REPORT DOCUMENTATION PAGE

Form Approved
OMB No. 0704-0188

PLEASE DO NOT RETURN YOUR FORM TO THE ABOVE ADDRESS.

1. REPORT DATE *(DD-MM-YYYY)*	2. REPORT TYPE	3. DATES COVERED *(From - To)*
032006	Final Report	15 June 2004 - 14 September 2005

4. TITLE AND SUBTITLE

Performance Testing of the Active Core Exhaust (ACE) Fluidic Mixing System

5a. CONTRACT NUMBER

5b. GRANT NUMBER

FA9550-04-1-0403

5c. PROGRAM ELEMENT NUMBER

6. AUTHOR(S)

R. J. Gaeta, B. Murdock, A. Churny and N. Hunter

5d. PROJECT NUMBER

5e. TASK NUMBER

5f. WORK UNIT NUMBER

7. PERFORMING ORGANIZATION NAME(S) AND ADDRESS(ES)

Georgia Institute of Technology
Aerospace and Acoustics Technologies Branch
GTRI/ATASL
Atlanta GA 30332-0844

8. PERFORMING ORGANIZATION REPORT NUMBER

9. SPONSORING/MONITORING AGENCY NAME(S) AND ADDRESS(ES)

USAF/AFRL
AFOSR
875 North Randolph Street
Arlington VA 22203

10. SPONSOR/MONITOR'S ACRONYM(S)

AFRL-SR-AR-TR-06-0214

12. DISTRIBUTION/AVAILABILITY STATEMENT

Distribution Statement A. Approved for public release; distribution is unlimited.

13. SUPPLEMENTARY NOTES

14. ABSTRACT

This report describes the work performed by the Georgia Tech Research Institute (GTRI) under a grant funded by the Air Force Office of Scientific Research (AFOSR). This grant was facilitated by the Air Force Research Laboratory's (AFRL) Air Vehicle Directorate to evaluate an existing fluidic jet mixing design system. Specifically, the operational design space of the Active Core Exhaust (ACE) Control system was explored.

15. SUBJECT TERMS

16. SECURITY CLASSIFICATION OF:			17. LIMITATION OF ABSTRACT	18. NUMBER OF PAGES	19a. NAME OF RESPONSIBLE PERSON
a. REPORT	b. ABSTRACT	c. THIS PAGE			19b. TELEPHONE NUMBER *(Include area code)*
U	U	U	UU	83	

Final Report

GTRI Report A7470/2006

Performance Testing of the Active Core Exhaust (ACE) Fluidic M\ixing System

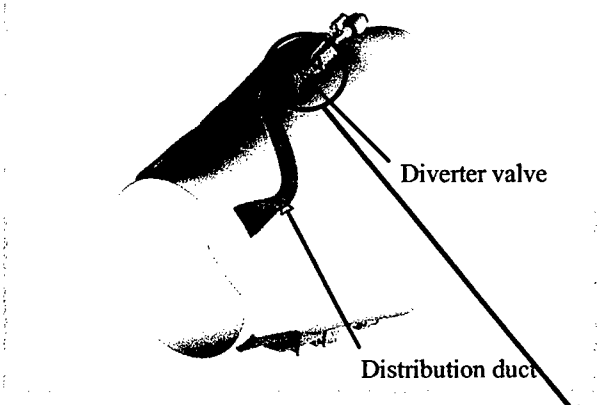

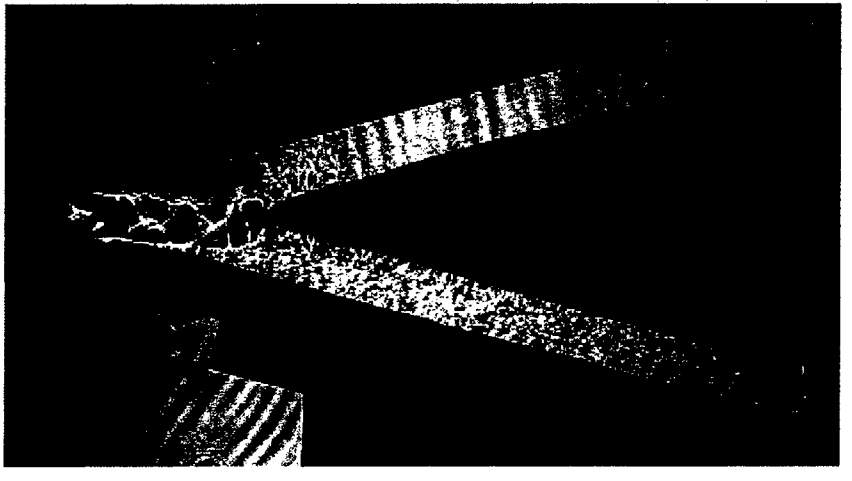

R. J. Gaeta, B. Murdock, A. Churny and N. Hunter
Georgia Institute of Technology,
Aerospace and Acoustics Technologies Branch
GTRI/ATASL
Atlanta, Georgia 30332-0844

Submitted to:
Col. Rhett Jeffries
AFOSR
801 North Randolf St.
Arlington, VA 22203-1977
FA9550-04-1-0403

MARCH 2006

Georgia Tech Research Institute

Acknowledgements

This work was funded by the Air Force Office of Scientific Research. Hardware was provided by The Boeing Company and Honeywell Engines and Systems. Throughout the course of this research, David Smith and Kurt Matthews of Boeing and John Thurston and Bill Ryan of Honeywell provided valuable information and feedback regarding the operation of the fluidic systems and components. The authors would also like to acknowledge Georgia Tech graduate student Paul Wickersham who wrote most of the data acquisition codes and helped with hardware set up. Finally, the first author acknowledges the support and encouragement of Tom Presdorf of AFRL's Vehicle Directorate.

Final Report

Executive Summary

This report describes the work performed by the Georgia Tech Research Institute (GTRI) under a grant funded by the Air Force Office of Scientific Research (AFOSR). This grant was facilitated by the Air Force Research Laboratory's (AFRL) Air Vehicle Directorate to evaluate an existing fluidic jet mixing design system. Specifically, the operational design space of the Active Core Exhaust (ACE) Control system was explored.

The ACE system was designed to mix the PW-F117 turbofan core exhaust for the C-17 aircraft. Previous research efforts on the ACE system were conducted with a two-fold objective: 1) Examine the performance the ACE system that proved to unsuccessful in a full scale PW F117 turbofan engine test and 2) draw on the lessons learned from this failure to design a new prototype ACE system. These objectives were achieved over the course of three years in programs funded by DARPA and AFRL. A full scale prototype was designed and fabricated to be installed on a PW F117 engine/nacelle package. Its performance was verified at GTRI facilities. This prototype was the culmination of a system re-design that both simplified the distribution system and delivered a more consistent pulse train to the jet's shear layer. These tests demonstrated the successful operation of a fluidic pulsing system designed to mix the core plume of a PW F117 turbofan.

However, it became clear that the system behaved unpredictably at certain supply pressures. Specifically, the system exhibited a tendency to naturally produce a pulse at certain frequencies regardless of the controlled input frequency. This suggested that the bi-stable diverter valve and/or the distribution duct system interacted with each other to force a condition that was not desired. In a continuing effort to understand the ACE system and its design implications, a series of tests were planned to assess the system's performance over a wide range of pressures and frequencies. These tests were guided under the auspices of AFRL with funding provided through an AFOSR grant. This report represents the findings of these tests. Key contributions to the test hardware were made by the Boeing Company and the Honeywell, Engine and Systems Company. It is hoped that a better understanding of the physics of the system will lead to a better guide to designers.

All data in this program was acquired without a main jet, so mixing performance was not addressed. The purpose was to delineate the operating map for the ACE system as a function of pressure and frequency. The work here was conducted to define the system's operational limitations.

Results indicate that at low system pressures, the area ratio (diverter valve exit to the system exit area) tends to dominate the valve switching phenomenon. At high pressures, resonance becomes a large factor and can control the diverter valve switching. This resonance frequency is predictable and is a function of the distribution duct length and the mean flow velocity in the duct. Thus, a tradeoff between exit slot area and duct length should be undertaken to optimize the operating envelope of the ACE system. Improvement in the pressure range of the pilot oscillating valve can extend the system envelope as well as increasing the control flow.

This study in conjunction with the previous work performed by GTRI on the ACE system represent a body of knowledge that allow the system integration aspects of ACE to be understood. The physics of the jet mixing technique are well established and a rational design approach has been applied. This jet mixing flow control technology is mature and the only remaining questions to be answered require on-wing testing to demonstrate it can meet operability demands. Finally, the data acquired for this report represent a large database from which analysis tools and CFD models can be validated.

List of Figures

Page

List of Figures

Page

List of Figures

Page

Final Report

1.0 INTRODUCTION

1.1 BACKGROUND

Previous research efforts on the ACE system were conducted with a two-fold objective: 1) Examine the performance the ACE system that proved to unsuccessful in a full scale PW F117 turbofan engine test and 2) draw on the lessons learned from this failure to design a new prototype ACE system. These objectives were achieved in two programs funded by DARPA and AFRL which are detailed in reference 1. A full scale prototype was designed and fabricated to be installed on a PW F117 engine/nacelle package. Its performance (consisting of the quality of pulse delivered and its ability to mix a jet) was verified at GTRI facilities. This prototype was the culmination of a system re-design that both simplified the distribution system and delivered a more consistent pulse train to the jet's shear layer. These tests demonstrated the successful operation of a fluidic pulsing system designed to mix the core plume of a PW F117 turbofan. Mixing was quantified for the idle-reverse cycle point using both cold and hot system air temperatures and is documented in reference 1. Although all the nozzle cycle points could not be duplicated in the GTRI facility, the ACE system could be operated over a wide range of pressures and frequencies. After successful mixing of the idle-reverse condition was demonstrated, higher ACE supply pressures were used to assess the pulse quality at different cycle conditions.

It became clear that the system behaved unpredictably at certain supply pressures. Specifically, the system exhibited a tendency to naturally produce a pulse at certain frequencies regardless of the controlled input frequency. This suggested that the bi-stable diverter valve and/or the distribution duct system interacted with each other to force a condition that was not desired. The questions were asked: Could this self-resonance be predicted and understood? How amenable is this technology to generic design rules that can be applied to a wider range of applications?

1.2 PROGRAM OBJECTIVES

In a continuing effort to understand the ACE system and its design implications, a series of tests were planned to assess the system's performance over a wide range of pressures and frequencies. These tests were guided under the auspices of AFRL with funding provided through an AFOSR Grant. Key contributions were made by the Boeing Company and the Honeywell, Engine and

Systems Company. Boeing provided the distribution duct hardware and other test hardware used in this effort and Honeywell provided the key bi-stable jet or diverter valve that provided the pulsing flow to the system. Both companies also contributed through valuable discussions with GTRI regarding testing and hardware design. It was hoped that a better understanding of the physics of the system would lead to a better guide to designers.

2.0 TECHNICAL APPROACH

The general ACE system consists of a single pilot oscillator valve that provides a control flow to two larger oscillator valves (diverter valves). The pilot oscillator itself is provided control flow from a small torque motor. The diverter valves are designed to divert the air down alternate exit paths of the valve that have a distribution ducts attached in order to deliver a pulse train of flow. This jet mixing technology has a firm foundation in physics and an established track record of success in the laboratory over the past 25 years[2-10]. Indeed, a full-scale demonstration on a mixed-flow turbofan was demonstrated in 1997[11], however this system was not flight-worthy and was not built to be housed in an engine nacelle like the current ACE system.

Figure 2.1 shows the old and the new ACE system design as would be installed on a core nozzle. Significant differences exist between the two designs, the latter of which was the beneficiary of previous work. The new design was also demonstrated on a full scale jet that simulated a pertinent engine cycle point of operation. Measured jet mixing at full scale was in agreement with small scale jet mixing experiments as shown in Figure 2.2. In short, it was shown that the system integration problems that plagued the initial ACE design were overcome. Furthermore, the ACE system was run at a wide range of pressures and frequencies in the laboratory in order to ascertain its performance envelope. It was crucial that a definition of acceptable performance be established, thus a map of pressure and frequency could be produced that indicated regions of acceptable and unacceptable system operation. In reference 1, a metric was developed that attempted to measure the "quality" of the pulse produced by the ACE system. Small scale jet mixing experiments revealed how the quality of the pulse affected the mixing . Parameters like DC offset and how faithfully the pulse resembled a square, sine, or impulse wave form were examined. It was found that the system exhibited a tendency to naturally produce a pulse at certain frequencies regardless of the controlled input frequency. This suggested that the bi-stable diverter valve and/or the distribution duct system interacted with each other to force a condition that was not desired.

The approach used in the current study was to isolate the effect of the distribution ducts on the system by building straight ducts of varying length and measuring system performance. Furthermore, duct terminations (exit spades) were fabricated that had the ability for exit area

adjustments. These ducts were built by Boeing. Then, in order to see how the distribution ducts affect the diverter valve, a special valve was built by Honeywell that allowed optical access of the critical flow regions within the valve. Schlieren and shadow-graph imaging was used to visualize the air flow as it switched from one path to another. Although the switching control ports were fixed and the distance from the valve throat to the splitter was fixed, the observed flow was correlated with the overall performance of the system. However, further performance metrics were developed to aid in understanding the resulting measurements.

2.1 METRICS TO ASSESS ACE PERFORMANCE

Assessing the quality of a pulse produced by the ACE system is, by nature, subjective. It has been determined via small-scale experiments that the quality of the square wave produced can be non-ideal and still result in excellent jet mixing. In fact, a sine wave can also be used with success as well. Since the present experimentation does not include a jet from which mixing can be quantified, the ACE system performance was couched in terms of pulse quality that was produced at a given supply pressure and frequency. One can look at a time history of the slot exit total pressure pulses and make a qualitative assessment as to its potential effectiveness. Things to look for include amount of DC offset, modulated frequencies, and general Gaussian noise. Other than examining the pulse time histories individually for a given pressure and frequency, several metrics were developed to help quantify the quality of the pulse delivered by the system.

Square and Sine Wave Quality

Given an input supply pressure and frequency, an ideal square wave was constructed. Each measured total pressure time trace (at least 10 periods) was then compared to this ideal. A mean square of the error between the ideal and actual was normalized for each case producing a single number representing the total error. If this number was zero, then the measured wave was a perfect square wave. Theoretically, this number has no upper bound. The larger this number, the worse the pulse quality. The steps below demonstrate the details of the calculation of the quality factor.

1. The top and bottom of the square wave is estimated from the pressure data.

2. An ideal square wave is generated and has the following properties:
    a. zero phase
    b. the desired pulsing frequency (i.e. the frequency input to the torque motor)
    c. the estimated top and bottom (from above)
3. The mean square error (MSE) between this ideal wave and the actual wave is calculated:

$$MSE=\frac{1}{n}\sum_{i=0}^{n-1}(x_i-y_i)^2$$

Where: n = the number of data points
x_i = the i^{th} actual pressure data point
y_i = the i^{th} ideal pressure data point

4. The phase of the ideal wave is shifted in 1.8° increments up to a total shift of 360° and the MSE is calculated for each phase shift.
5. The minimum MSE value is chosen as the one that is the best phase match for the two waves (actual and ideal).
6. The Quality is calculated as the MSE which has been normalized for square waves of all amplitudes as follows:

$$Q=MSE\cdot\left(\frac{1}{A}\right)^2$$

Where: A = Top – Bottom (the amplitude)
Q = quality

The square wave quality for an ideal square wave is zero. Thus the lower the quality, the better the fit. Figure 2.3 shows an example of how this metric is created from real data, this case, the quality is quite good. In addition to these cases where the error is computer generated, if the waveform is not square in shape or difficult to fit a square wave to, then the quality factor will be

high (i.e. bad). Figure 2.4 is an example of a poor quality sine or square wave. The same procedure can be done by fitting the data to an ideal sine waveform.

A different way to use this parameter is to produce a contour plot on a plane of input frequency and upstream total pressure (P_{ch}). This plane can be referred to as the performance plane. The color magnitude of this plot indicates the value of the square or sine wave quality. Figure 2.5 shows an example of this type of plot for a particular slot exit and a distribution duct configuration.

Input/Output Frequency

Another measure of the performance of the ACE system is the ability for it to produce a pulse at the desired (input) frequency. Thus, if 80 Hz is input, one should expect that a Fourier transform of the resulting pulse time history to have a peak amplitude frequency of 80 Hz. Plotting contours of constant amplitude on a 2D plane of input frequency versus resulting frequency can give an indication of how well the system responds to the driving frequency. Figure 2.6 shows an example of this contour plot. If a line of constant input frequency is cut through the contour, one would see the resulting frequency domain of the time history (see top figures). Note that the highest magnitudes in the contour plot occur around a line that is 45^0 from the origin. This shows that the system is indeed producing the maximum amplitude at the input frequency. Note also that several sub-harmonics are visible (the lighter-colored lines that have a shallower angle than 45^0).

Frequency Power Ratio

If the energy at the input frequency is quantified and compared to the total energy in the spectrum, then a contour plot of this parameter can be used to gain insight into the system's performance. The Frequency Power Ratio (FPR) is the fraction of energy at the input frequency relative to the total. Its value is from 0 to 1 and Figure 2.7 shows an example of how it could be mapped in the performance plane.

Switching Parameter - ϕ

Finally, with all of the myriad ways to quantify performance it was desired to produce a parameter that could give a "go – no go" type result. That is, if possible, come up with a set of criteria that will be a good indication of whether the diverter valve (or pilot valve) switched properly. Three indicators from the time history of a pulse will be computed. First, a parameter called Valve Ratio is calculated:

$$VR = \frac{Avg.Max_{slot\#1}}{Avg.Max_{slot\#2}} \qquad (1)$$

where the average pulse maximum and minimum are defined as in Figure 2.8 for one slot and its alternate slot. Second, a DC offset parameter is computed that examines just one pulse time history and calculates:

$$DCO = \frac{Avg.Max}{Avg.Min} \qquad (2)$$

Finally, a measure of valve control authority is determined by comparing the input frequency with the frequency of peak output and determining if the difference is within +/- 1 Hz:

$$-1Hz \le f_{input} - f_{peak\ output} \le 1Hz \qquad (3)$$

If all of the criteria (1 – 3) are satisfied, a parameter, ϕ, is given the value 1 and the valve is said to have switched. If one of the criteria is not satisfied then $\phi = 0$ and the valve is said not to have switched. For each upstream pressure and input frequency, ϕ can be computed and plotted as a contour in the performance plane. Figure 2.9 shows an example of this.

2.2 DISTRIBUTION DUCT PARAMETERS

The distribution ducts were fabricated by Boeing to mimic the internal cross sectional area of the new ACE duct design (specifically, a 2.3inch x 0.35inch rectangular duct). These ducts were modular such that the overall length of the ducts could be altered. Nominally, three duct lengths were available: a 12, 21 and a 49 inch duct that bolted to the exit of the diverter valve. In

addition, a so-called spade exit was made for each duct which added approximately 11 inches to each duct. This type of exit simulated a typical slot that interfaced with the main jet to initiate the mixing process. The exit area of the slot had the capability of changing height so the exit area could be either increased or decreased +10% and -20% from a nominal value. Finally, 90^0 bend sections were fabricated to examine their effect on the pulse quality. Thus, distribution duct length, exit area, and turning were varied parameters in the current study. Figure 2.10 and 2.11 show the distribution duct hardware. Table 2.1 summarizes the test hardware configurations of the distribution ducts.

Duct Configuration	Inlet Area	Exit Area	Area Ratio
L = 12"	0.863 in^2	0.863 in^2	1.000
L = 23" w/Spade Exit; nominal area	0.863 in^2	0.829 in^2	1.040
L = 23" w/Spade Exit; +10% increase from nominal area	0.863 in^2	0.912 in^2	0.946
L = 23" w/Spade Exit; -10% increase from nominal area	0.863 in^2	0.746 in^2	1.156
L = 23" w/Spade Exit; -20% increase from nominal area	0.863 in^2	0.663 in^2	1.300
L = 21"	0.863 in^2	0.863 in^2	1.000
L = 32" w/Spade Exit; nominal area	0.863 in^2	0.829 in^2	1.040
L = 32" w/Spade Exit; +10% increase from nominal area	0.863 in^2	0.912 in^2	0.946
L = 32" w/Spade Exit; -10% increase from nominal area	0.863 in^2	0.746 in^2	1.156
L = 32" w/Spade Exit; -20% increase from nominal area	0.863 in^2	0.663 in^2	1.300
L = 49"	0.863 in^2	0.863 in^2	1.000
L = 60" w/Spade Exit; nominal area	0.863 in^2	0.829 in^2	1.040
L = 60" w/Spade Exit; +10% increase from nominal area	0.863 in^2	0.912 in^2	0.946
L = 60" w/Spade Exit; -10% increase from nominal area	0.863 in^2	0.746 in^2	1.156
L = 60" w/Spade Exit; -20% increase from nominal area	0.863 in^2	0.663 in^2	1.300
L = 42" w/90^0 w/Bend	0.863 in^2	0.863 in^2	1.000
L = 42" w/90^0 w/Bend and Spade Exit	0.863 in^2	0.829 in^2	1.040

Table 2.1 Distribution duct test hardware configurations.

2.3 QUALITATIVE DIVERTER VALVE PERFORMANCE

The bi-stable jet that forms the basis of the diverter valve is the key to producing oscillatory flow needed for jet mixing. Air at high pressure is fed into a plenum where it is accelerated through a two-dimensional throat. It is then allowed to expand into an area leading to two pathways. The expanding jet, left alone, will "choose" a path and stay in quasi-equilibrium. At approximately 4

throat heights downstream of the throat, slots are cut to deliver control flow. That is, alternating flow through these slots can force the jet to go down one pathway or the other. The diverter valve is two dimensional with the width being approximately 2.3 inches. Honeywell fabricated one such valve that had the sides made amenable for optical glass to be installed. This allows a clear view of the valve's two-dimensional flow path. Figure 2.12 shows this "optical diverter valve". A double diode YAG 532 nm laser was collimated and passed through the valve side glass walls. The resulting schleiren image was focused into a high speed camera to capture the flow field structure within the valve. With the capability of thousands of frames a second, the camera easily was able to detect switching frequencies over 100 Hz.

3.0 EXPERIMENTAL FACILITIES AND DATA ACQUISITION

3.1 TEST RIG FOR THE ACE PULSE MIXING SYSTEM

The ACE pulse mixing system consists of a main flow supply that is split into two paths (via flexible hoses) leading to two diverter valves which produce alternating flow that exit out of two ports. Distribution ducts are attached to the diverter valve exhaust and they deliver air through a high aspect ratio slot. In all of the tests performed in the current study, the jet exhausts into a quiescent room. The alternating flow through the diverter valve is provided by control flow inputs on either side of the valve throat. The control flow is delivered by a smaller diverter valve called the pilot valve. This flow originated from a different source than the main flow. Finally, the control flow needed for the pilot valve was from still a different source. A smaller torque motor or electro-pneumatic solenoid valve was used. The frequency of the entire pulsing system is controlled by a function generator which drives the solenoid valve.

The main flow for the diverter valves was supplied from a 300-PSI air source and controlled with a Valtek Mark II computer controlled valve. The flow passed through a plenum/combustion chamber and thus could be heated or unheated. It arrived via a 4 inch insulated pipe and passed through a 1-inch throat diameter venturi flow meter before splitting into two flexible stainless steel hoses that connected to the diverter valves.

Control flow for the diverter valves arrived from the pilot valve via copper tubes. Main flow for the pilot valve was supplied from the 300-PSI air source controlled by a Norgren R18 pressure regulator. This flow also passed through a 0.5-inch throat diameter venturi flow meter and was delivered to the pilot valve. Control flow for the pilot valve came from the torque motor and arrived through 3/8" diameter copper tubes. The torque motor was supplied with 100-PSI shop air and flow input was measured with a 0.25-inch throat diameter venturi flow meter.

Each leg of the ACE system was bolted to an optical table to minimize vibration. Figure 3.1 shows the test rig set up schematically. It consists of a primary flow duct that is split into two equal length flexible steel pipes. Each flow stream feeds a diverter valve that has two distribution ducts attached to the valves exit. Figure 3.2 shows the actual test rig as installed in

GTRI's laboratories. The constituent parts of the diverter valve are shown in Figure 3.3 and Figures 3.4 and 3.5 show a typical installation of distribution ducts associated with one diverter valve.

3.2 PRESSURE, TEMPERATURE, AND FLOW MEASUREMENT

Mass flow at three different locations was measured using venturi flow meters to determine the total mass flow of the system. The three locations were: diverter valve main flow, pilot valve main flow, and torque motor flow. For each of these venturis, a high and low (inlet and throat) pressure was measured to calculate the mass flow. The most accurate way to do this was to measure the high pressure (P_{high}) and the change in pressure (ΔP) across the venturi. The low pressure was then calculated from these measurements. For the diverter valve and pilot valve flows, P_{high} was measured with Omega PX302 pressure transducers and ΔP was measured with Validyne P305D differential transducers. For the torque motor flow, P_{high} and ΔP were measured using a Pressure Systems Netscanner 98RK rackmount with Model 9816 Pressure modules installed.

Static temperature was measured in the bottom diverter valve inlet using a type-T, plug like thermocouple. Based on flow symmetry, we assumed the static temperature was the same for the top diverter valve inlet as well.

Total pressure was measured at a number of locations using Endevco unsteady pressure transducers of various pressure ranges. In the previous phase of this project that was determined that total pressure tubes of sufficiently short length could be used to measure unsteady pressure with virtually no loss of accuracy. This was verified by comparing measurements made by Endevco transducers screwed into custom built total pressure tubes against measurements made with a Dantec hot wire anemometer. Four 0-100 PSIG unsteady transducers measured the duct exit total pressures via total pressure tubes. Four 0-100 PSIG unsteady transducers also measured diverter exit total pressure in the same way. Two 0-50 PSIG unsteady transducers measured total pressure at the pilot oscillator exit.

Static Pressure was measured in two of the diverter control input ports using flush-mounted Endevco unsteady pressure transducers.

3.3 DATA ACQUISITION

All of the measurements (except for those made with the Pressure Systems rackmount) were tied into a National Instruments AMUX 64-T Multiplexor. The multiplexor allows up to 32 differential analog input connections. To get the cleanest signals possible, shielded wires, differential inputs, and powered all transducers with a 12-volt car battery are used. Excitation voltage for the unsteady transducers was dropped to 10 volts via a potentiometer added in series. The Multiplexor was connected to a NI PCI-6035E multifunction data acquisition board. This board has a TTL output that was used to control the pulsing frequency. LabView software was used to write all of the needed programs. Two main programs were written for data acquisition and control. One program controlled the pulsing frequency and measured the diverter inlet temperature and all mass flow rates. It has the added capability of performing a frequency sweep by inputting a starting frequency, and increment, and an ending frequency. A second program performs all of the unsteady pressure measurements (total and static). It was written in such a way that it could be run in manual mode or automatic mode. In manual mode, the user decides when to make the pressure measurements. In auto mode, the program is linked to the first program such that with each increment in frequency, the program automatically measures all of the unsteady pressures and stores them to a file for later processing. This data acquisition automation provided a smooth and efficient method of gathering a lot of performance data for the ACE system.

3.4 SCHLIEREN SYSTEM FOR DIVERTER VALVE FLOW VISUALIZATION

The schlieren system consisted of a laser whose beam which was allowed to pass through an aperture to produce a point light source. The light was then collimated with a 6-inch diameter lens and passed through the test section, which consisted an ACE diverter valve with the sidewalls removed and replaced with quality optical glass. Finally, the collimated beam is re-focused over a knife edge with another 6-inch diameter lens and is terminated into the lens of a Vision Research Phantom high speed digital camera. Figure 3.6 shows the optical test setup for a typical run.

4.0 RESULTS AND DISCUSSION

Before reconfiguring the ACE pulse delivery system to test the effects of distribution duct changes on the performance, the full-scale baseline ACE system that was mounted on the simulated core nozzle was tested on the new bench test set-up. This was done to ensure that performance of the system was representative of the previous experiments run in previous tests.[1,2] It also provided data that was used to explore new data analysis techniques. Results of these tests are presented first, followed by results of distribution duct length changes and duct exit area changes. Finally, qualitative results of the flow field within the diverter valve are presented and correlated with system performance.

4.1 THE BASELINE ACE PULSE DELIVERY PERFORMANCE

The baseline ACE pulse delivery system that was documented in references 1 and 2 was removed from the simulated core nozzle and rigged for mounting on a test bench, as shown in Figure 4.1. Selected time histories of total pressure at the exit slots of the "S-Duct" configuration are shown in Figure 4.2. While the pulse trains are not identical, they agree very well considering the differences in the two test set ups. This provided confidence that the ACE bench rig set up was behaving as the full-scale simulated nozzle test set up.

4.2 EFFECT OF DISTRIBUTION DUCT LENGTH ON PULSE QUALITY

Previous experience with ACE system performance has identified that the desired pulse delivery depended on supply total pressure, pulsing frequency, control flow quality, and distribution duct configuration. The latter manifested itself as a loading or back pressure on the diverter valve that allowed it to pulse (i.e., switch) adequately. In addition to the distribution duct's role, the supply pressure can prevent the valve from switching properly due to over-expansion of the valve's internal flow. This will be shown qualitatively in the flow visualization data.

4.2.1 SLOT EXIT PRESSURE TIME HISTORIES

The effect of distribution duct length was explored by attaching straight ducts of differing lengths to the diverter valves. Distribution ducts are necessary components of the ACE system because the alternating flow from the diverter valve has to be delivered to opposite sides of a large (on the order of 30 inches) diameter jet. Thus, the pulse quality from the diverter valve and

the performance of the diverter valve will be modified by the presence of the ducts. Figure 4.3 shows selected time histories of total pressure at the duct exit for an upstream pressure of 30 psig and input frequency of 10 Hz. Three duct length configurations are compared from short (top) to long (bottom). It is clear that the additional duct length helps deliver the strongest quality pulse. The short duct fails to produce flow that switches from one slot exit to the other significantly. The medium length duct shows signs of valve switching and the long duct demonstrates full switching at 10 Hz. Figure 4.4 shows the same type of pressure time histories for 100 Hz. Again the additional duct length allows the diverter valve to switch properly. At higher pressure, the added distribution duct length improves the pulse quality as at lower pressures. This is shown in Figure 4.5.

4.2.2 PULSE QUALITY CONTOURS

Figure 4.6 shows square wave quality contour plots for both the pilot oscillator output (the left side of the page) and one of the two diverter valve outputs (the right side of the page). The quality of the pilot oscillator doesn't appear to be affected much by the increased length of the distribution duct, but clearly the output from the duct exits are affected. The medium length duct has higher quality output than the shorter duct, while the long duct a region of good square wave quality that bridges the low and high pressure conditions.

The effect of the distribution duct length on overall performance can also be demonstrated by looking at the overall performance of the system in the pressure-frequency domain. Figure 4.7 shows contours of the switching parameter f for the pilot oscillator valve output (the left column) and the duct output attached to diverter valve #2 (the right column). In these contour plots, the green represents successful operation (see Section 2.1) and there is a trend towards more green space is observed as the duct length increases. Additional back pressure generated by the additional length plays an important role in determining if the diverter valve works properly. In this case, additional back pressure is provided by the increased friction of the longer duct (this corresponds to a smaller effective flow area due to boundary layer build up).

4.2.3 PEAK FREQUENCY CONTOURS

Section 2.1 presents an alternate way of looking at the ACE system performance that involves the frequency of peak amplitude compared to the desired input driving frequency. Figure 4.8 shows this peak frequency contour plot for the three tested duct lengths. These are each at a

constant chamber pressure of 30 psig. Two observations to note are the increase in the "signal-to-noise" as the duct length is increased and the appearance of vertical bands of high amplitude, particularly around 100 Hz. It should also be pointed out that in all of these types of plots, the vertical band of high amplitudes occurring near 0 Hz is an artifact that these periodic pulses do not oscillate around a zero mean. Thus a DC component will always be present.

Further interpretation of Figure 4.8 reveals that when the input frequency gets close to 100 Hz, the output pulse frequency "locks" on to 100 Hz. Subsequent vertical lines of lesser amplitude are visible at 200 Hz and 300 Hz, indicating that these are higher harmonics of 100 Hz. This phenomenon appears to be related to the duct length (Figure 4.8c) and the result of flow-acoustic interactions, that is, a resonance phenomenon. Figure 4.9 and Figure 4.10 show peak frequency contour plots for a chamber pressure of 30 psig and 120 psig, respectively. The peak frequency contour plots for the control ports that "switch" the diverter valve are also shown for these two cases. Two things to note: 1) the resonance becomes stronger as the chamber pressure increases and 2) the resonance is evident in the control port lines. Further discussion of this resonance will be discussed in Section 4.4.

4.3 EFFECT OF DISTRIBUTION DUCT EXIT AREA ON PULSE QUALITY

It has been shown that increased duct length can improve the operation of the ACE system by introducing a back pressure due to viscous effects. Another way to describe the effect of increased viscous forces is that the increased boundary layer produces a smaller flow area. The exit area of the distribution duct was changed by adding an exit spade that had an adjustable exit slot height (see Figure 2.11). The spade, which could be attached to any of the duct lengths, was approximately 11 inches long. The exit slot formed by the spade was nominally 0.155" high and 5.35" wide. Figure 4.11 shows the dramatic effect the spade has on the delivered pulse. At a chamber pressure of 30 psig and a frequency of 10 Hz, it shows the time history for the medium duct length (a) without the spade attached, (b) with spade attached and the exit area increased by 10%, and (c) with spade attached and the exit area decreased by 20%. It is clear that the case with the spade attached and a reduced area (Area ratio = 1.3) produces a "textbook" square wave pulse. Figure 4.12 shows similar configurations for a frequency of 80 Hz. The results at this higher frequency are not as dramatic, but still produce a useable pulse train with the exit area

reduced 20%. The progression of bad to good pulses can be seen in Figure 4.13 for a chamber pressure of 30 psig. For this particular slot exit, a non-existent pulse becomes a robust pulse at the increased area ratio.

Examination of the switching contour plots for the short duct length for four different slot exit area ratios shows clearly the benefit of having the proper exit area and thus, the proper diverter valve back pressure. This is shown in Figure 4.14 where the amount of green contour area increases with decreasing slot exit area. Similar data is shown in figures 4.15 and Figure 4.16 respectively, for the medium and long duct configurations at the slot exit area extremes (+10% nominal and -20% nominal).

Finally, to demonstrate that the exit area ratio can be a significant parameter in producing a quality pulse, the distribution ducts were removed and the diverter valve was allow to exhaust to ambient. Total pressure time histories were recorded with the valve unloaded and with a "restrictor plate" that closed the exit area by 20%. Figure 4.17 shows the results for 10 Hz and 80 Hz respectively, at a chamber pressure of 30 psig. The pulse for the unloaded diverter valve case is plagued by a large DC offset, with very minimal pressure pulse, while the restrictor plate case generates a clean square wave pulse in the 10 Hz case and a sinusoidal pulse in the 80 Hz case.

The effect of exit area on the diverter valve is summarized in Figure 4.18 where the unloaded valve exit, the 20% reduced restrictor plate, and the 20% reduced medium length distribution duct time histories are shown together for a chamber pressure of 30 psig and a frequency of 10 Hz. Although the main difference between the latter two cases is a duct length of 32 inches vs. no-duct, similar quality pulses are produced. This can provide some freedom when designing ACE-type systems for alternate engine-nacelle configurations.

4.4 FLOW-ACOUSTIC CONSIDERATIONS

The flow-acoustic phenomenon described in Section 4.2 and shown in Figures 4.8c, 4.9, and 4.10 is an important design consideration for this type of pulse delivery system. It was hypothesized that a longitudinal mode could be excited in the distribution duct (based on its length) that forced the diverter valve to switch at this excited frequency. This hypothesis was tested by examining

the theoretical longitudinal duct resonance modes and observing what the effect of flow has on this phenomenon.

It has been observed that the "lock on" frequency of the system is intensified under two conditions: 1) when the input frequency is close to the fundamental resonance frequency and 2) when the chamber pressure is elevated well beyond its design intent. Figure 4.19 shows three slot exit time histories. The first is at a chamber pressure 120 psig with an input frequency of 10 Hz. Note that the resulting output frequency is approximately 44 Hz with a noticeable 10 Hz modulation. The system is trying to deliver the 10 Hz pulse, but is being overridden by a 44 Hz pulse. The second plot shows a time history for the same chamber pressure condition, but with an input frequency of 44 Hz. Here the output frequency is approximately 47 Hz. The driving frequency is augmenting the resonance frequency. Finally the third plot shows a time history for an input frequency of 80 Hz. The output frequency is approximately 47 Hz again. (Note: the flat tops of the pressure pulses indicate "clipping" due to the pressure exceeding the transducers upper limit).

The resonance of the ducts must have a source to excite their modes. This source could be the input driving frequency or some strong broadband source from which the ducts respond to their preferred frequency. Given the physics of the flow through the diverter valve, it is quite likely that the significant turbulent flow and oscillating shock structures that occur as the inner jet "flops" from one side of the flow splitter to the other is the broadband source. The longitudinal acoustic mode of a rigid duct produces resonance at frequencies prescribed by the solutions of the wave equation. Depending on the boundary conditions, the following resonance frequency and its harmonics can exist[12]:

For an Open-Closed Duct –

$$f_{\text{Res}} = \frac{(2n-1)c}{4\left[l + \frac{8}{3\pi} r_{eq}\right]} \qquad (4)$$

For an Open-Open (or Closed-Closed) Duct –

$$f_{\text{Res}} = \frac{nc}{2\left[l + \frac{8}{3\pi} r_{eq}\right]} \qquad (5)$$

In both cases, c is the speed of sound, l is the duct length, and r_{eq} is the equivalent radius of the duct exit area. The term modifying the length ($8*r_{eq}/3*\pi$) is known as the end correction[12]. Also, n = 1,2,3,.....and represents the mode numbers. The actual boundary conditions are not known precisely, especially at the diverter valve exit. However, it has been shown theoretically that the refection coefficient of an open end duct is near unity for very low frequencies[13] (or low $k*r_{eq}$, where k is the wave number). Thus, it is plausible that the ends of the distribution ducts could behave like a closed-closed boundary condition. In reality, the end near the "source" (i.e., the diverter valve end) probably behaves somewhere in-between a closed and open boundary condition. Figure 4.20 shows how the theoretical resonance fundamental frequency varies with duct length. Two curves are shown. The upper curve uses equation (4) which is valid for an acoustic wave traveling along a duct with no mean flow. However, the wave equation can be modified to account for a mean flow as follows[13]:

$$f_{\text{Res}} = f_{res_{NOFLOW}} \left[1 - M^2\right]^{0.5} \qquad (6)$$

Where M is the mean Mach number in the duct. The lower curve in Figure 4.20 shows the effect of having a Mach number of 0.85 in the duct, a realistic number for a chamber pressure of over 100 psig. The primary effect of the mean flow is to reduce the resonance frequency and for a duct length of approximately 32 inches, a Mach number of 0.85 reduces the fundamental frequency from approximately 102 Hz to 50 Hz.

It is important to note that as the chamber pressure increases, the mean flow in the distribution duct increases. Therefore in the pressure-frequency domain, one should see evidence of the "lock on" or resonance frequency reducing as the chamber pressure increases. Figure 4.21 shows the fundamental resonance frequency plotted against mean Mach number (or approximately chamber pressure) for selected duct lengths using both equation (4) and (5). It becomes apparent that the shape of these curves is similar to the region of good quality pulses in the square or sine wave quality contour plots. Figure 4.22 shows contours for both sine wave and the switching parameter for the long duct configuration. A trend similar to the one shown in Figure 4.21 is observed (indicated with a red line).

To further confirm the idea that what is being observed in the ACE bench data is evidence of a flow-acoustic resonance, an acoustic test was set up to measure duct resonances with an acoustic

driver as a source at one end. Figure 4.23 shows the long distribution duct with a speaker attached to one end. A microphone with a probe tube attachment was placed inside the open end of the duct, approximately 5 inches from the exit. This, of course, doesn't mimic the ACE system exactly because there is no mean flow and the upstream boundary condition for the duct is not equivalent to having a diverter valve in place. However, it can affirm the notion that the lock on frequency can be correlated with the excitation of the longitudinal mode. Figure 4.24 shows the sound pressure level spectra of the microphone in the duct under broadband excitation from the speaker. A resonance phenomenon is clearly observed as evidenced by the sharp peaks in the spectra. Data was collected for the long duct without the exit spade, with the exit spade and just the exit spade itself. The spectrum for the straight 49 inch duct shows a much defined fundamental resonance peak and several higher harmonics. The addition of the 11 inch spade exit (making the duct 60 inches in length) shows how the fundamental resonance frequency moves from 153 Hz to 135 Hz, which is expected due to the lengthening of the duct. However, the fundamental and the first harmonic are more attenuated in the latter case. This is quite likely due to the change in duct geometry with the addition of the spade exit (see Figures 2.10 and 2.11). Finally, the spectrum for just the spade exit (L = 11 inches) is shown. A fundamental resonance is observed at 526 Hz.

These resonance frequencies observed with no mean flow and with a broadband acoustic source are consistent with theoretical longitudinal mode calculations. Their values fall between the two boundary condition extremes expressed in equations (4) and (5). Figure 4.25 shows three runs where the fundamental and harmonic resonance frequencies were measured with the long duct configuration. The data fall between the two extremes defined by equation (4) and (5).

4.5 EFFECT OF 90^0 BENDS ON PULSE QUALITY

The effect of a 90^0 bend occurring in an otherwise straight distribution duct is summarized in Figure 4.26 and Figure 4.27. Figure 4.26 shows time histories of duct exit pulses. The red traces are for the medium duct configuration with no spade exits or 90^0 bends. The blue trace is with the 90^0 bends and an exit spade. The bends help improve the pulse quality significantly for both low and high input frequencies. This is most likely due to the increased back pressure that the bends produce, making the diverter valve think a much longer duct exists.

Figure 4.27 shows switching parameter contours for the medium duct with no exit spade as well as contours for the medium duct with 90^0 bends and an exit spade. Due to data acquisition problems, chamber pressures below 70 psig were lost. However, the plots still reveal the increased operating envelope for the duct with 90^0 bends. Thus, a designer can use a strategic bend in the distribution duct to improve the system operation. One should be cautioned that bends also introduce non-uniform outlet flow (due to centrifugal forces). However, as demonstrated with the S-duct configuration, bends to one direction and then the opposite direction can be used to cancel these non-uniformities in the flow.

4.6 EFFECT OF NEW PILOT OSCILLATOR DESIGN ON PULSE QUALITY

The pilot oscillator valve that has been used for all of the data presented thus far was not specifically designed for high operating pressures. It was felt that perhaps the operating envelope of the ACE system could be extended by redesigning the pilot oscillator valve for better high pressure operation. Recall, this valve provides a pressure pulse to the diverter valve to initiate switching of the two dimensional jet. Honeywell provided a redesigned pilot oscillator valve that was inserted into the ACE bench system at GTRI and is shown in Figure 4.28.

A pressure time history comparison of unloaded (exits exhausting to ambient) pilot valves is shown in Figure 4.29 for an equivalent chamber pressure setting of 30 psig. Both a low (10 Hz) and a high (80 Hz) input frequency are shown. The results indicate that while the pressure pulse quality improves, it does not improve significantly. That is, the delivered pulse for both the original and redesigned pilot valve is adequate at low operating pressures. However, the redesigned pilot valve dramatically improves the pulse quality at high operating pressures. Figure 4.30 shows similar time history comparisons for an equivalent chamber pressure of 100 psig. There is clear indication that the newly designed pilot oscillator valve improves its switching operation at higher pressures.

The new pilot valve was connected to the entire ACE system and results for the medium duct with spade configuration were obtained. Figure 4.31 shows time history comparisons of the slot exit pressures for the old and the new pilot valve. Note that there is not much change in the low pressure cases, but that there is significant improvement at 100 psig. However, only marginal

improvement is observed at the highest pressure tested (120 psig). The main conclusion from this study is that improvement in all components of the ACE system work together to deliver the best possible pulse train over the largest operating range.

Finally, the operating envelope of the ACE system can be extended by regulating the control flow used to switch the diverter valves. That is, a particular region of the ACE operation that is not delivering a proper pulse can be fixed by increasing the control mass flow (the flow through the pilot oscillator). Figure 4.32 shows a series of exit pressure time histories for a range of control mass flows. An almost non-existent pulse can be transformed into an excellent pulse by increasing the control flow to the diverter valve. This extra bit of control can be used in critical situations that arise during operational use.

4.7 VISUAL EVIDENCE OF DIVERTER VALVE FLOWFIELD BEHAVIOR UNDER CHANGING DISTRIBUTION DUCT CONDITIONS

In an effort to understand more about the flow behavior inside the diverter valve, a special valve with glass sidewalls was fabricated and inserted into one side of the ACE bench set up. Figures 2.12 and 3.6 show the optical diverter valve and bench test set-up respectively for flow visualization of the internal flow field of the bi-stable jet inside the diverter valve. The objective of this qualitative test was to see how flow at the different chamber pressure settings interacted with the splitter and to witness the flow field during instances when the valve was not working properly. The flow was visualized using schlieren and shadow-graph techniques. Density gradients were produced from natural expansion and shock waves present. A double diode YAG 532 nm laser was used as the light source and a Vision Research Phantom high speed digital camera was used to stream images to a computer hard drive.

Figure 4.33 shows still photographs from a typical run where the valve was switching properly. The input frequency is 5 Hz; the chamber pressure is 40 psig with 10% control flow. The photographs show the two-dimensional jet in three phases of its travel from one wall to the other. Clearly visible are the shock waves and expansion waves of the emerging over-expanded jet. Other turbulent structures are also visible. Note the increase in distortion and turbulence of the jet as it "flops" across the splitter. It is possible that this could produce a broadband source that could excite duct modes downstream. Figure 4.34 shows another series of still photographs

taken of the diverter valve internal flow field. The driving frequency was 15 Hz with a chamber pressure of 30 psig.

Figure 4.35 show a progression of still photographs for an unloaded diverter valve (no downstream ducts). Above 50 psig, the reduced back pressure makes the jet emerging from the throat over-expand into the valve, filling both flow passages with shock and expansion waves. The control flow merely nudges each side near the throat that just makes the waves flutter in harmony with the driving frequency. Figure 4.36 shows a comparison between an unloaded diverter valve and one with a medium length duct attached. Exit pulses resulting from this flow field (an example is shown in Figure 4.37), have large amounts of DC offset and thus would have a difficult time mixing a jet significantly.

Over 100 GB of high speed camera data was recorded for several different system configurations. A selected amount of this data is provided on a DVD that is included in this report.

5.0 CONCLUDING REMARKS

A design approach has been outlined which can guide designers of a fluidic mixing system of the ACE-type. This methodology is represented in the experimental work and analysis of this report along with references 1 and 2. Key information can aid the designers such as the appropriate momentum ratio needed for good jet mixing, the appropriate placement of the high amplitude pulses on the periphery of the jet, the effect of distribution ducts on the bi-stable jet operation, and the appropriate frequency for best mixing. For jets on the order of 30 inches in diameter (e.g., the PW 117 core exhaust), one can bound the frequencies that would be needed for a fluidic system similar to one described in this report. Figure 5.1 shows a design space for forcing frequency and the exhaust velocity of the jet to be mixed. It assumes a 31-inch diameter jet, an optimum momentum ratio of 0.15 and an optimum non-dimensional frequency of 0.1 – 0.2. This design space is bounded by frequencies as low as 5 Hz (for a 120 ft/s jet) to 130 Hz (for a 1750 ft/s jet).

Results have indicated that at low system pressures, the area ratio (diverter valve exit to the system exit area) tends to dominate the valve switching phenomenon. At high pressures, resonance becomes a large factor and can control the diverter valve switching. This resonance frequency is predictable and is a function of the distribution duct length and the mean flow velocity in the duct. Thus, a tradeoff between exit slot area and duct length should be undertaken to optimize the operating envelope of the ACE system. Improvement in the pressure range of the pilot oscillating valve can extend the system envelope as well as increasing the control flow.

This study in conjunction with the previous work performed by GTRI on the ACE system represent a body of knowledge that allow the system integration aspects of ACE to be understood. The physics of the jet mixing technique are well established and a rational design approach has been applied. This jet mixing flow control technology is mature and the only remaining questions to be answered require on-wing testing to demonstrate it can meet operability demands. Finally, the data acquired for this report represent a large database from which analysis tools and CFD models can be validated.

Further study of this type of fluidic mixing system would focus on extending the operational envelope of the diverter valve. This valve, which relies on the bi-stable action of a two dimensional jet, is limited in its effectiveness by the extreme changes in its internal flow field due to changing upstream pressure conditions. Basic fluid-dynamic research on finding an optimum control port placement, proper splitter geometry or splitter location would go a long way in producing a robust flow control system that had a wide operating range.

6.0 REFERENCES

[1] Matthews, K. & Gaeta, R. "Active Core Exhaust (ACE) Control System Phase IIA Test Report, Revision A – Final Report for 13 March 2001 – 31 August 2004", Air Vehicles Directorate / Air Force Research Laboratory, WPAFB, Ohio, 2004.

[2]Ho, Chih-Ming and Huang, Lein-Saing, "Subharmonics and Vortex Merging in Mixing Layers" *Journal of Fluid Mechanics*, Vol. 119, 1982, pp. 443-473.

[3]Gaster, M., Kit, E., and Wygnanski, I., "Large-Scale Structures in a Forced Turbulent Mixing Layer", *Journal of Fluid Mechanics*, Vol. 150, 1985, pp. 23-39.

[4]Raman, G., Rice, E. J., and Reshotko, E., "An Experimental Study of Natural and Forced Modes in an Axisymmetric Jet", NASA TM-105225, 1991.

[5]Raman, G. and Rice, E., "Axisymmetric Jet Forced by Fundamental and Subharmonic Tones", *AIAA Journal*, Vol. 29, No.7, 1991, pp. 1114,1122.

[6]Freund, J. B. and Moin, P., "Jet Mixing Enhancement by High-Amplitude Fluidic Actuation", *AIAA Journal*, Vol. 38, No. 10, 2001, pp. 1863,1870.

[7]Wiltse, J. M, and Glezer, A., "Direct High-Frequency Excitation of Turbulence in Free Shear Flows", AIAA Paper 96-0309, *34th Aerospace Sciences Meeting,* 1996.

[8]Parekh, D. E., Cain, A. B., and Vaporean, C. N., "Characterization of Receptivity of Jet Flow Control" Final Report McDonnell Douglas Corporation, St. Louis, MO, 1997.

[9]Parekh, D. E., Kibens, V., Glezer, A., Wiltse, J. M, and Smith, D. M., "Innovative Jet Flow Control: Mixing Enhancement Experiments", AIAA Paper 96-0308, *34th Aerospace Sciences Meeting,* 1996

[10]Kibens, V., Parekh, D. E., Bingaman, D. C., Glezer, A., Mossman, M. F., and Rogers, C. B., "Innovative Jet Flow Control: Technology Transfer Process", AIAA Paper 96-0307, *34th Aerospace Sciences Meeting*, 1996

[11] Smith, D. M., Dorris, J. and Fields, R. "Active Core Exhaust (ACE) Control" Flight Dynamics Directorate, Wright Laboratory, WPAFB Ohio, 1998.

[12] Kinsler, L. E., Frey, A.R., et al. *Fundamentals of Acoustics*, John Wiley & Sons, 3rd Edition New York, 1982.

[13] Munjal, M. L. *Acoustics of Ducts and Mufflers (with Application to Exhaust and Ventilation System Design)* John Wiley & Sons, New York, 1987.

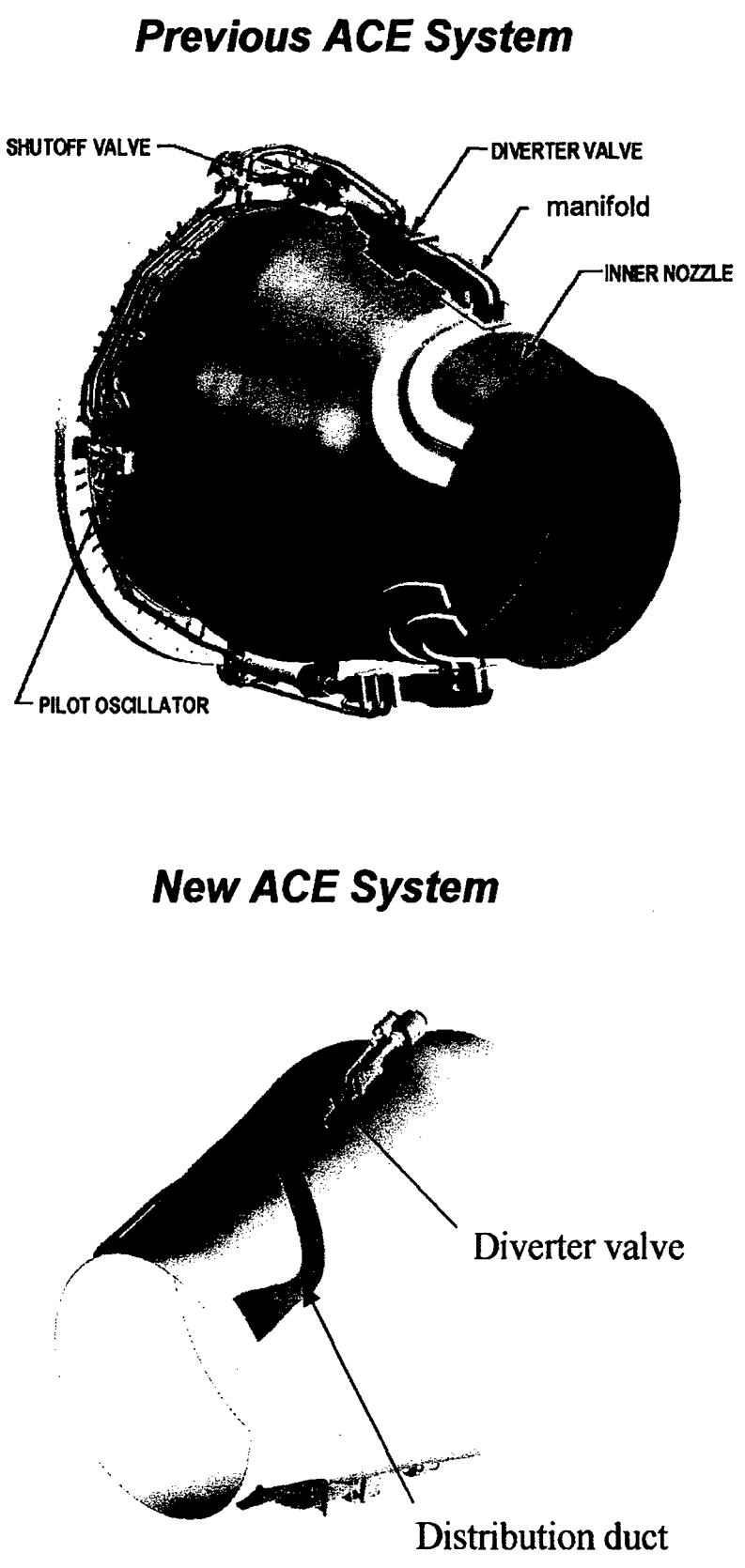

Figure 2.1 Schematic of old and new ACE system integrated with a PW F117 core nozzle.

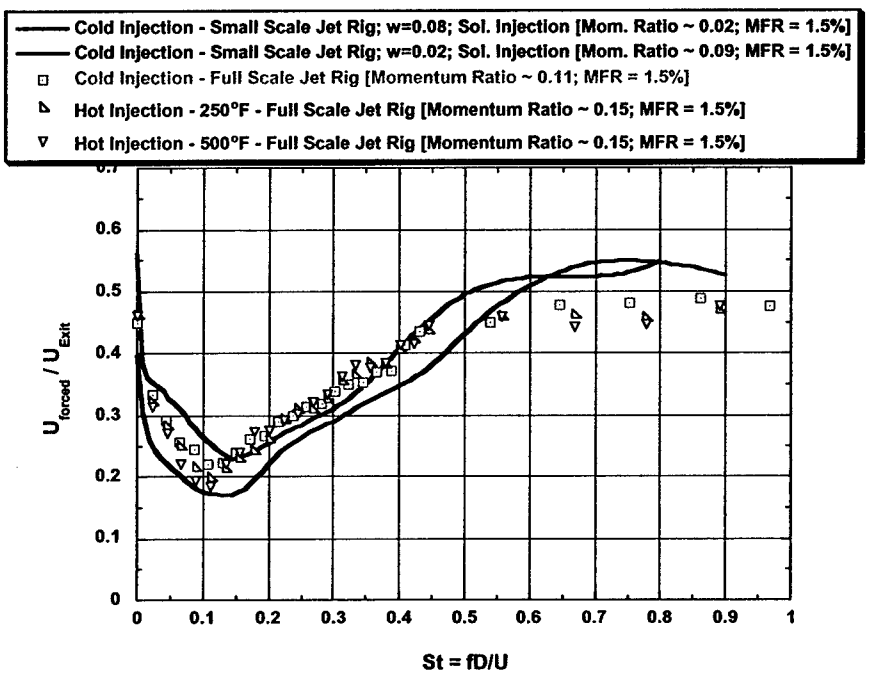

Figure 2.2. Mixing effectiveness as a function of non-dimensional frequency for small and large scale jet mixing experiments.

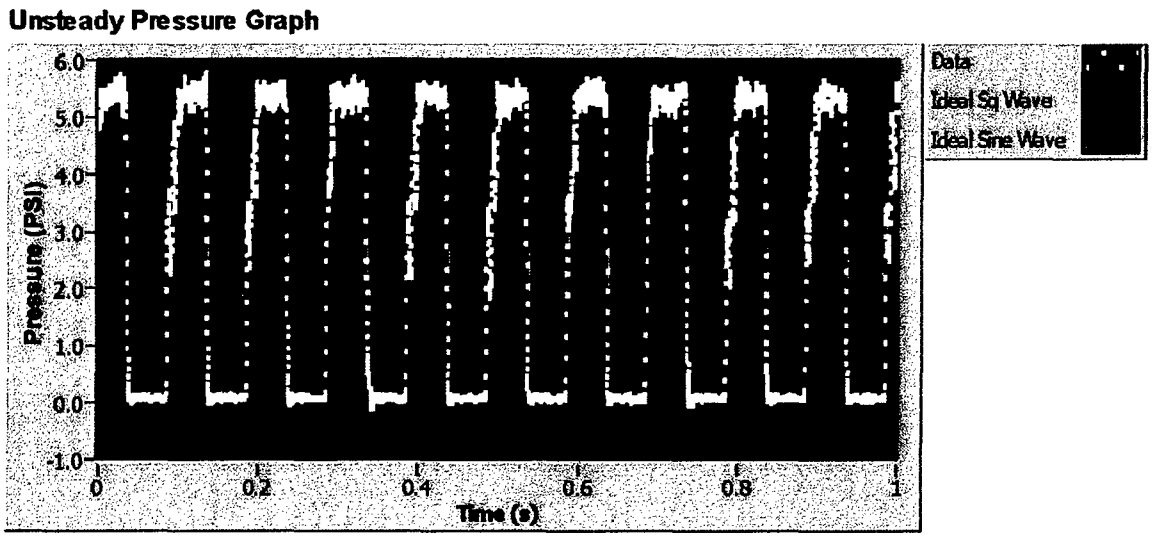

Figure 2.3. Example of a measured pulse that is of good quality.

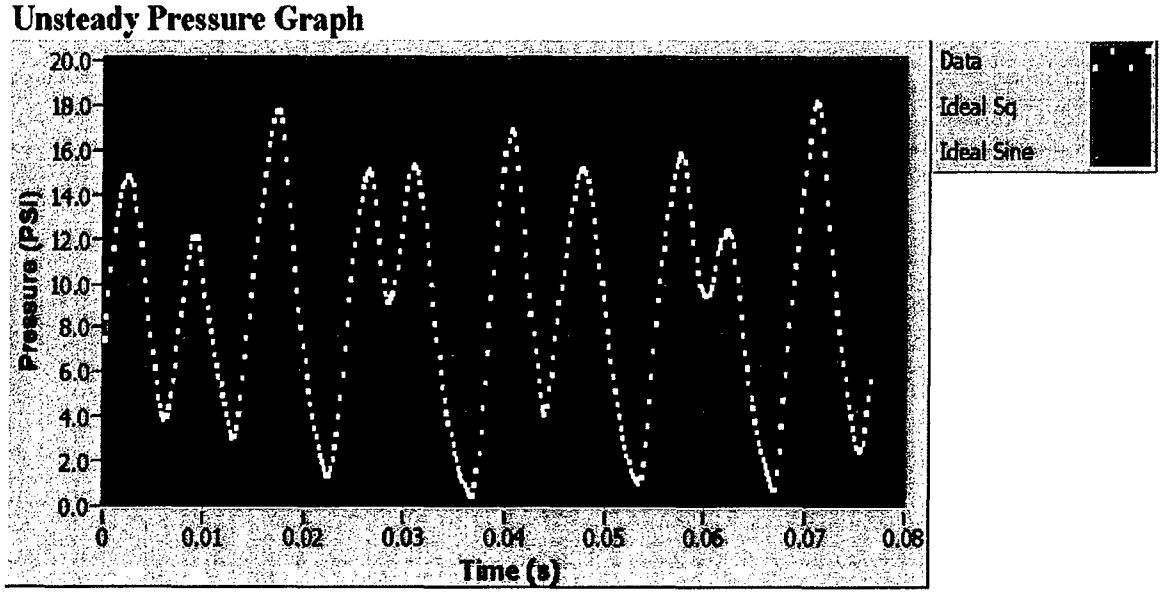

Figure 2.4. Example of a measured pulse that is of poor quality.

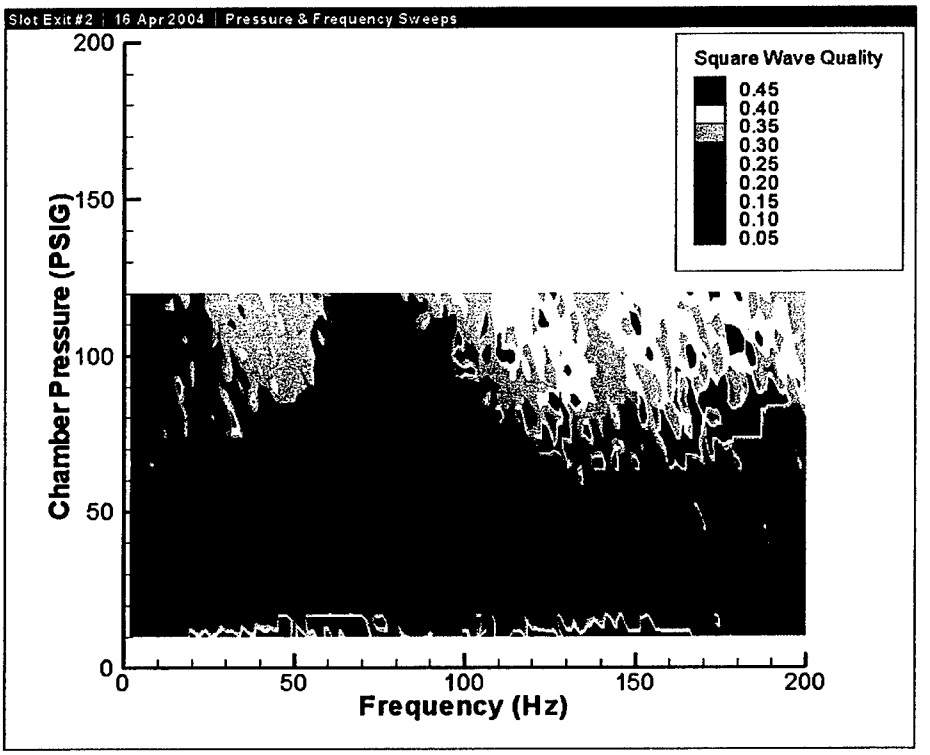

Figure 2.5. Example of square wave contour map in pressure-frequency domain.

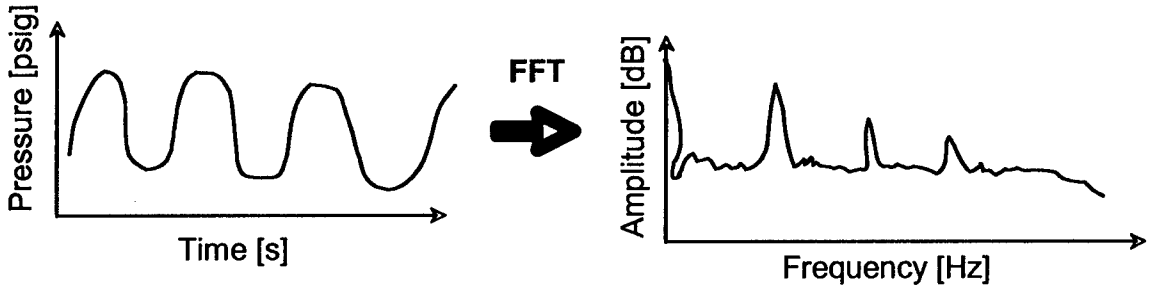

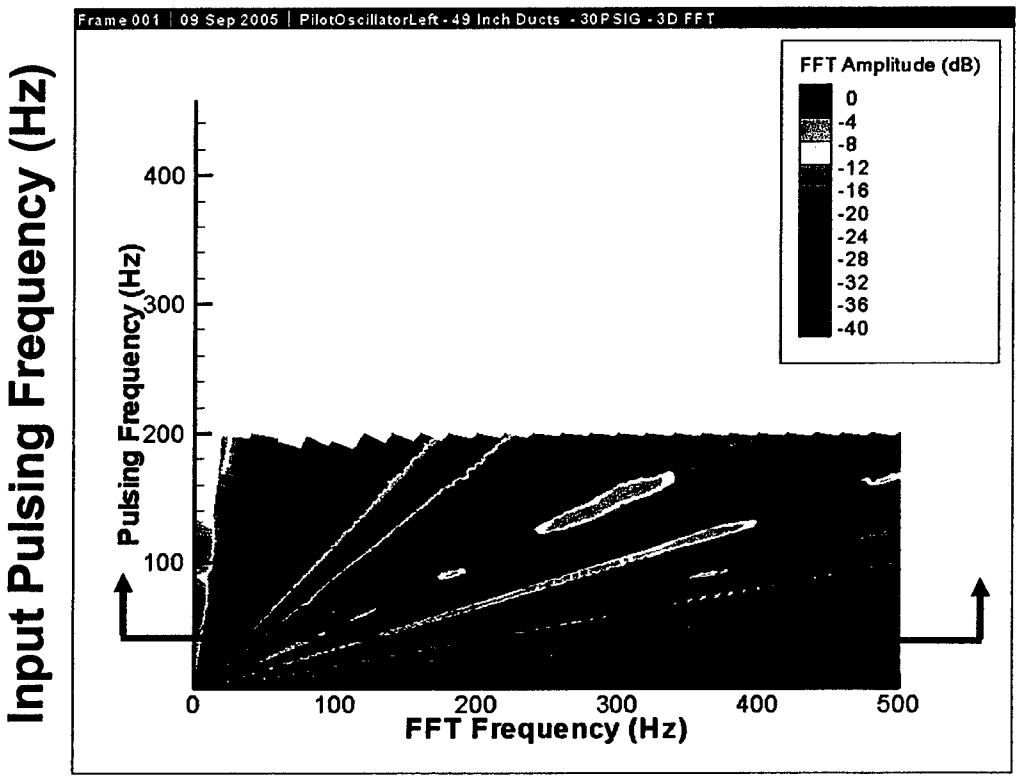

Figure 2.6. Example of peak frequency contour map: input frequency vs. measured output frequency.

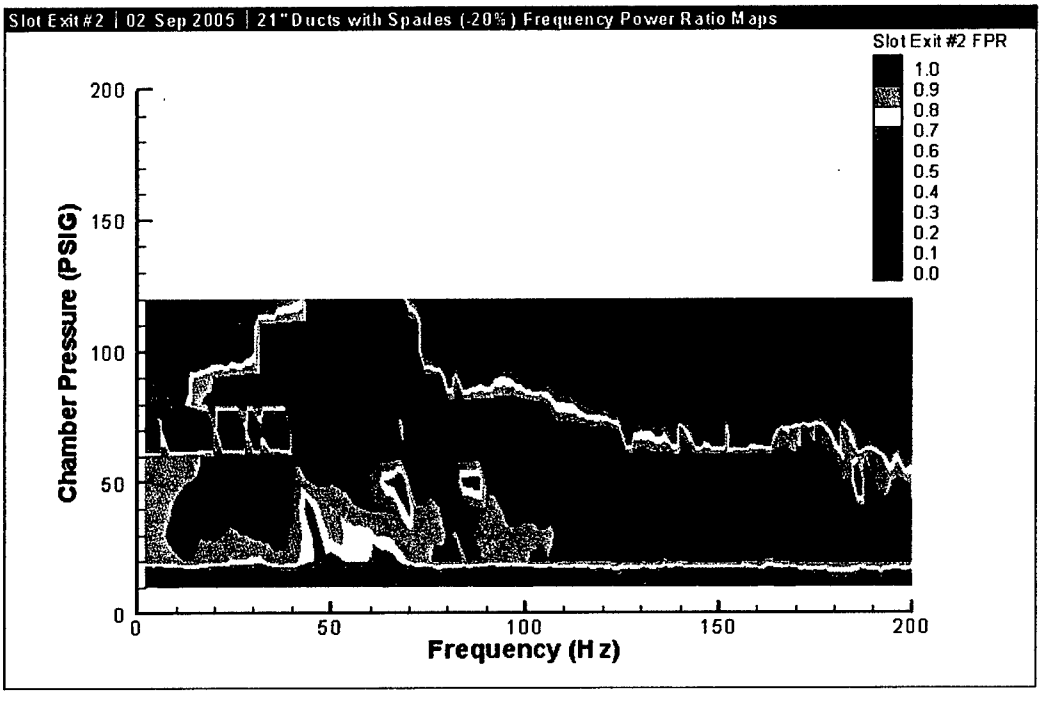

Figure 2.7. Example of frequency power ratio plot: power at output frequency relative to the power of the whole spectrum.

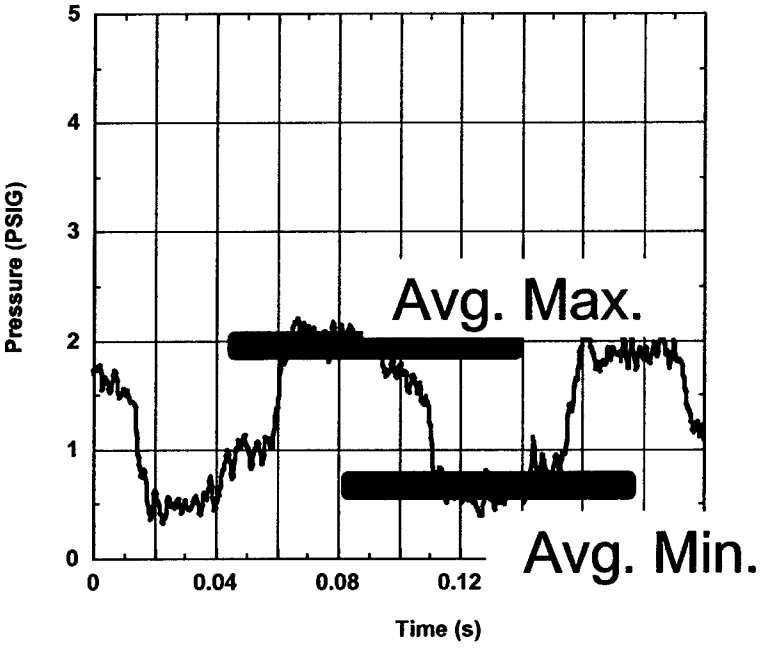

Figure 2.8. Determination of average maximum and minimum of pressure pulse as part of criteria for diverter valve switching.

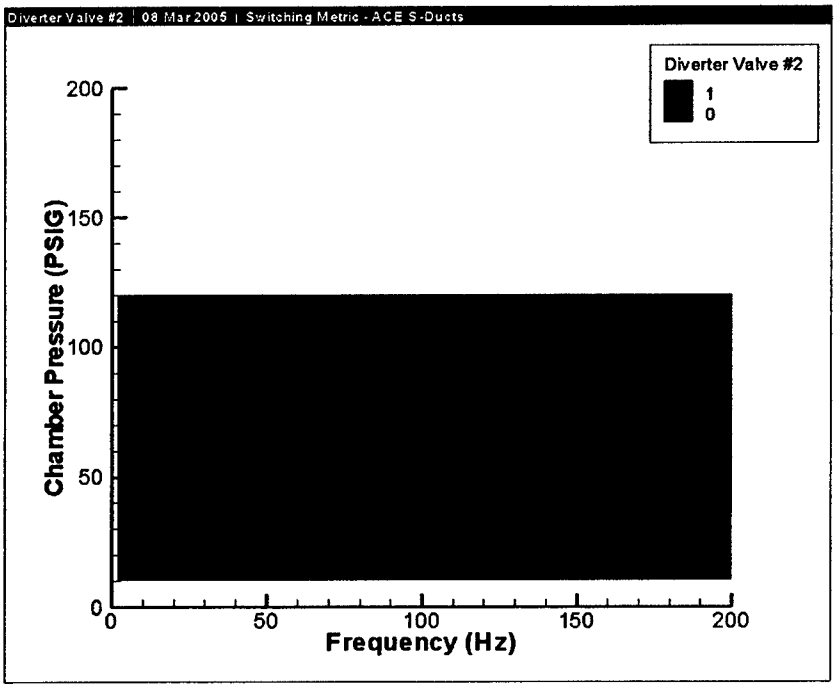

Figure 2.9. Example of switching contour plot; green regions indicate successful switching and quality of pulse from system.

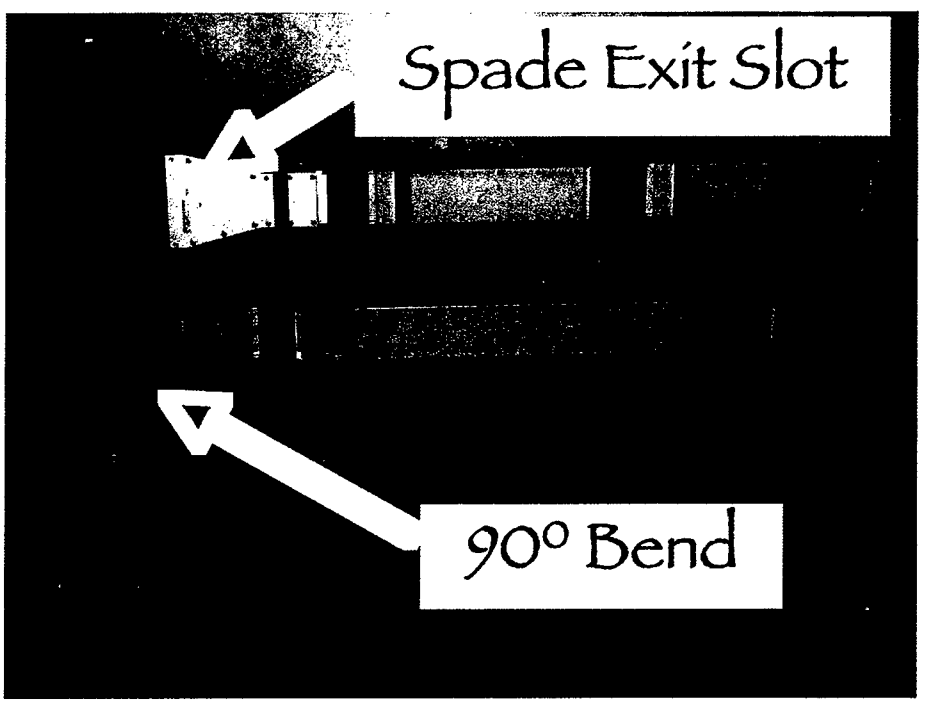

Figure 2.10. Modular distribution duct test hardware.

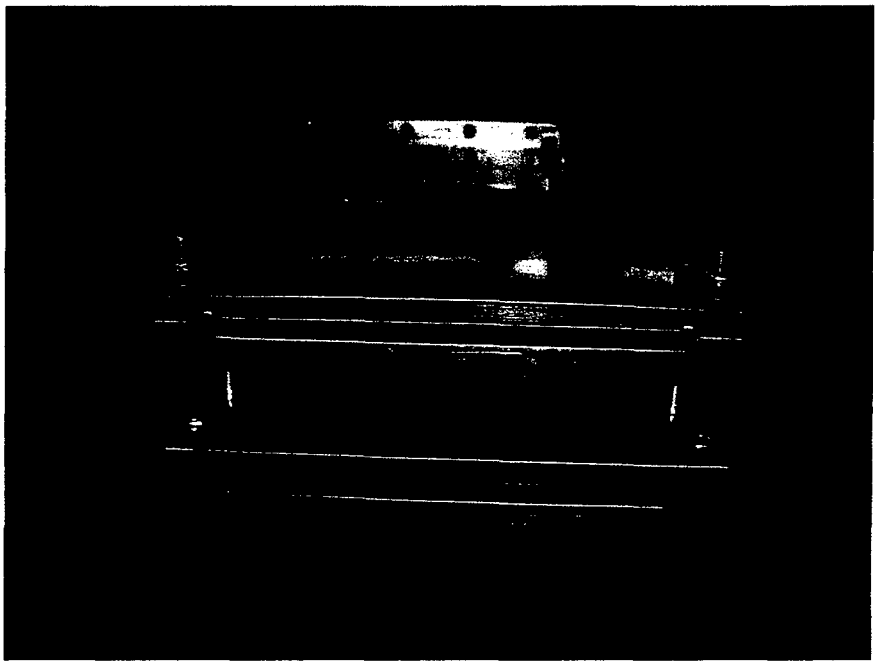

Figure 2.11 Adjustable slot exit height of spade hardware.

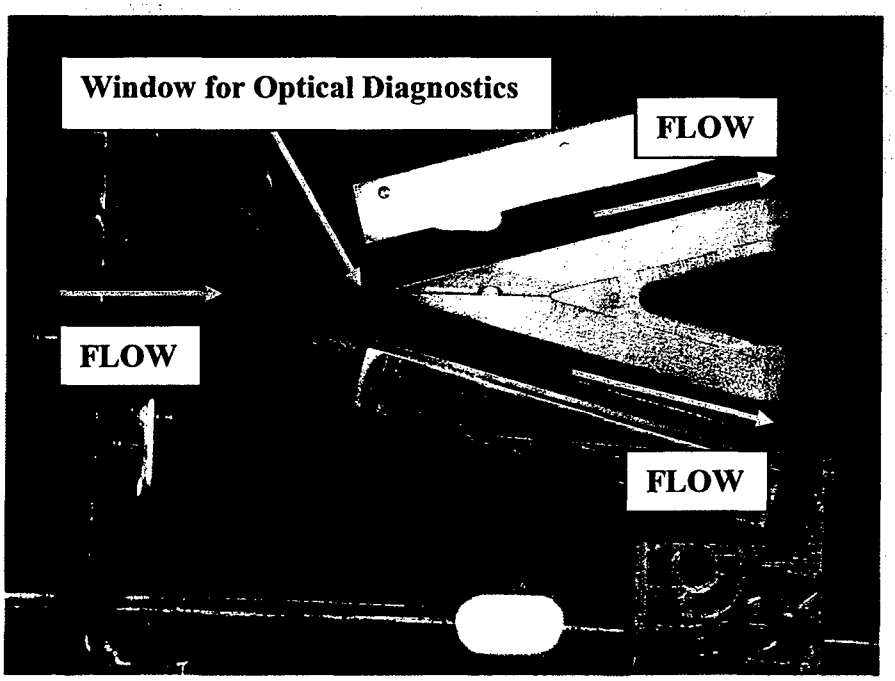

Figure 2.12 "Optical Diverter Valve" test hardware.

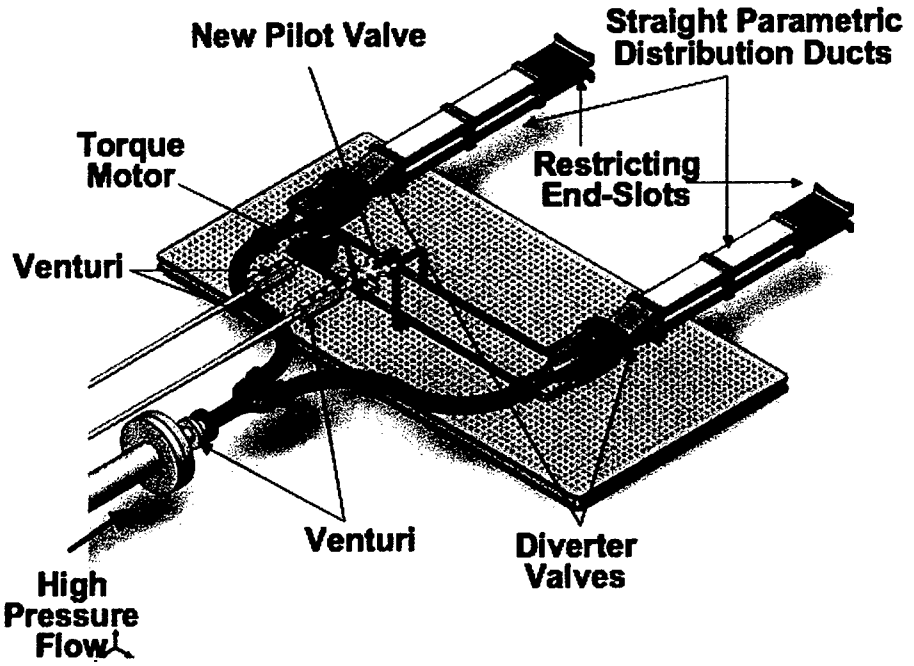

Figure 3.1 Schematic of ACE bench test rig.

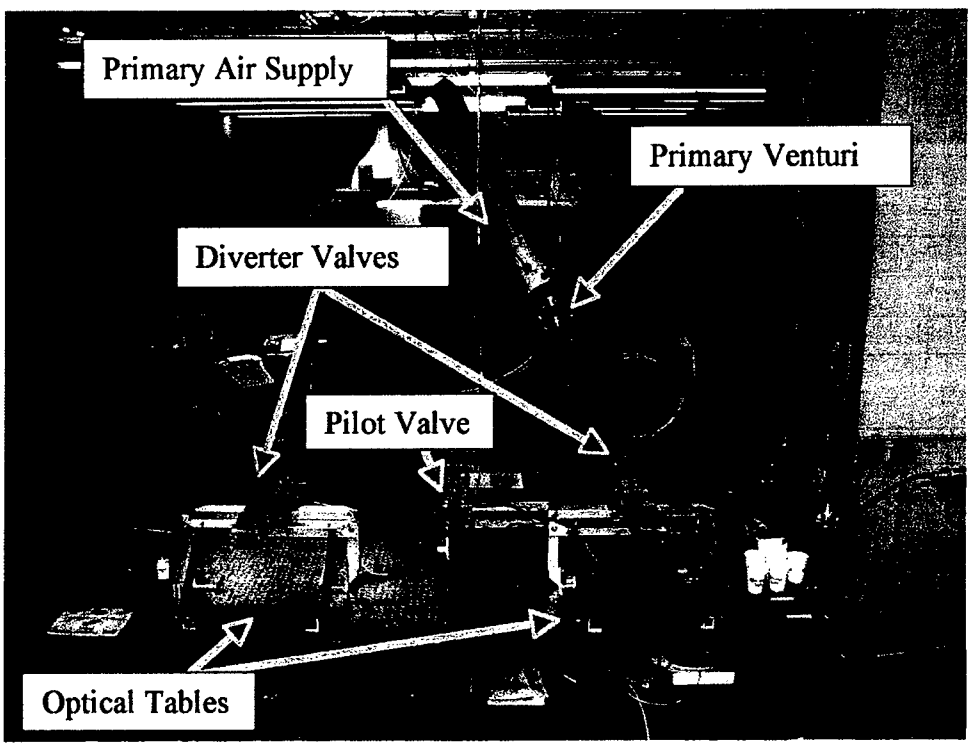

Figure 3.2 Actual bench test rig for ACE system at GTRI laboratories.

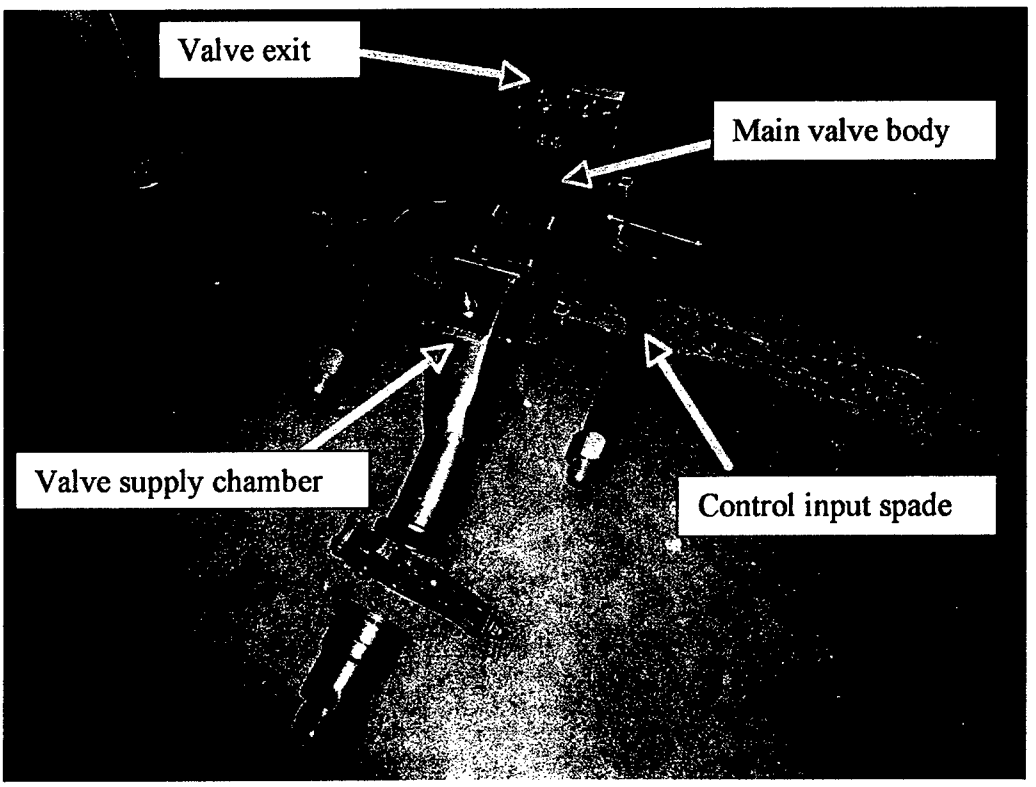

Figure 3.3 "Exploded" view of diverter valve components.

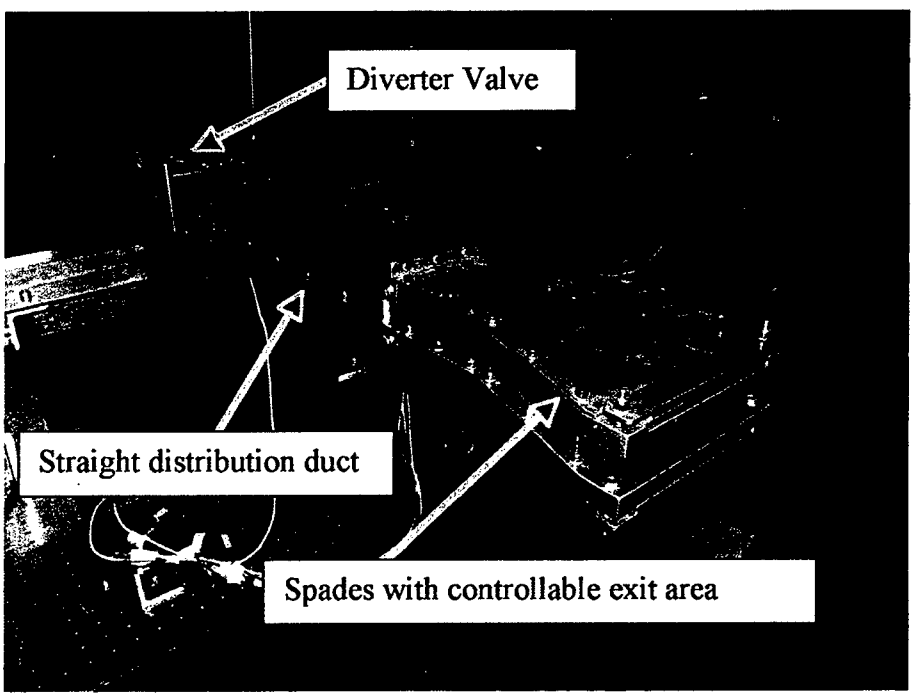

Figure 3.4 Medium length distribution ducts with exit spades installed in the test rig.

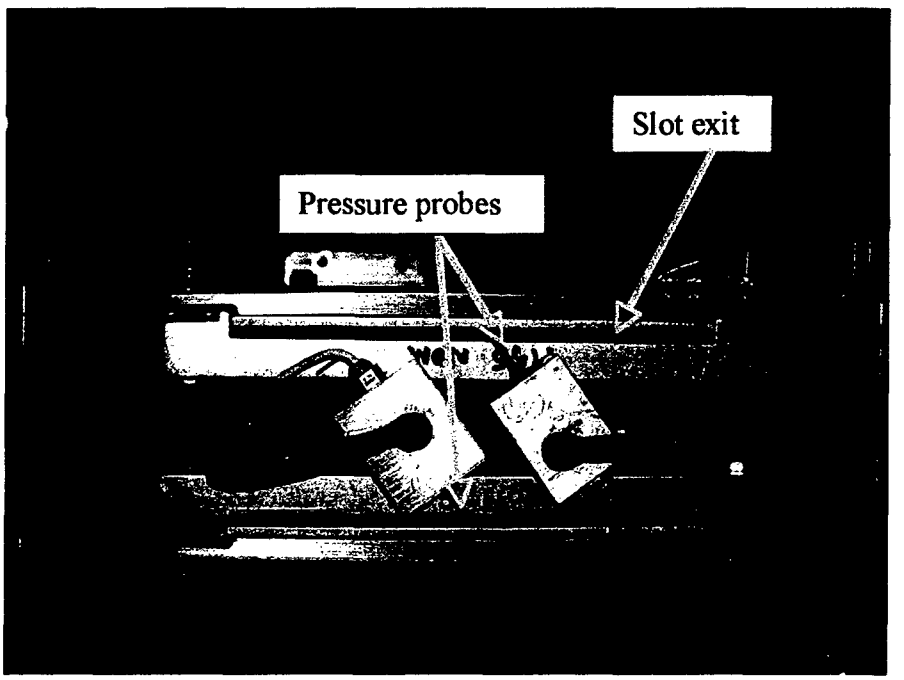

Figure 3.5 Total pressure probes at spade exit slot. Probes were attached to Endevco pressure transducers and placed in center of slot.

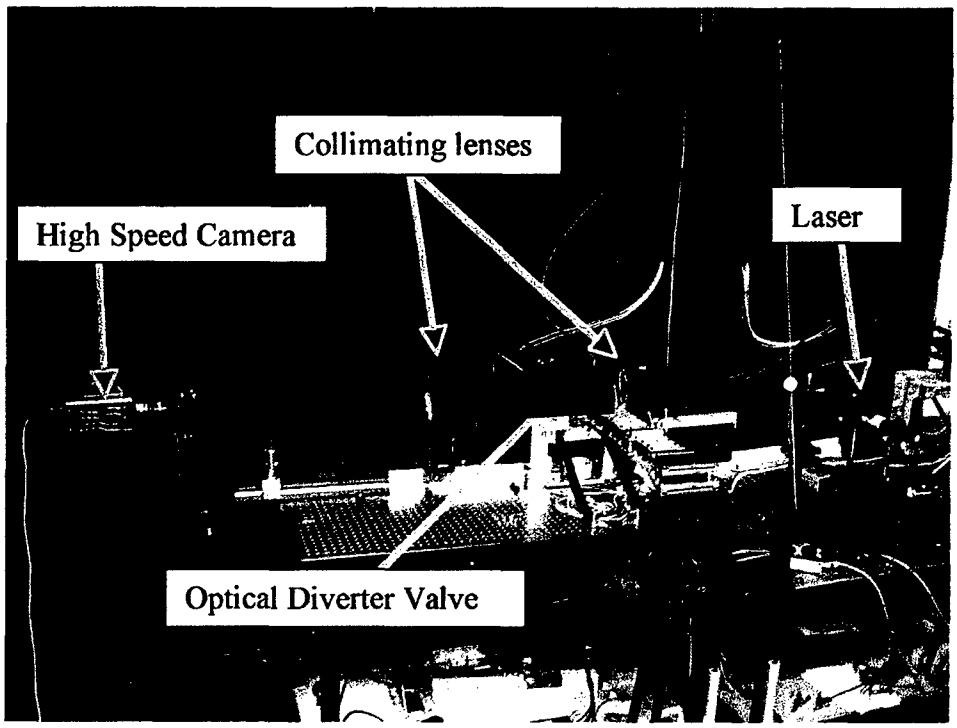

a)

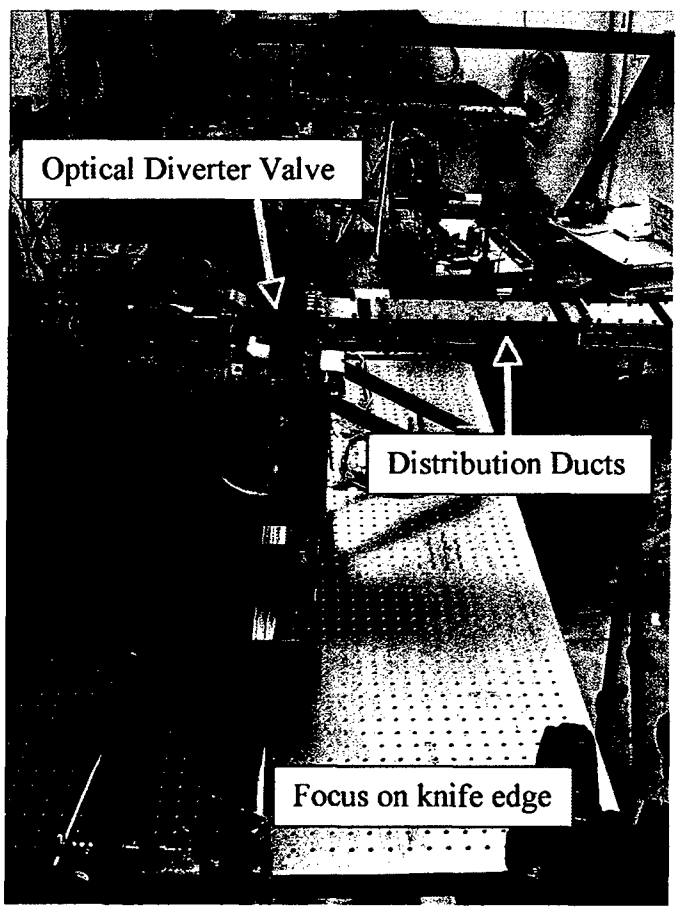

b)

Figure 3.6 Optical test set up for schlieren imaging of diverter valve internal flow.

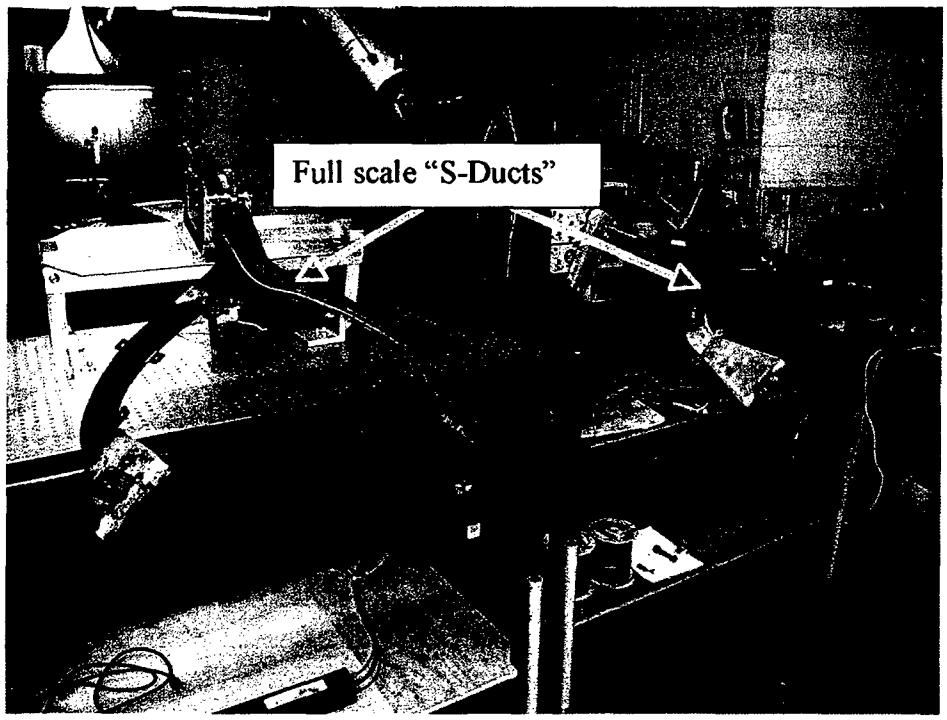

Figure 4.1 Original full scale "S-Ducts" ACE configuration set up on bench rig.

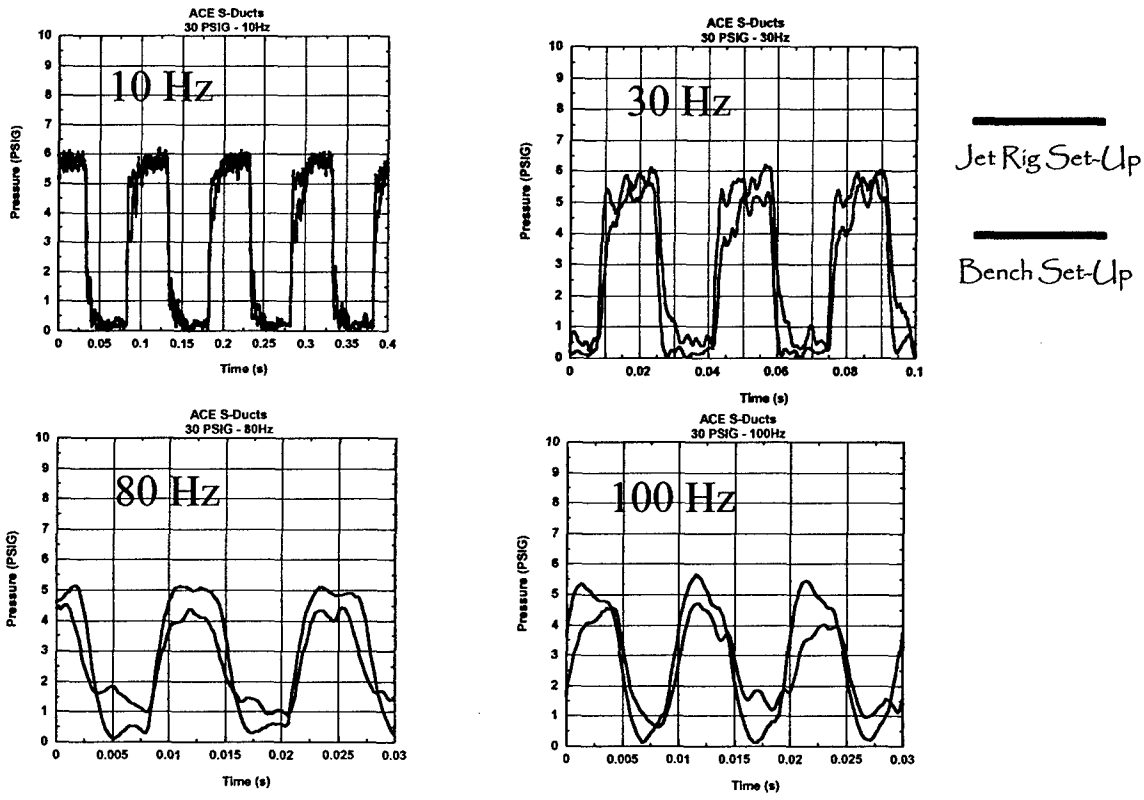

Figure 4.2 Comparison between ACE system output on jet rig vs. bench set-up.

f_{input} = 10 Hz

Short Duct
[L = 12 inches]

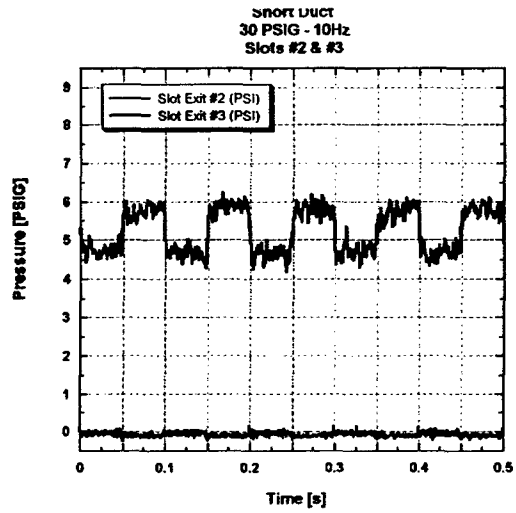

Slot Exit #2

Slot Exit #3

Medium Duct
[L = 21 inches]

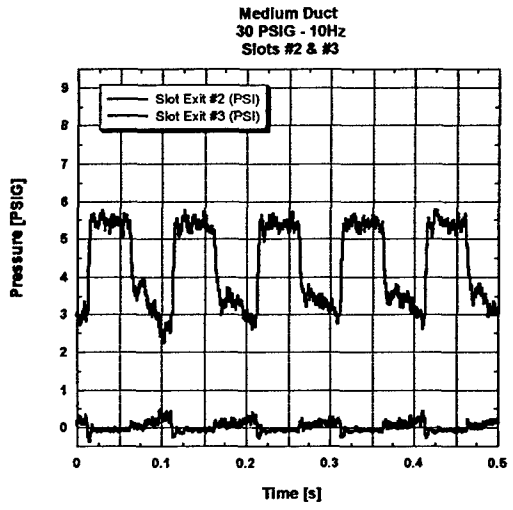

Long Duct
[L = 49 inches]

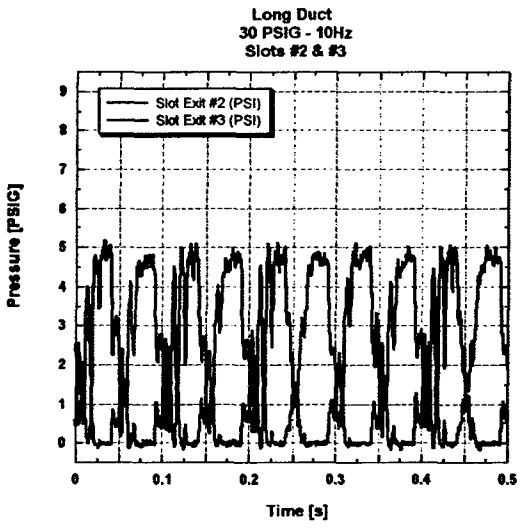

Figure 4.3 Effect of duct length on slot exit pulse; f_{input} = 10 Hz; P_{ch} = 30 psig.

Short Duct
[L = 12 inches]

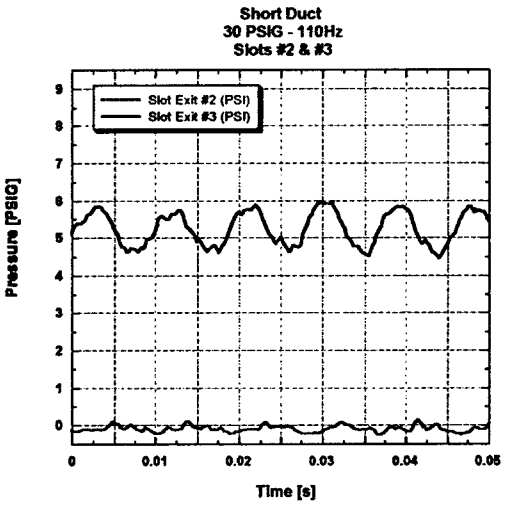

Slot Exit #2

Slot Exit #3

Medium Duct
[L = 21 inches]

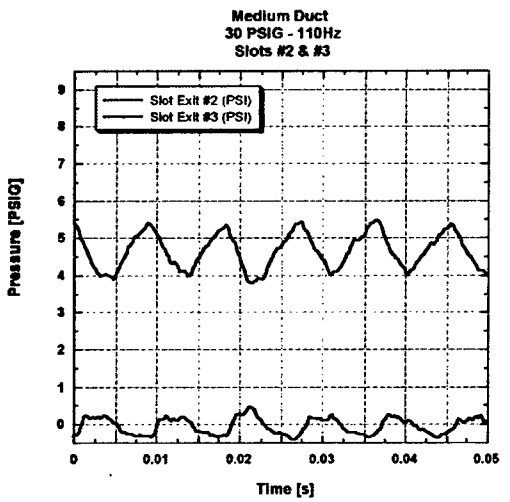

Long Duct
[L = 49 inches]

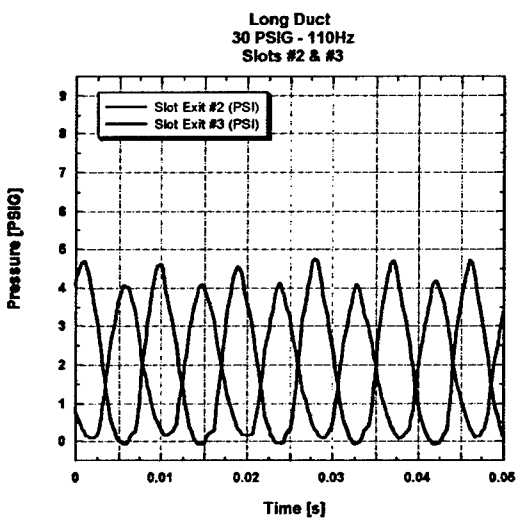

Figure 4.4 Effect of duct length on slot exit pulse; f_{input} = 100 Hz; P_{ch} = 30 psig.

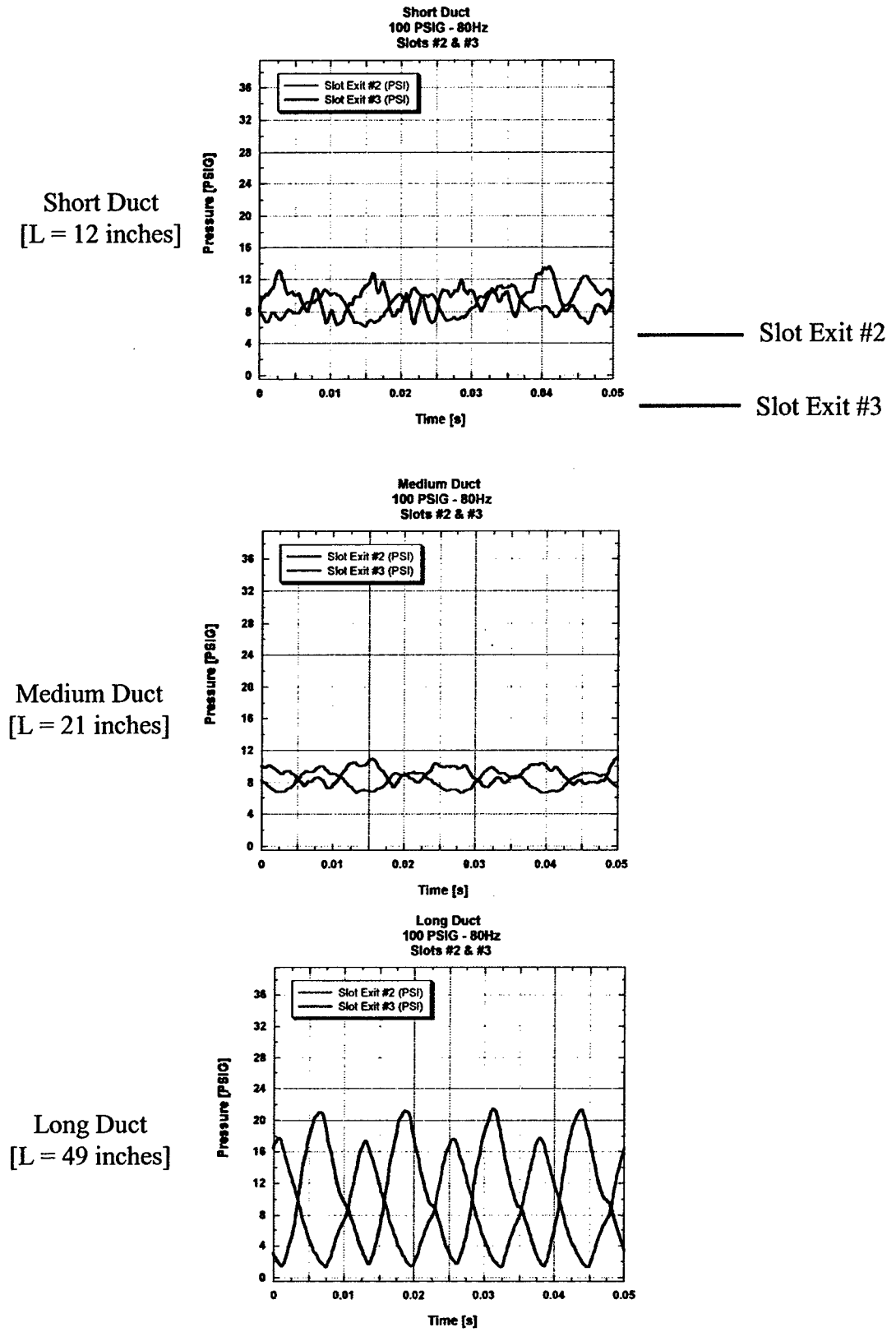

Figure 4.5 Effect of duct length on slot exit pulse; f_{input} = 80 Hz; P_{ch} = 100 psig.

Pilot Valve

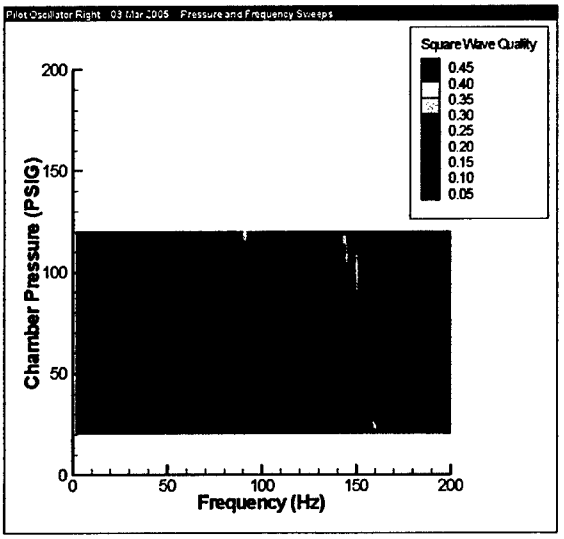

Diverter Valve #2

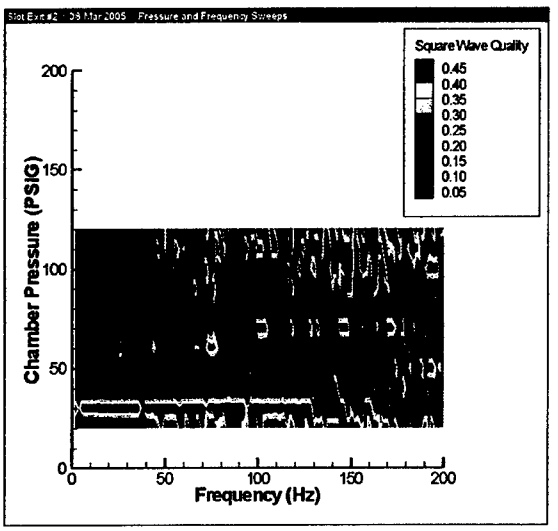

Short Duct

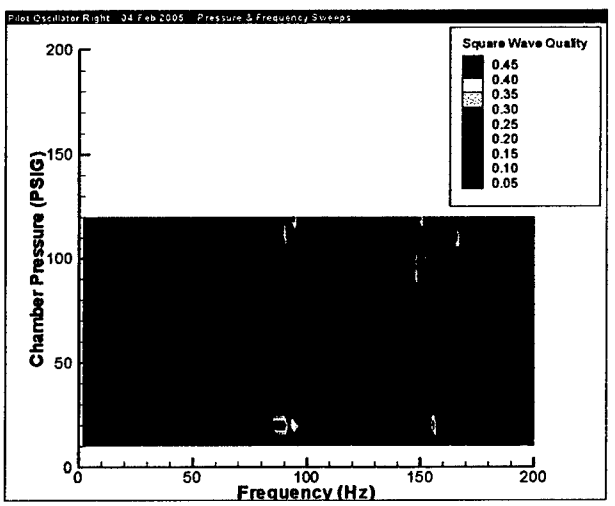

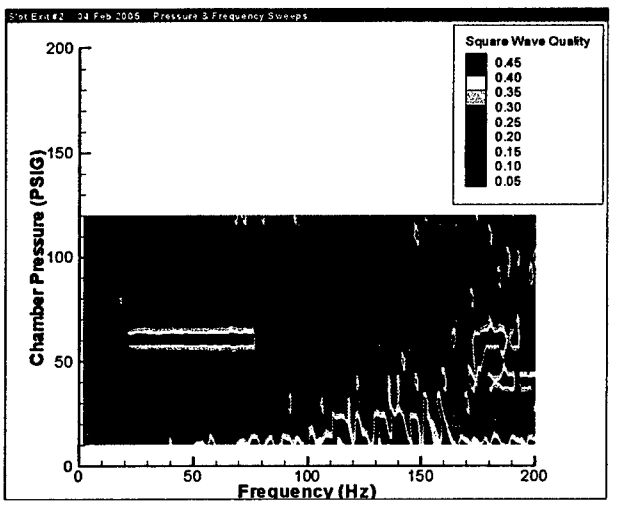

Medium Duct

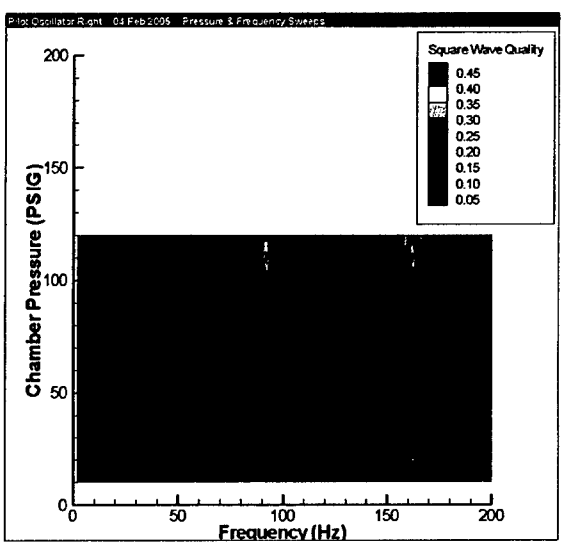

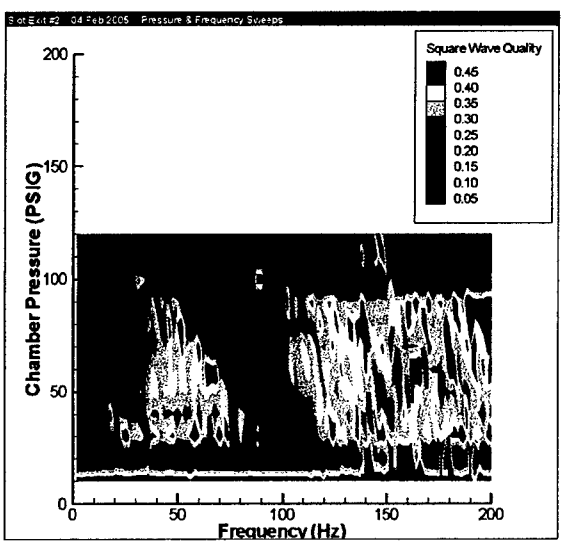

Long Duct

Figure 4.6 Comparison of square wave quality as a function of duct length; NO SPADES.

Pilot Valve

Diverter Valve #2

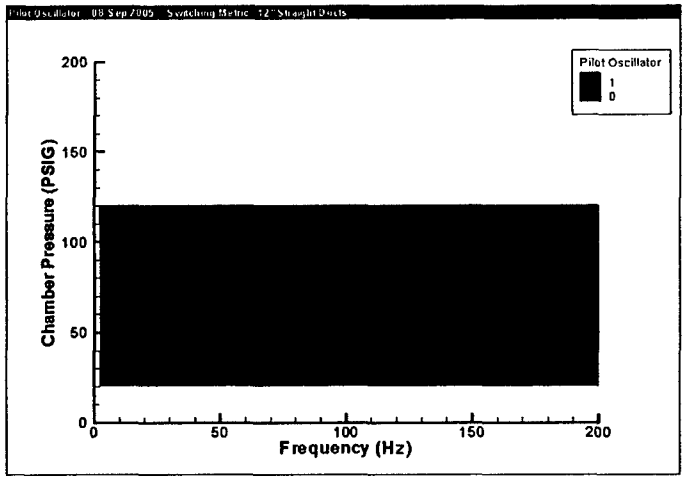

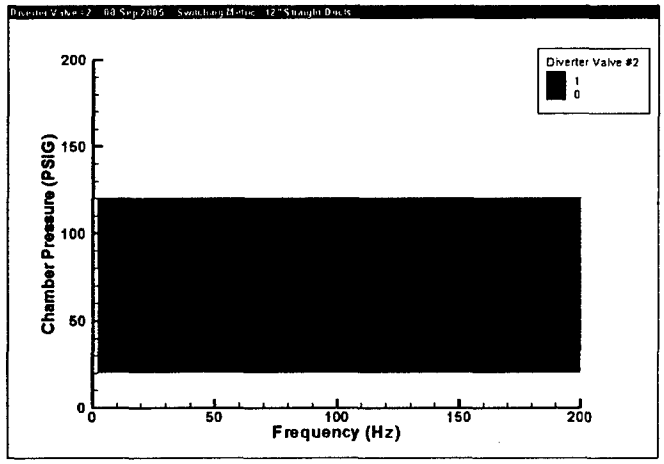

Short Duct

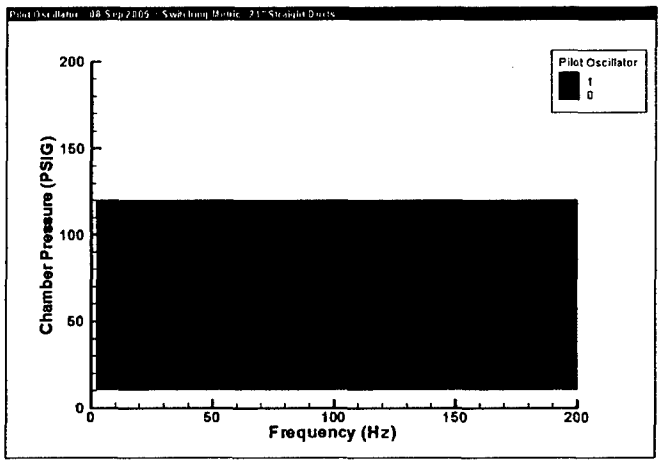

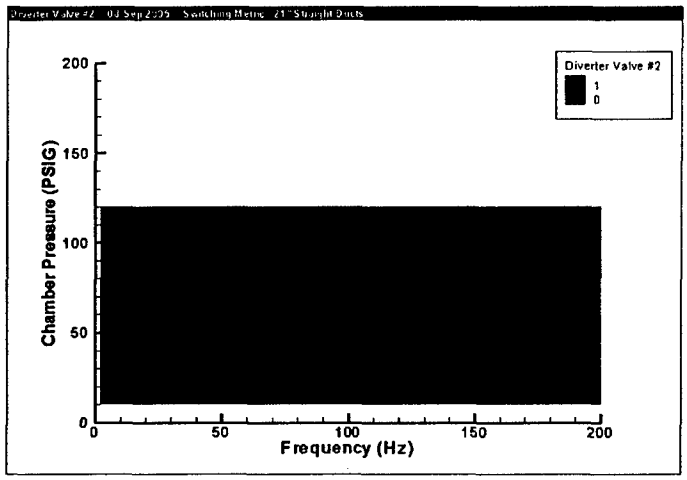

Medium Duct

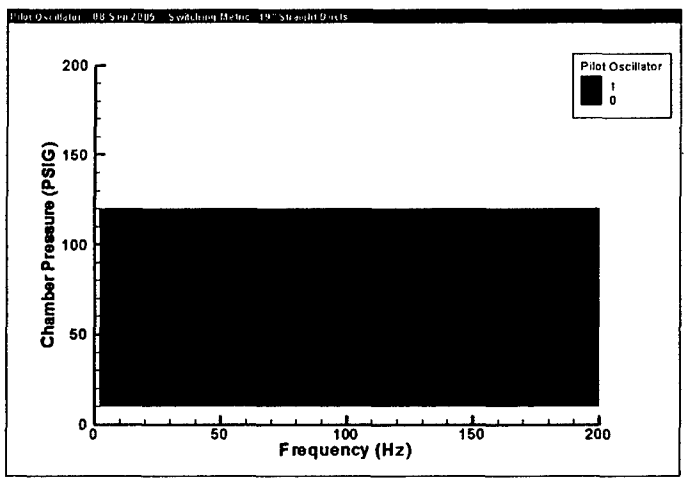

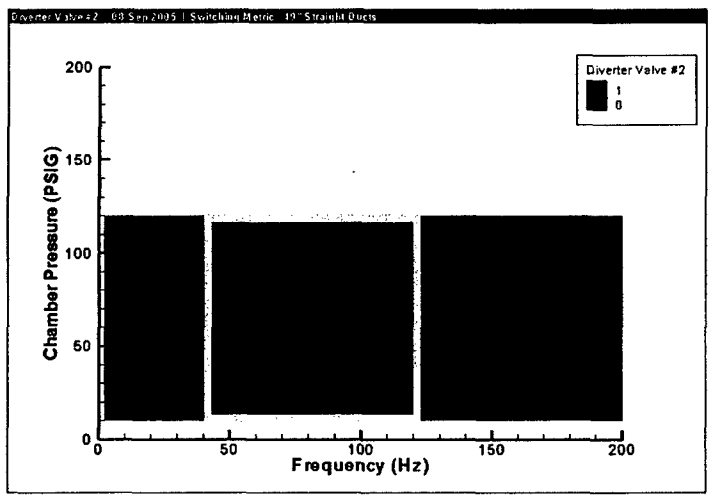

Long Duct

Figure 4.7 Effect of duct length on switching parameter; NO SPADES.

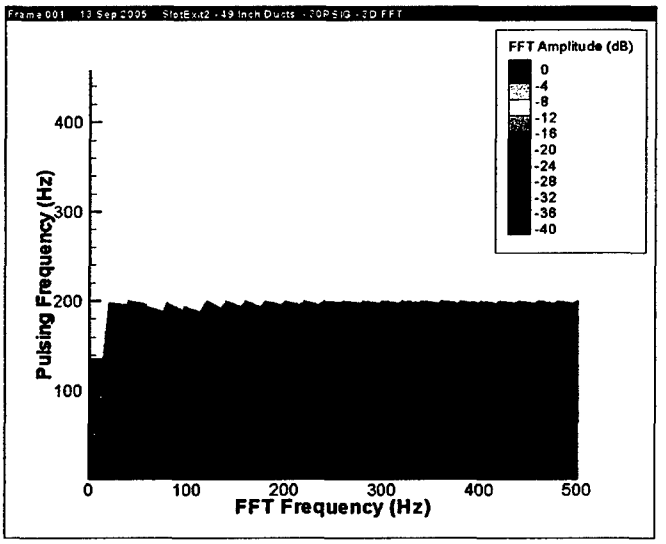

Short Duct

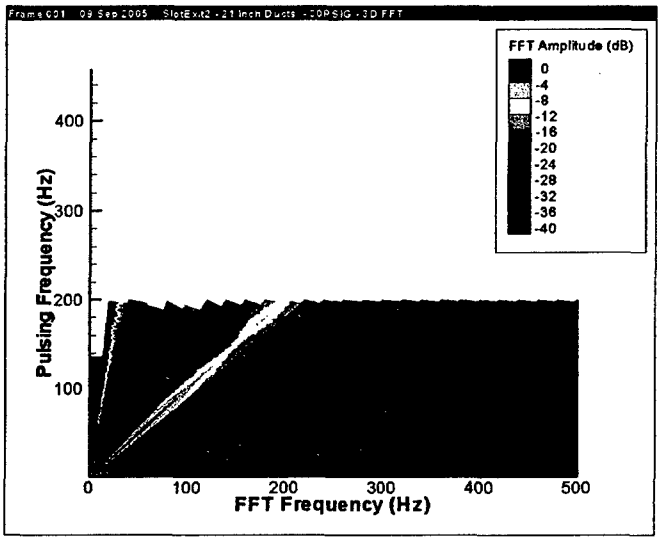

Medium Duct

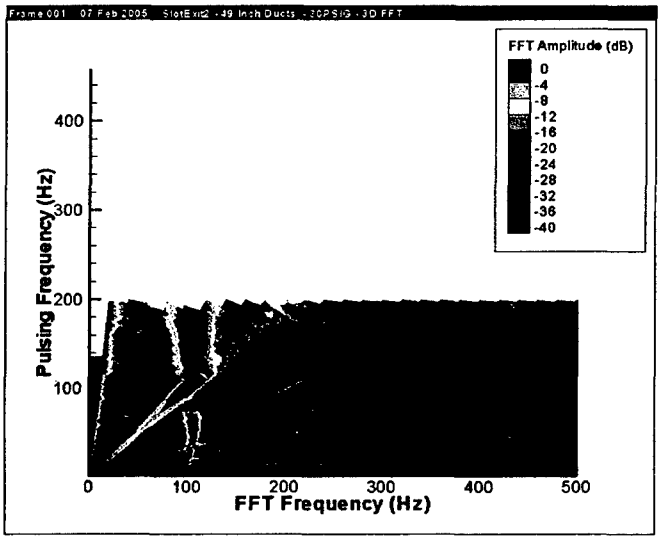

Long Duct

Figure 4.8 Input/ frequency versus output peak frequency of system as function of duct length.; P_{ch} = 30 psig

FFT Contours at P_{ch} = 30 psig

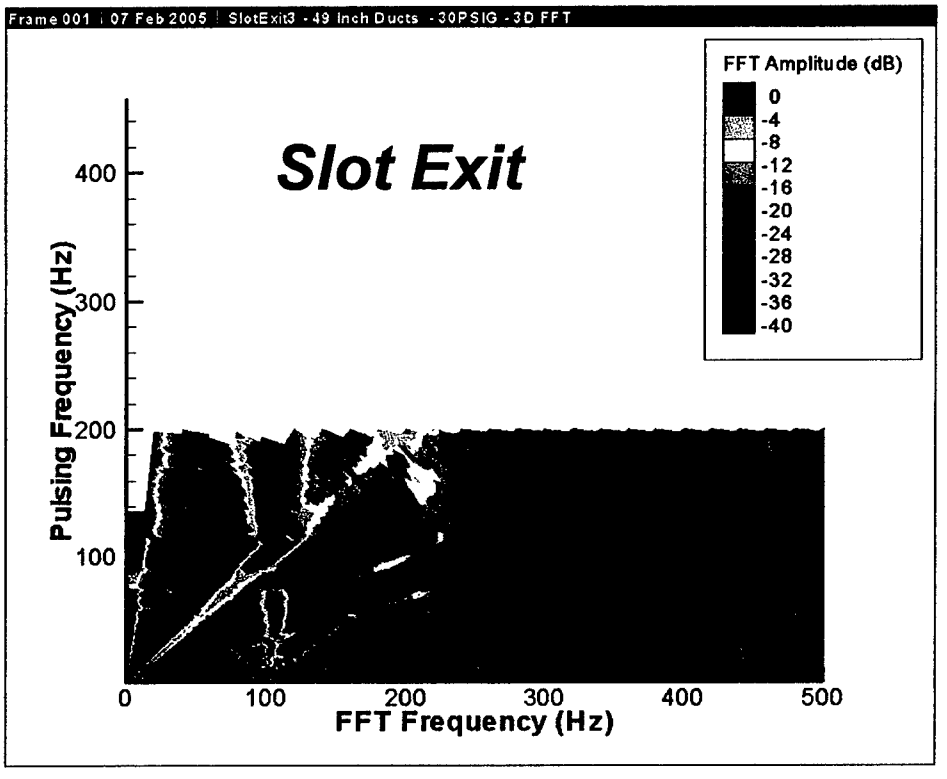

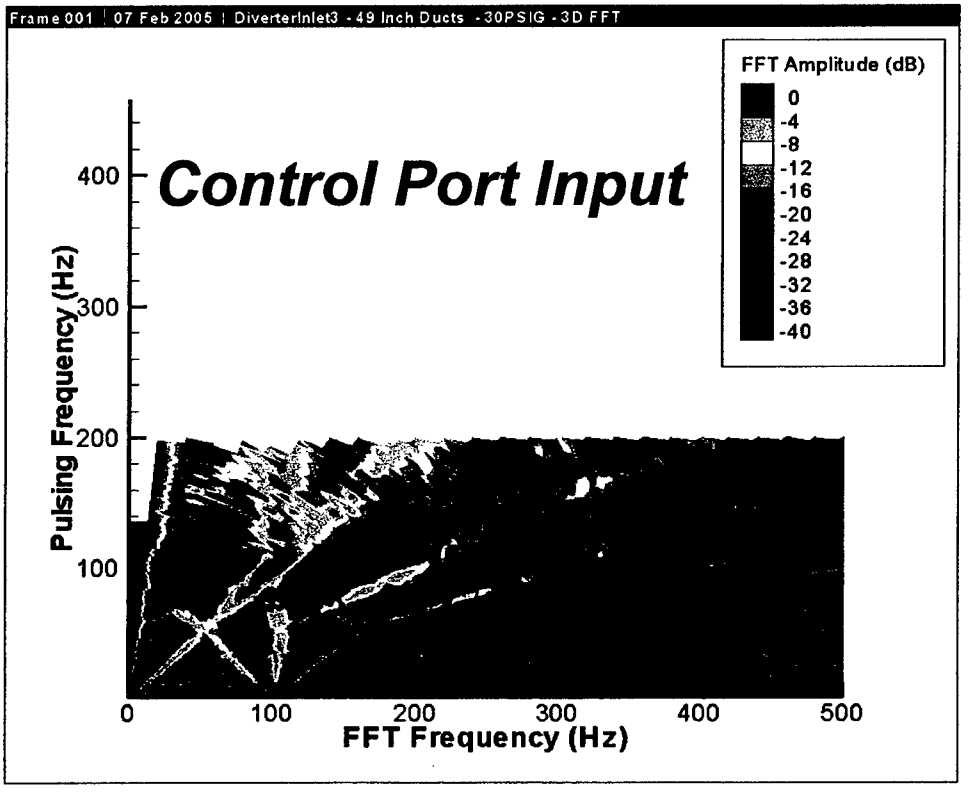

Figure 4.9 Slot exit and control port input peak frequency contours. Evidence of "lock on" frequency is observed in both cases; P_{ch} = 30 psig.

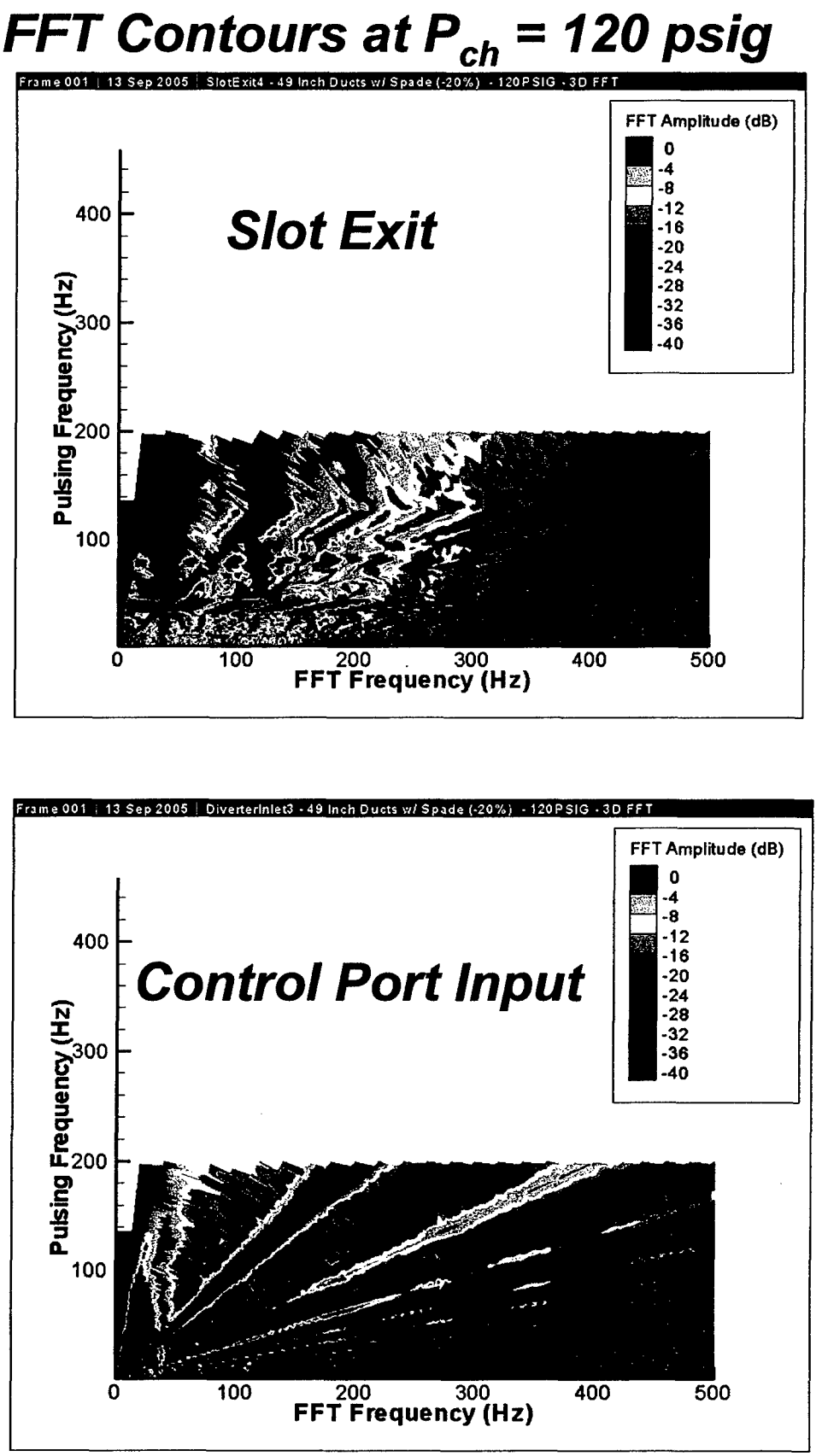

Figure 4.10 Slot exit and control port input peak frequency contours. Evidence of "lock on" frequency is observed in both cases; P_{ch} = 120 psig.

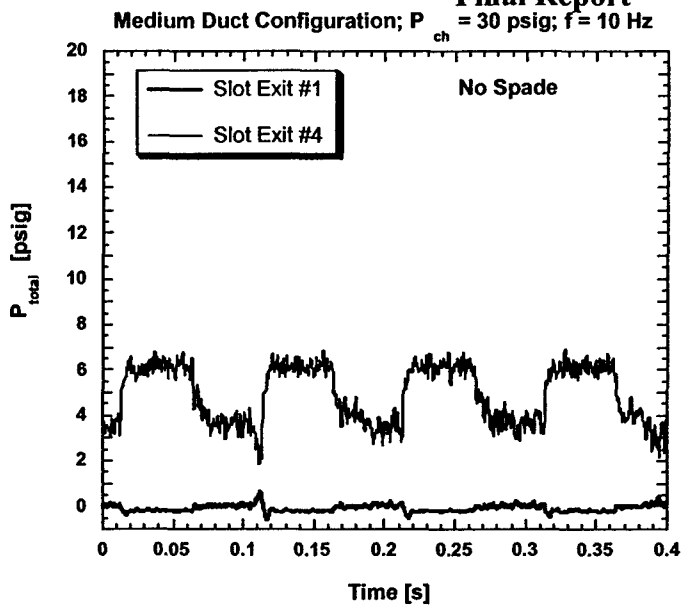

No Spade; +4% of nom. area
L = 21"

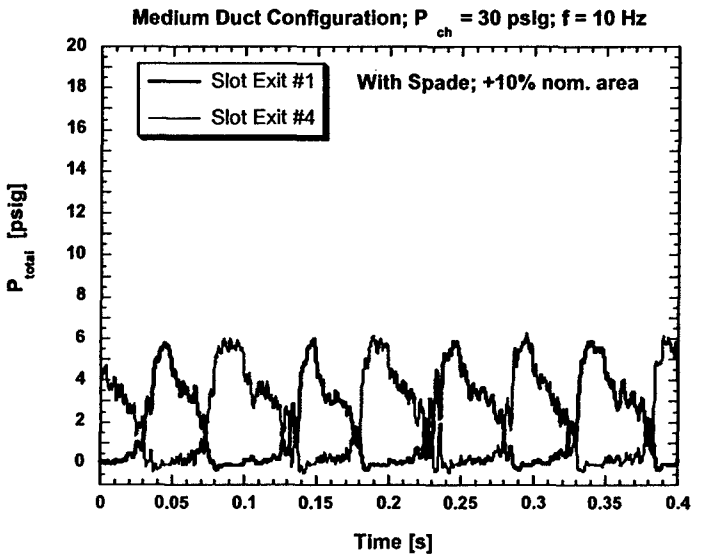

With Spade; +10% of nom. area
L = 32"

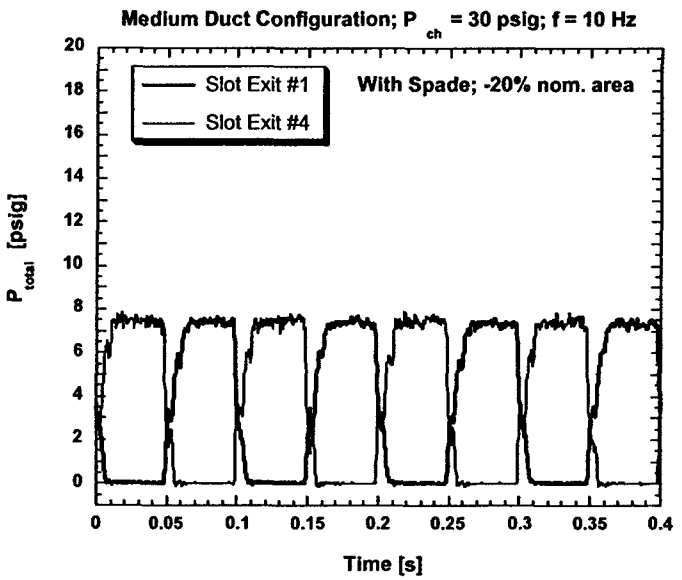

With Spade; -20% of nom. area
L = 32"

Figure 4.11 Effect of exit area and spade on system delivered pulse; P_{ch} = 30 psig; f = 10 Hz.

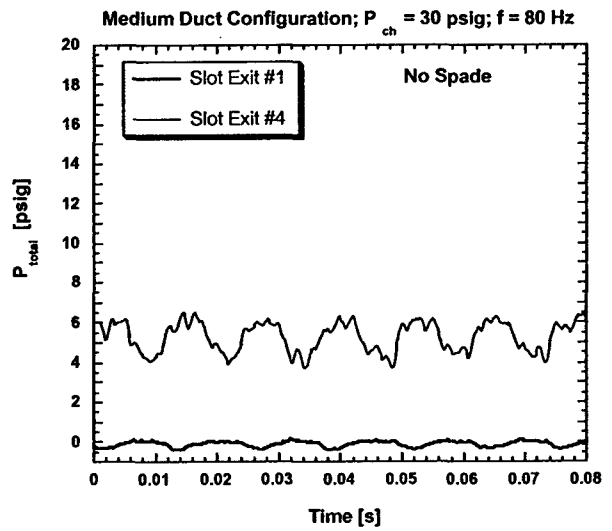

No Spade; +4% of nom. area
L = 21"

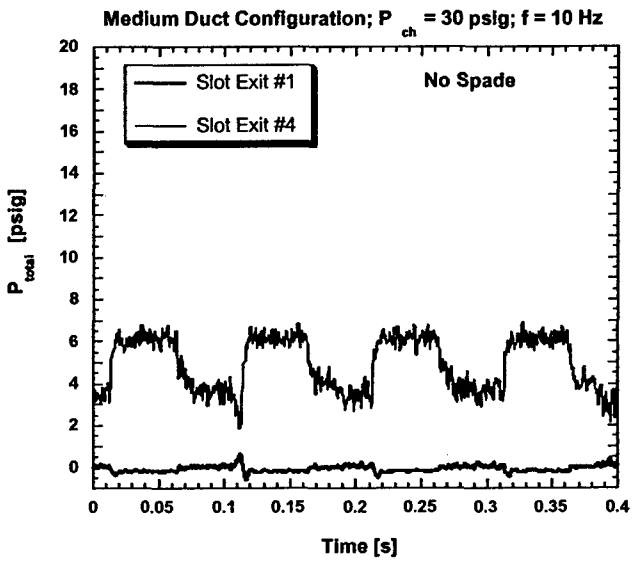

With Spade; +10% of nom. area
L = 32"

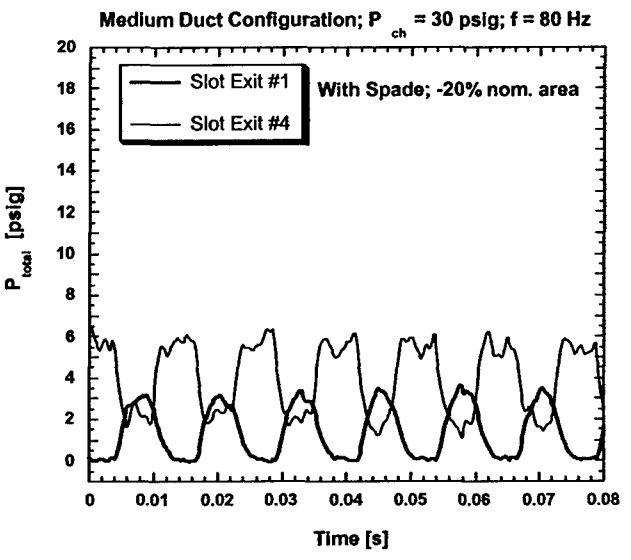

With Spade; -20% of nom. area
L = 32"

Figure 4.12 Effect of exit area and spade on system delivered pulse; P_{ch} = 30 psig; f = 80 Hz.

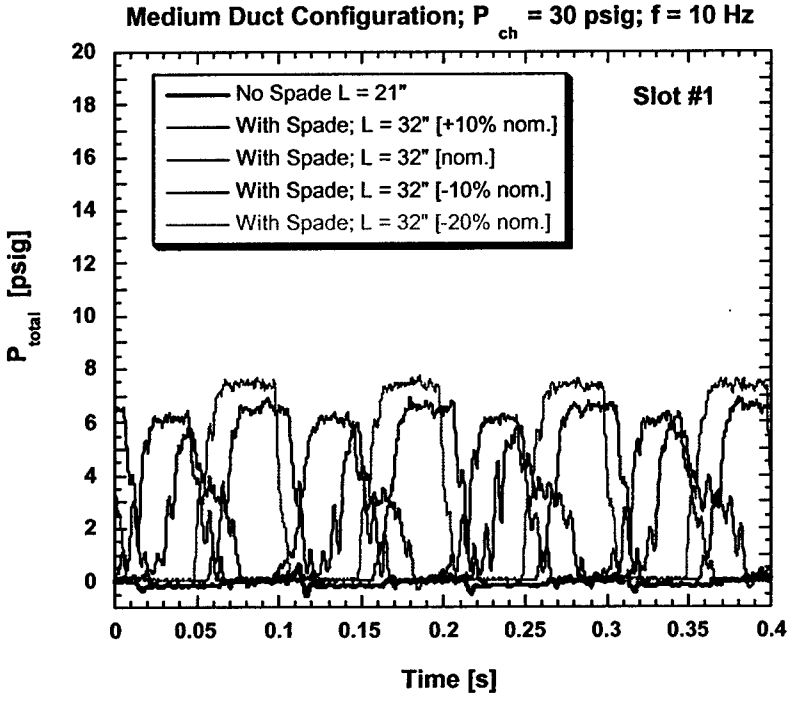

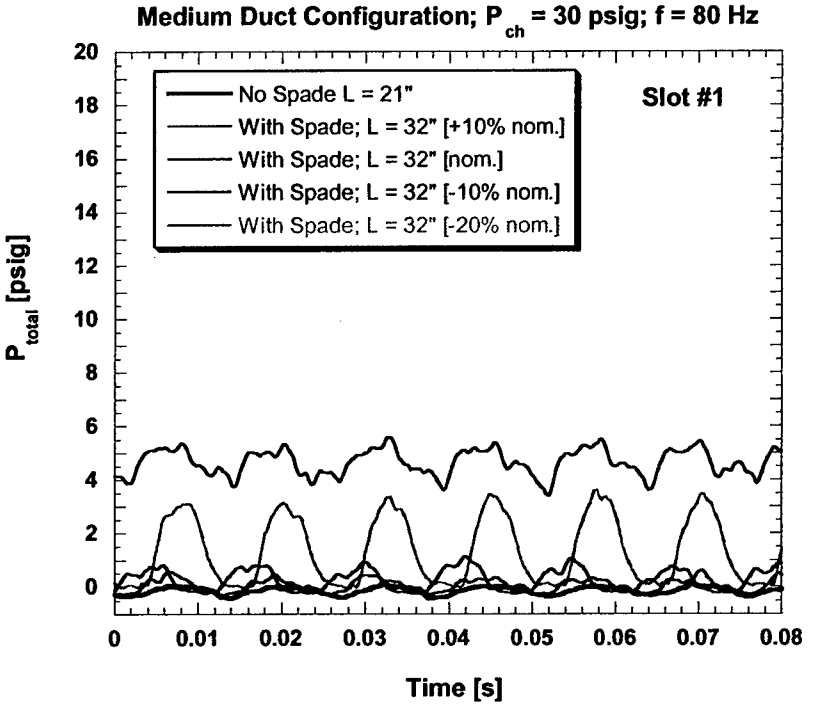

Figure 4.13 Progression of improving pulse quality with increasing inlet to exit area ratio; P_{ch} = 30 psig.

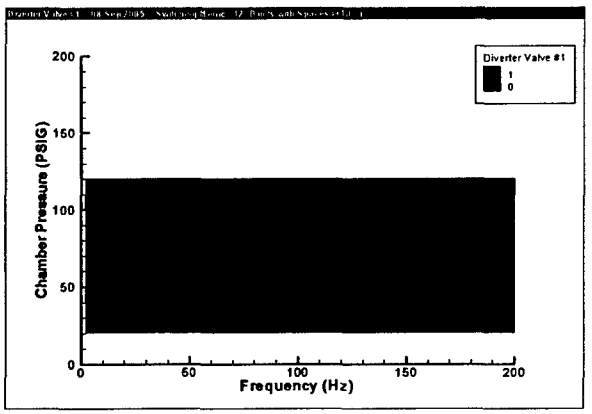

Exit Area at +10% of Nominal

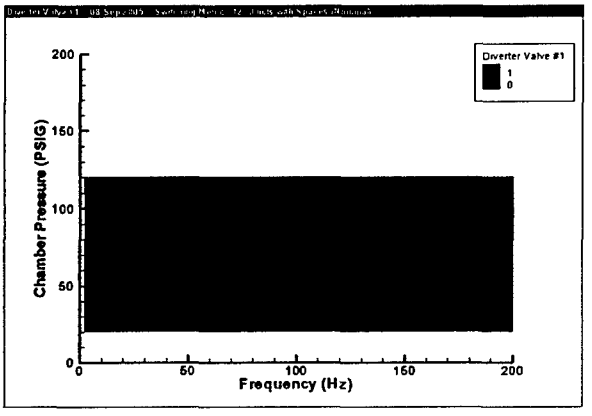

Exit Area at Nominal

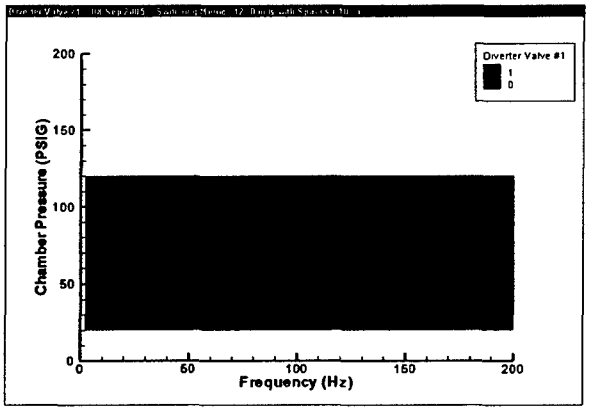

Exit Area at -10% of Nominal

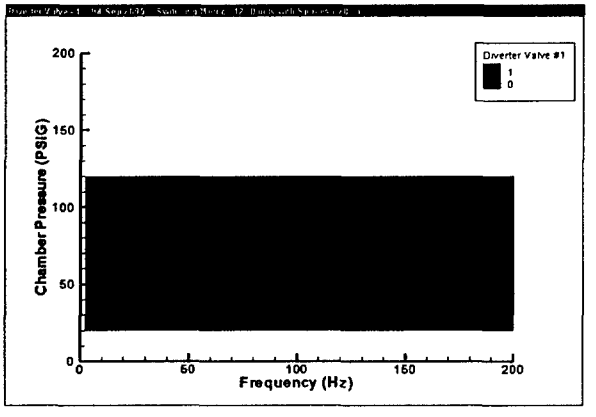

Exit Area at -20% of Nominal

Figure 4.14 Effect of duct exit area on valve switching performance; Short duct configuration L = 23 inch.

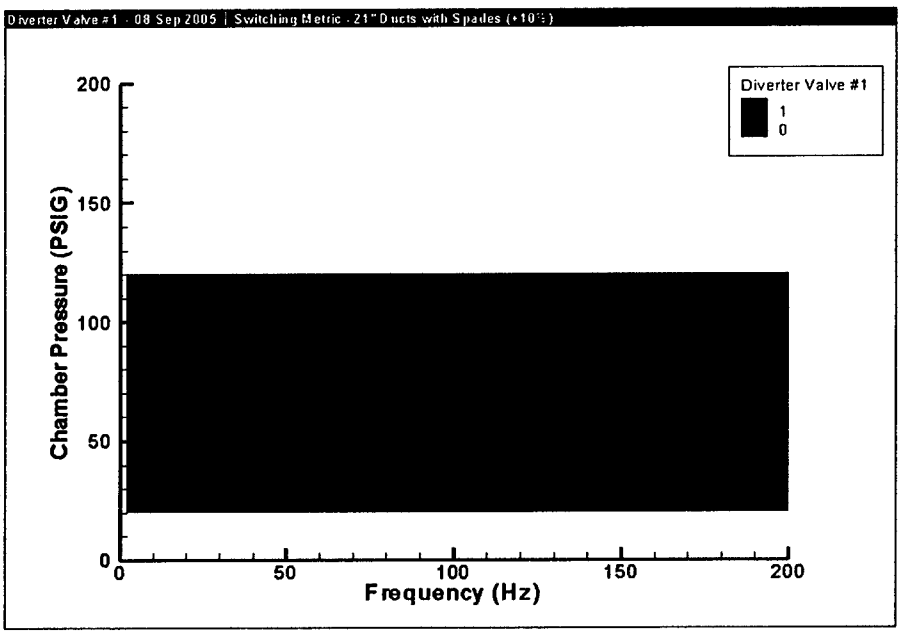

Medium duct +10% exit area

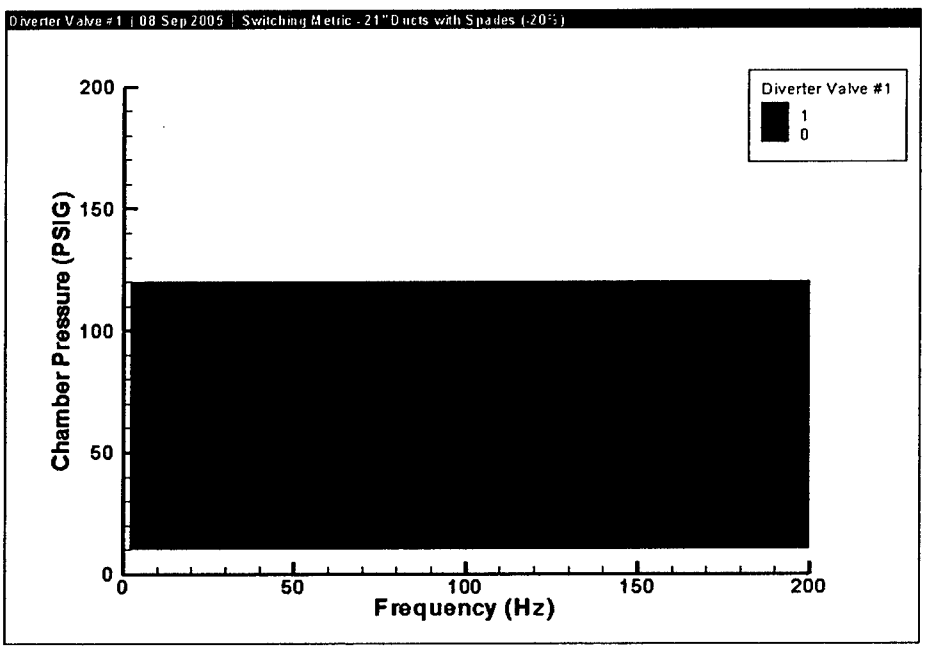

Medium duct -20% exit area

Figure 4.15 Effect of duct exit area on valve switching performance; Medium duct configuration L = 32 inch.

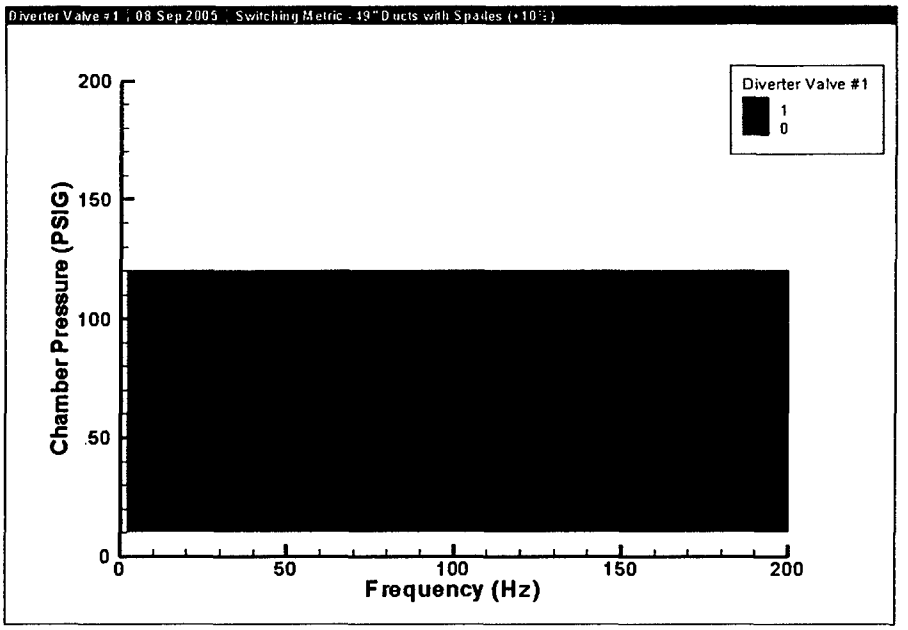

Long duct +10% exit area

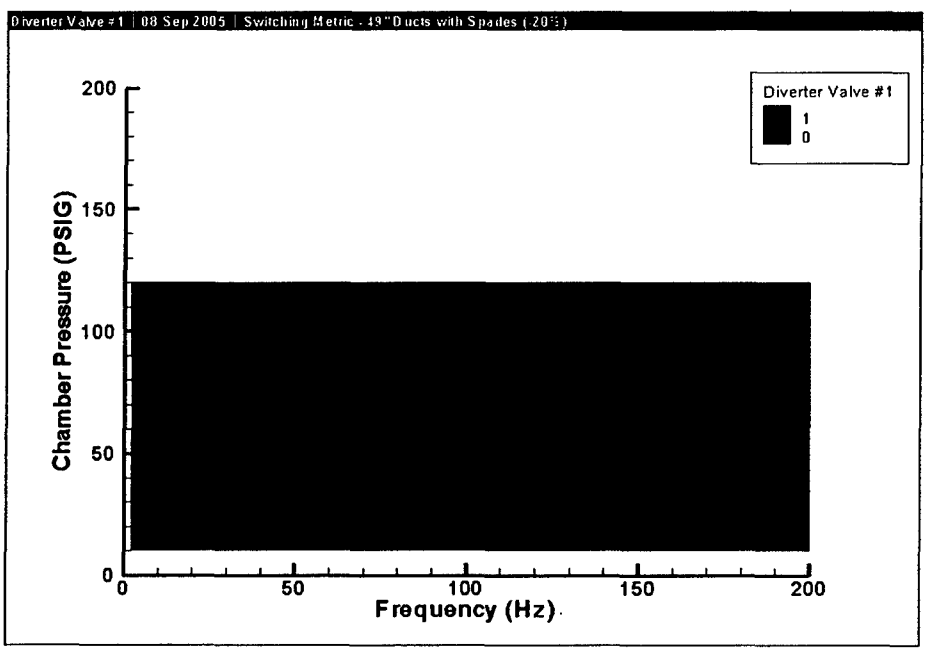

Long duct -20% exit area

Figure 4.16 Effect of duct exit area on valve switching performance; Long duct configuration L = 60 inch.

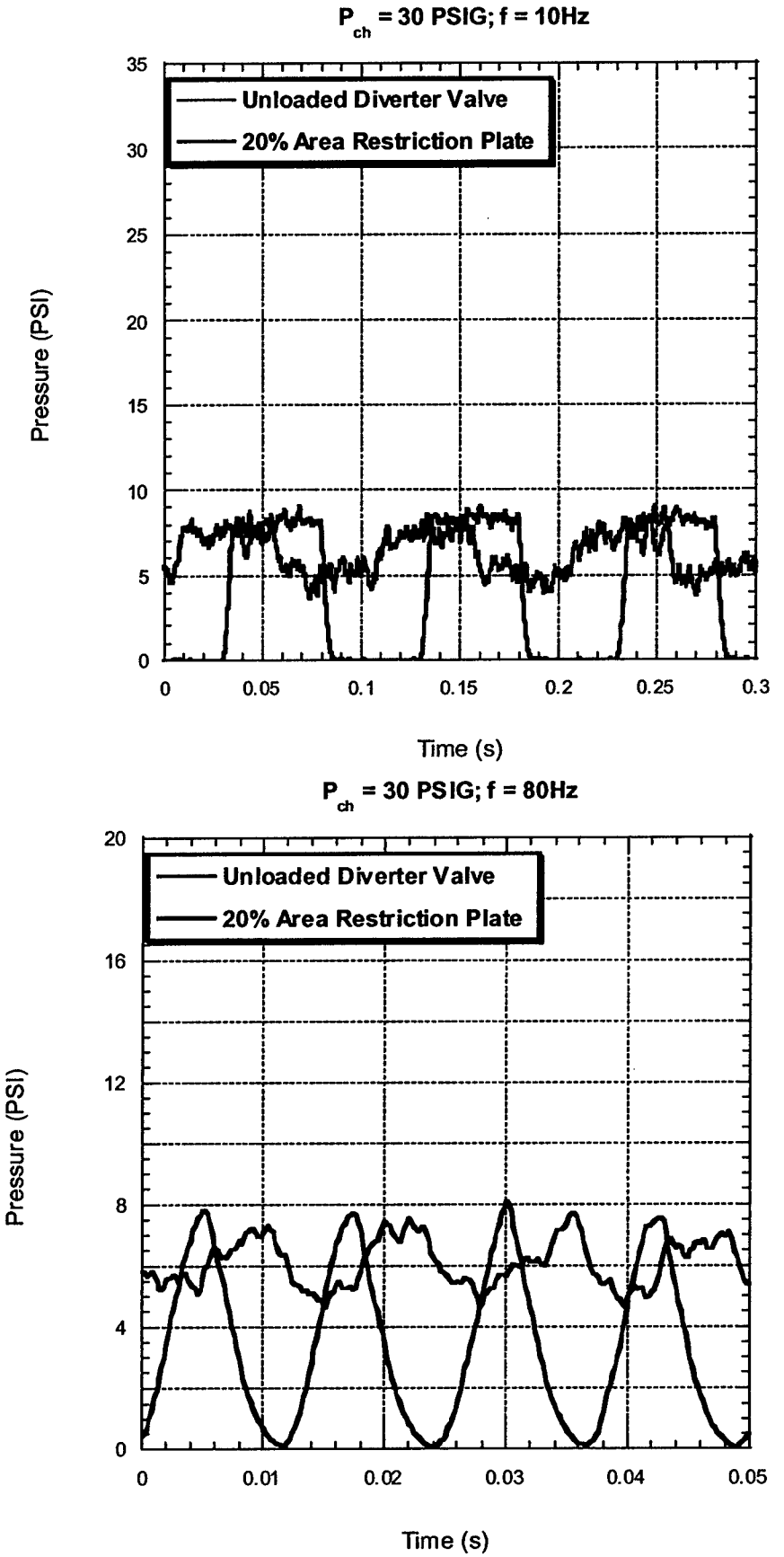

Figure 4.17 Improved pulse quality with "restrictor plate" closing 20% of the unloaded diverter valve exit area; P_{ch} = 30 psig.

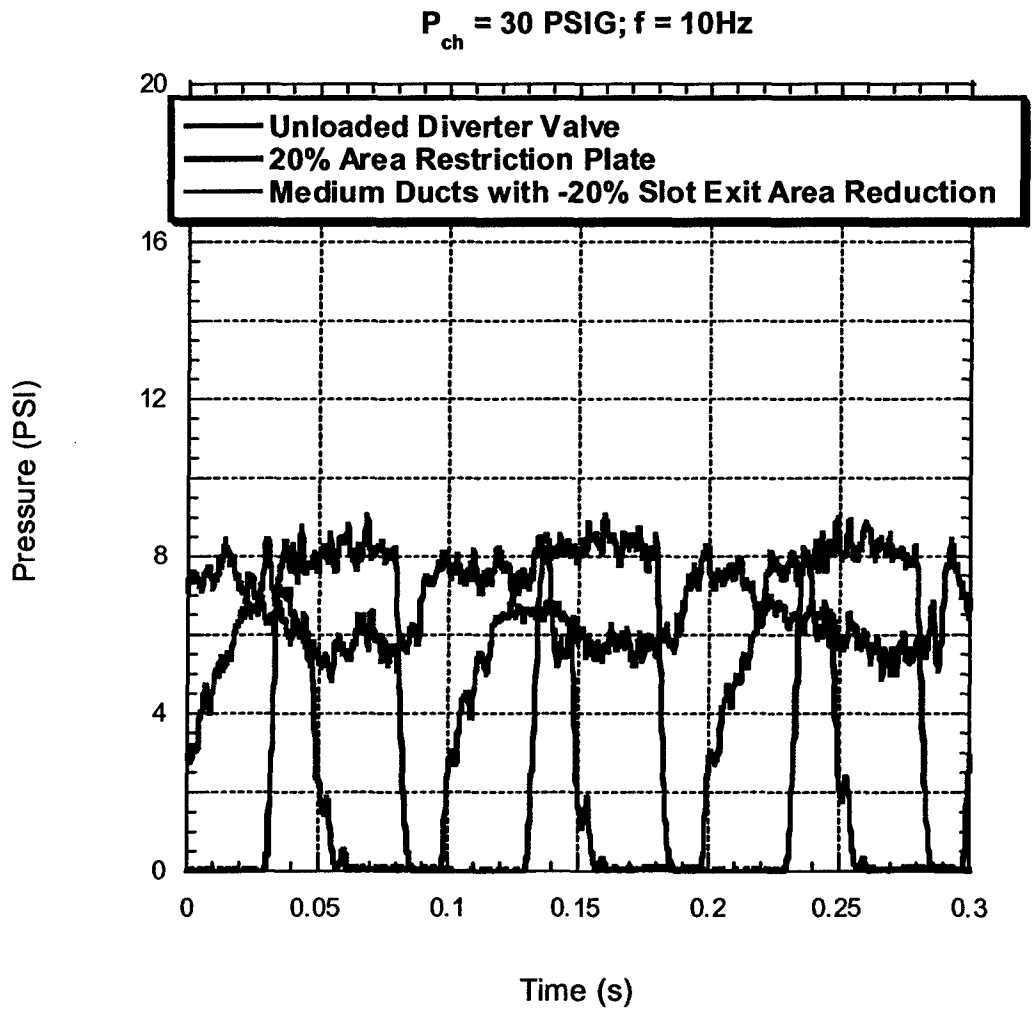

Figure 4.18 Adding distribution ducts has similar effect as adding "restrictor plate" to diverter valve exit; P_{ch} = 30 psig.

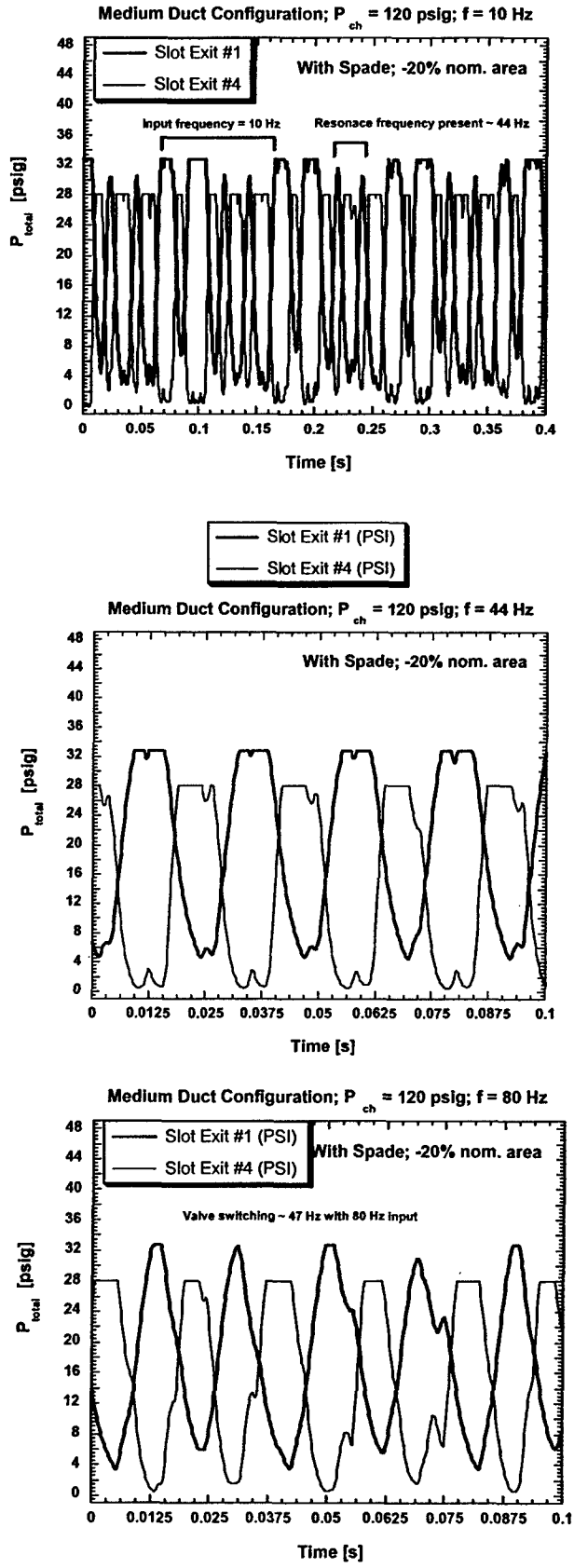

Figure 4.19 Evidence of "lock on" frequency from ACE system with medium duct configuration and exit spades; P_{ch} = 120 psig.

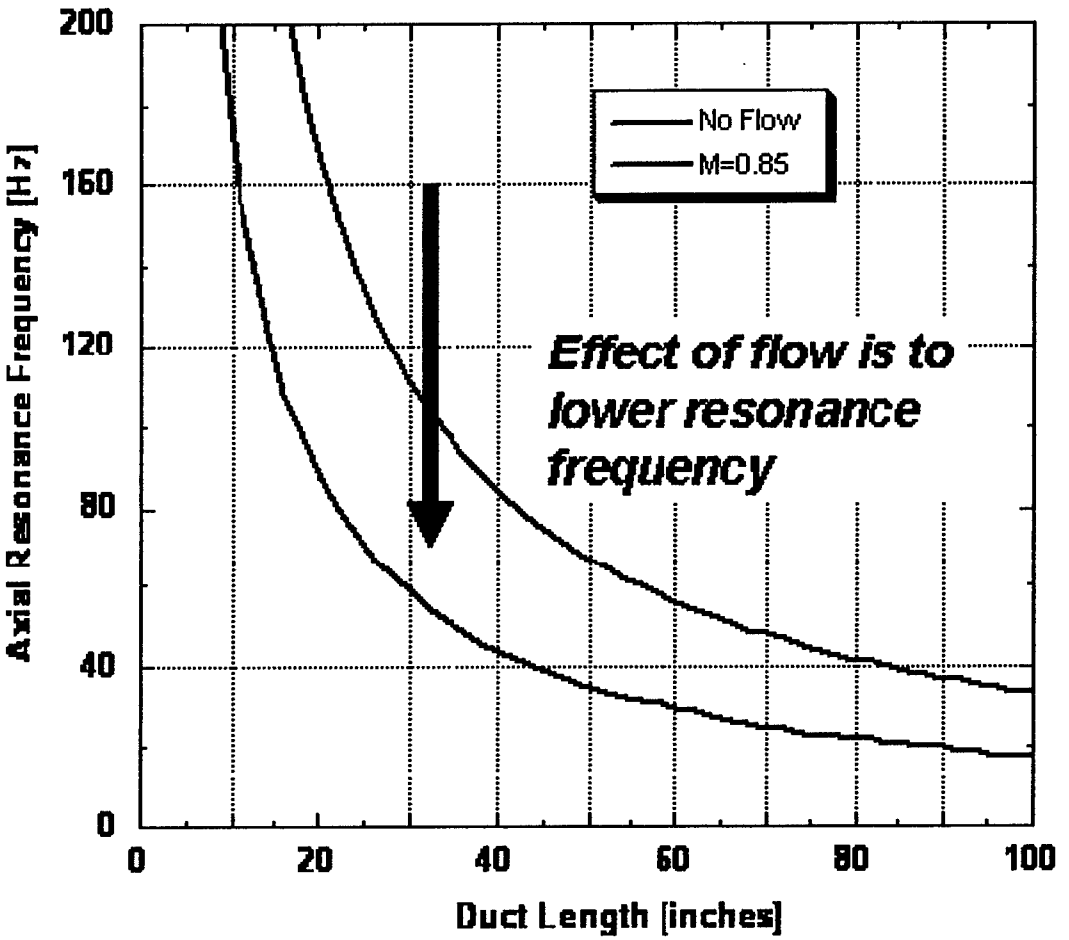

Figure 4.20 Effect of flow on theoretical longitudinal duct resonance frequency. Resonance as a function of duct length is shown for Open-Closed duct boundary conditions.

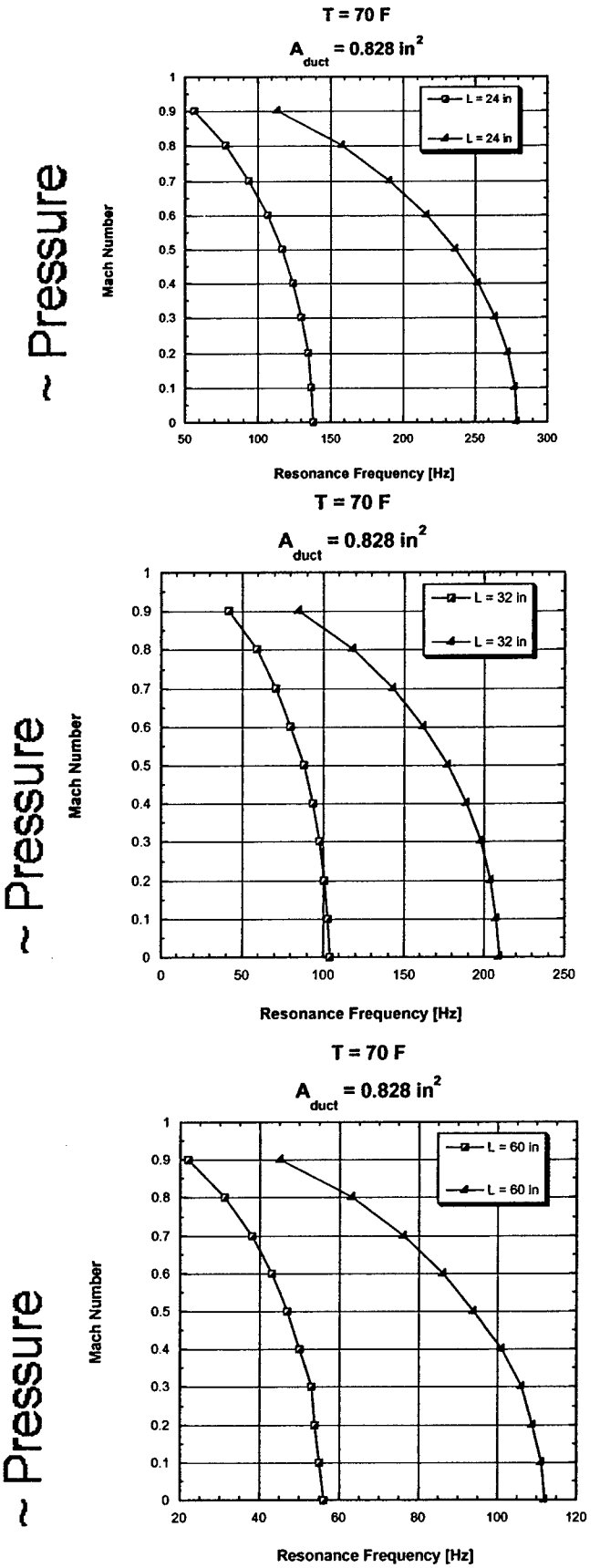

Figure 4.21 Effect of flow on theoretical longitudinal duct resonance frequency. Resonance frequency as a function of Mach number (or pressure) is shown for three different duct lengths.

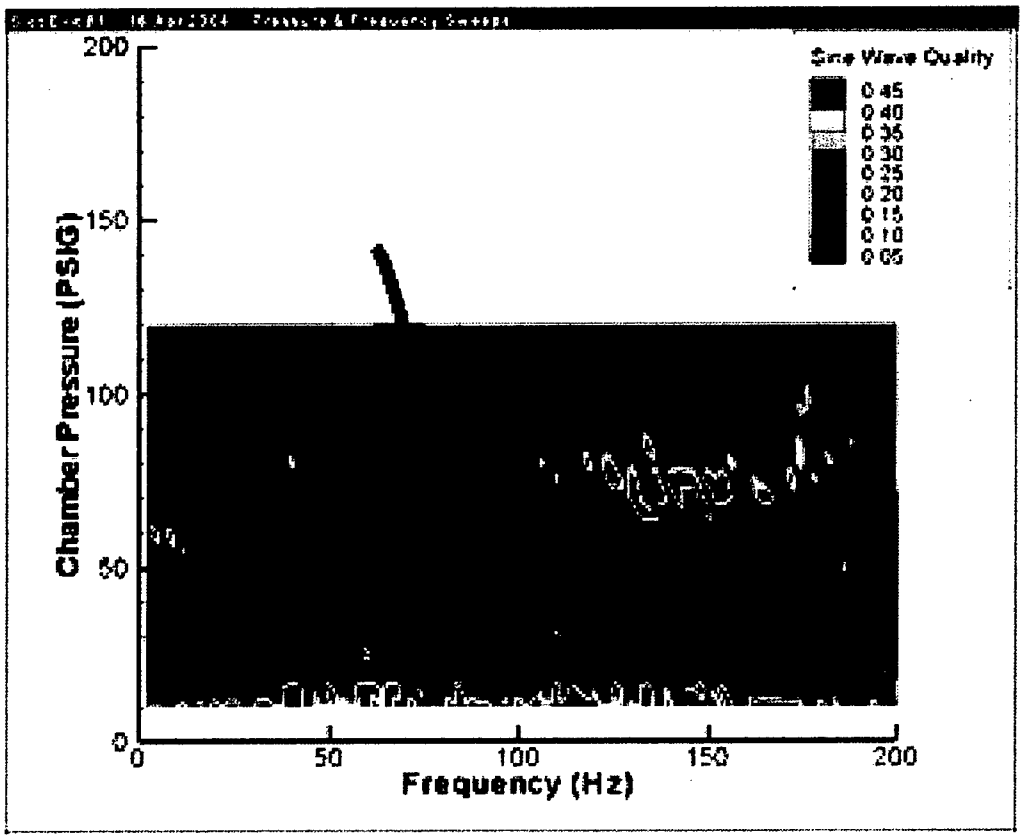

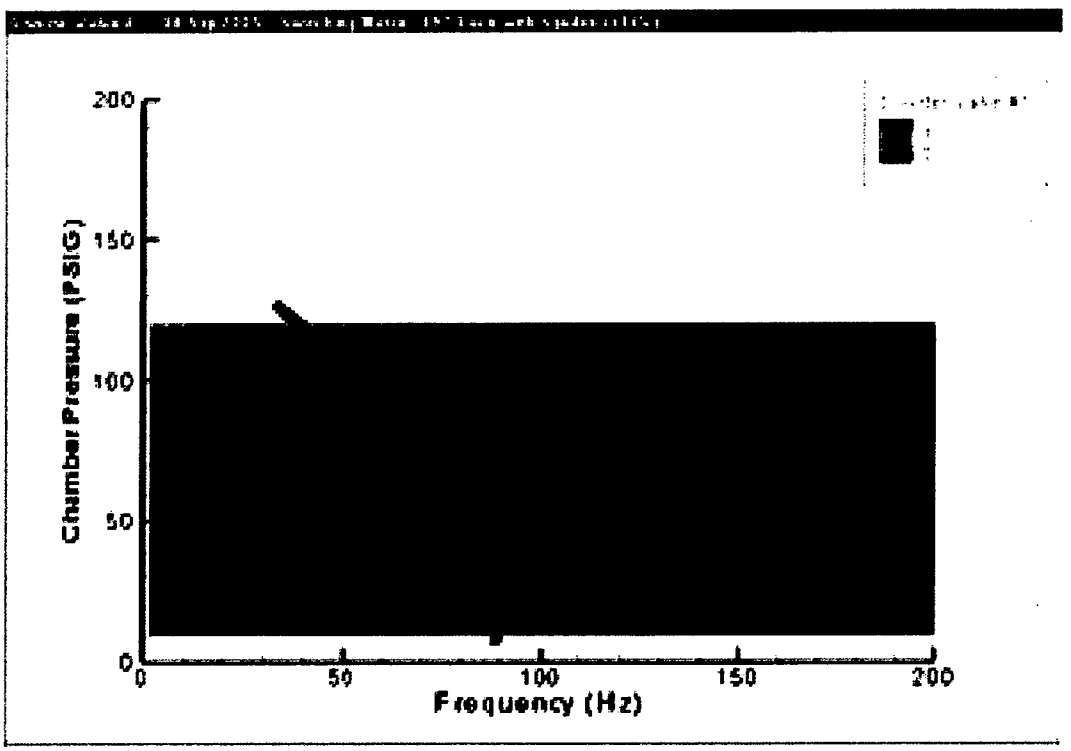

Figure 4.22 Evidence of longitudinal flow-acoustic resonance in pulse quality and switching parameter contour plots.

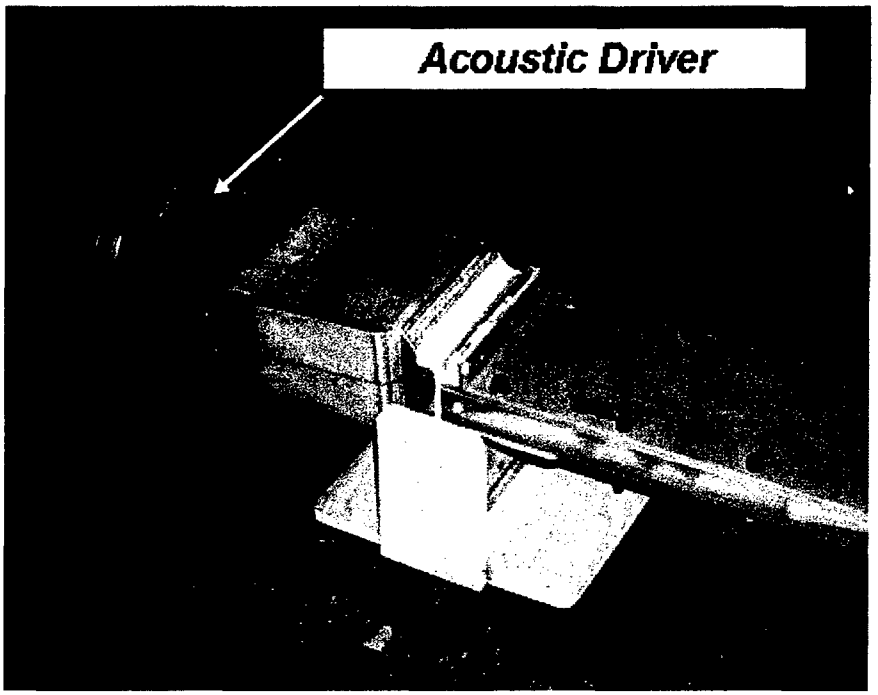

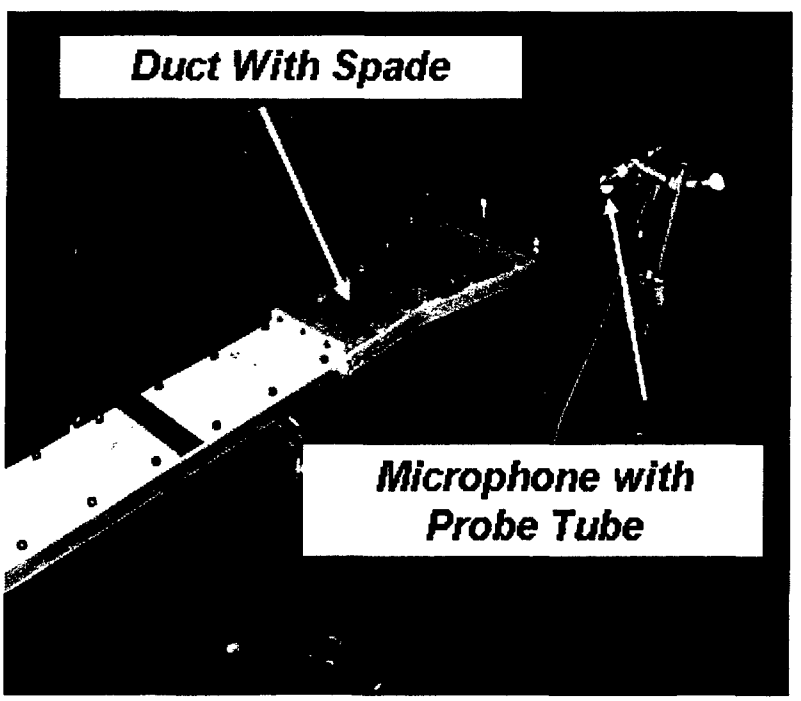

Figure 4.23 Experimental set-up for no-flow acoustic test on ACE distribution duct.

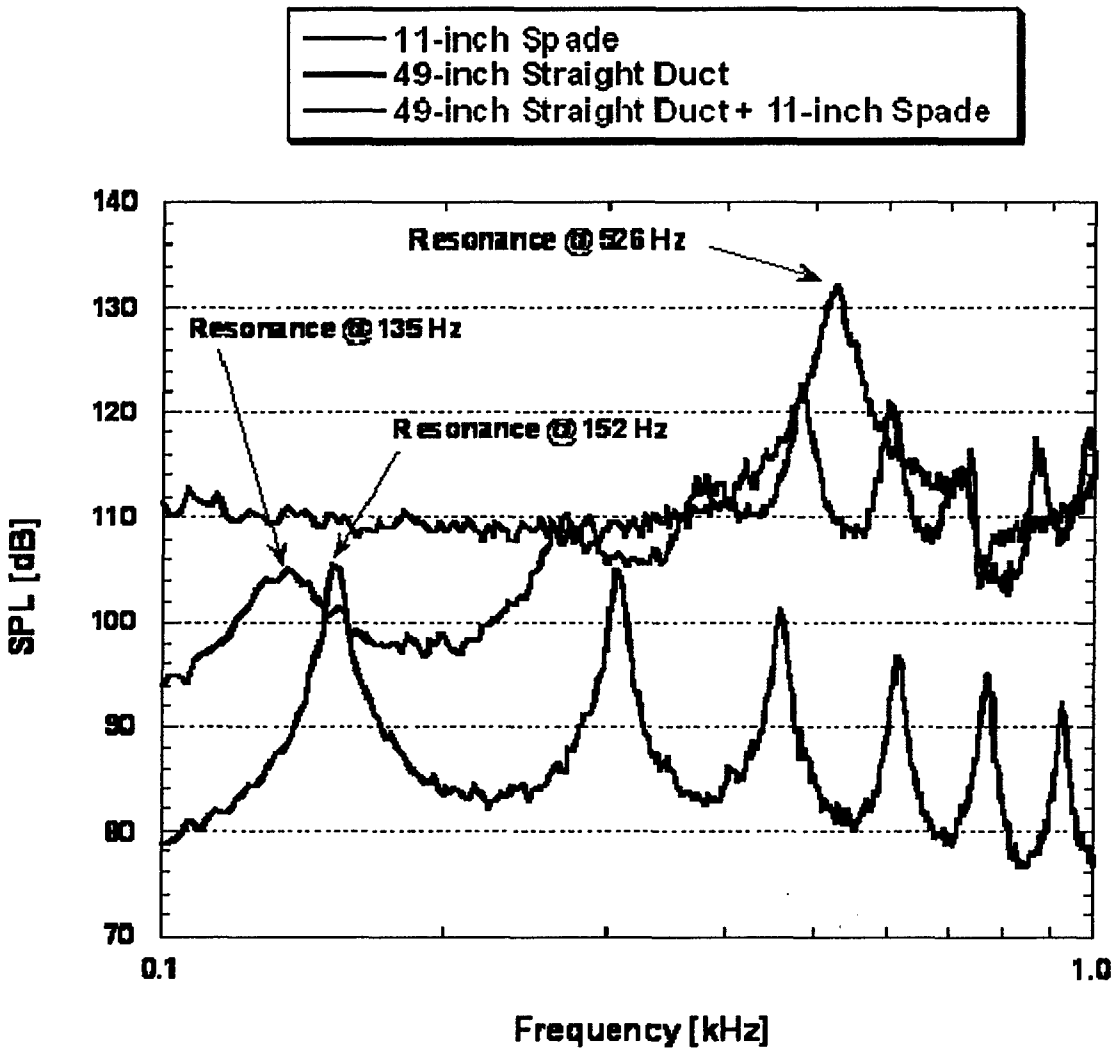

Figure 4.24 Sound pressure level spectra of ACE distribution duct exposed to broadband acoustic source. Clear evidence of longitudinal resonance is observed.

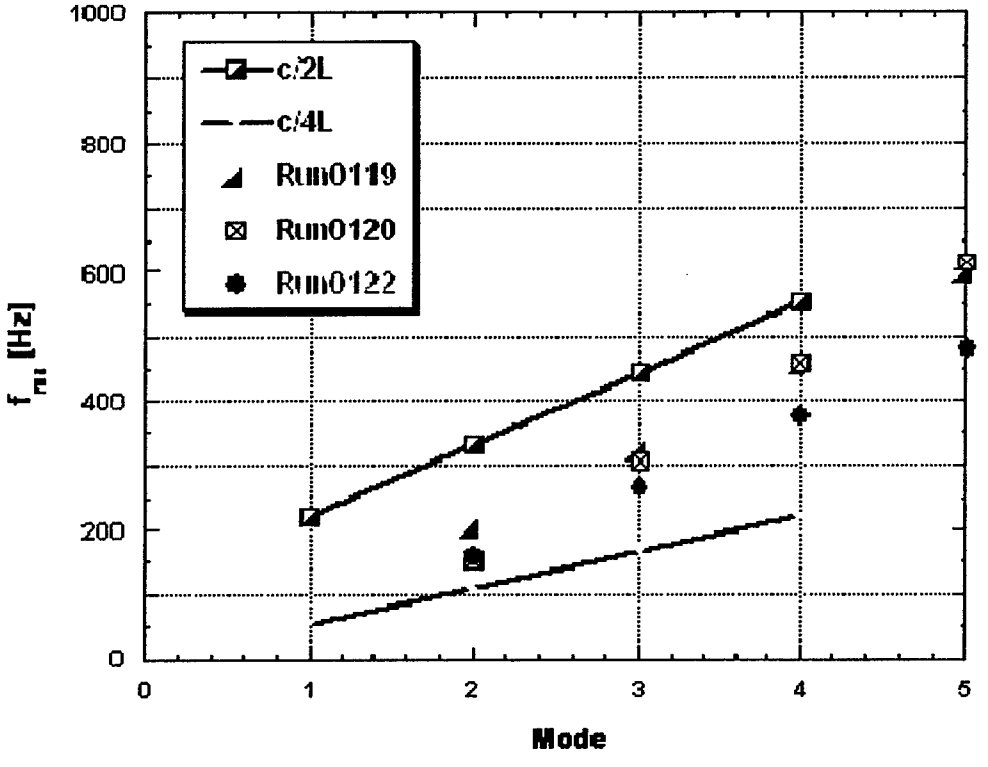

Figure 4.25 Fundamental and higher harmonic resonance frequencies measured in ACE duct exposed to broadband excitation.

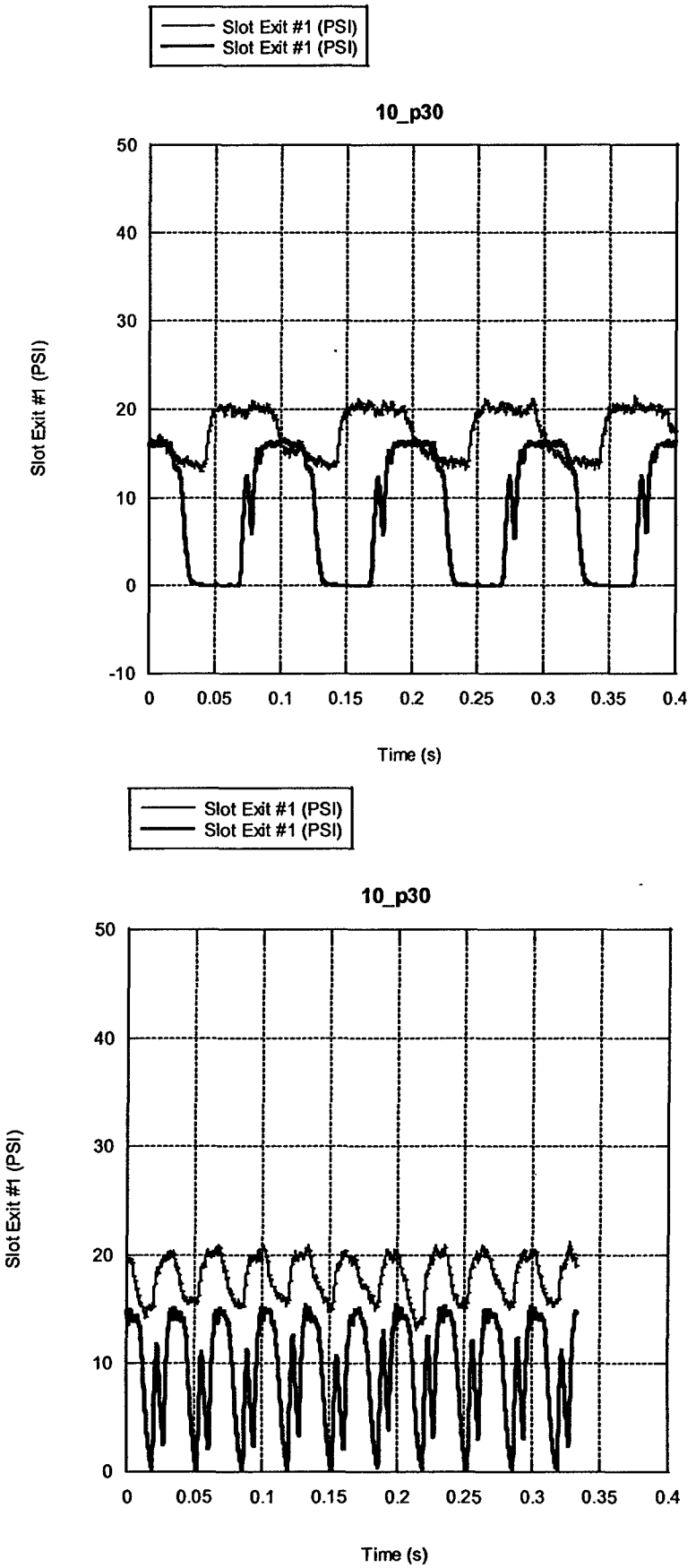

Figure 4.26 Improved pulse quality with addition of 90^0 bend onto straight medium length duct.; P_{ch} = 30 psig.

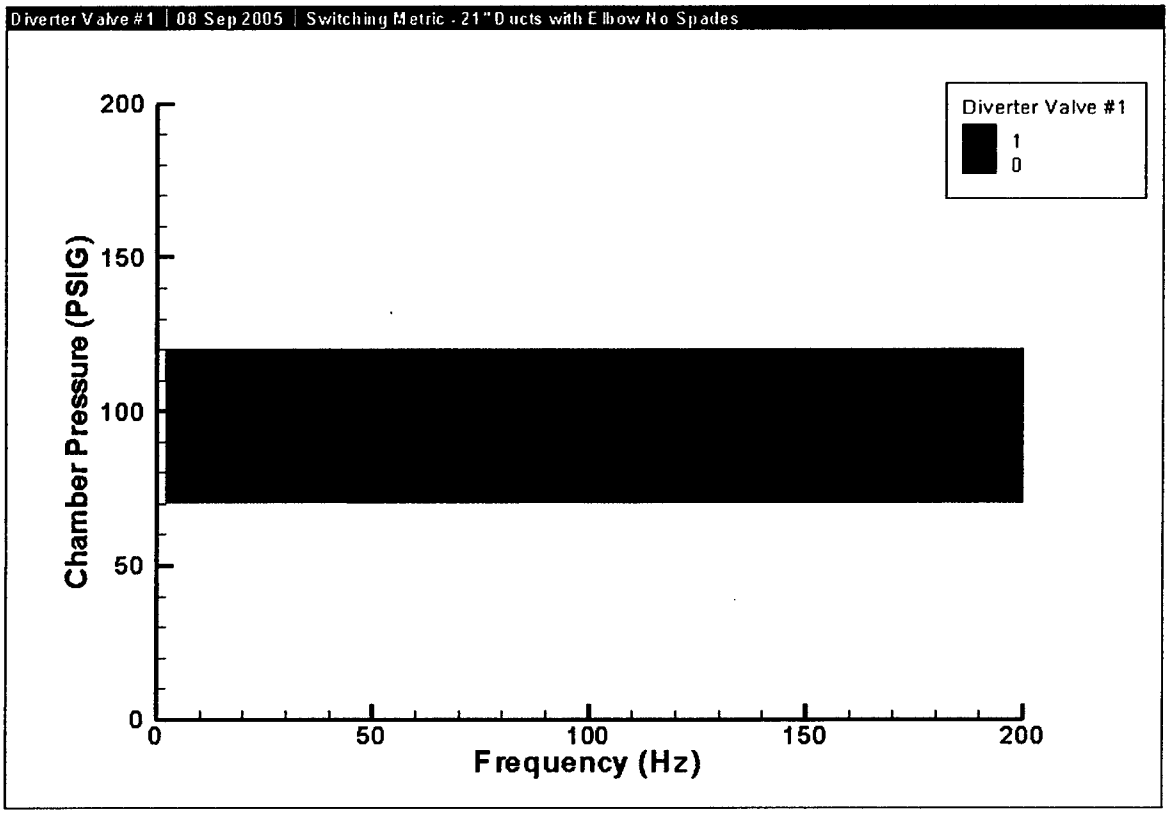

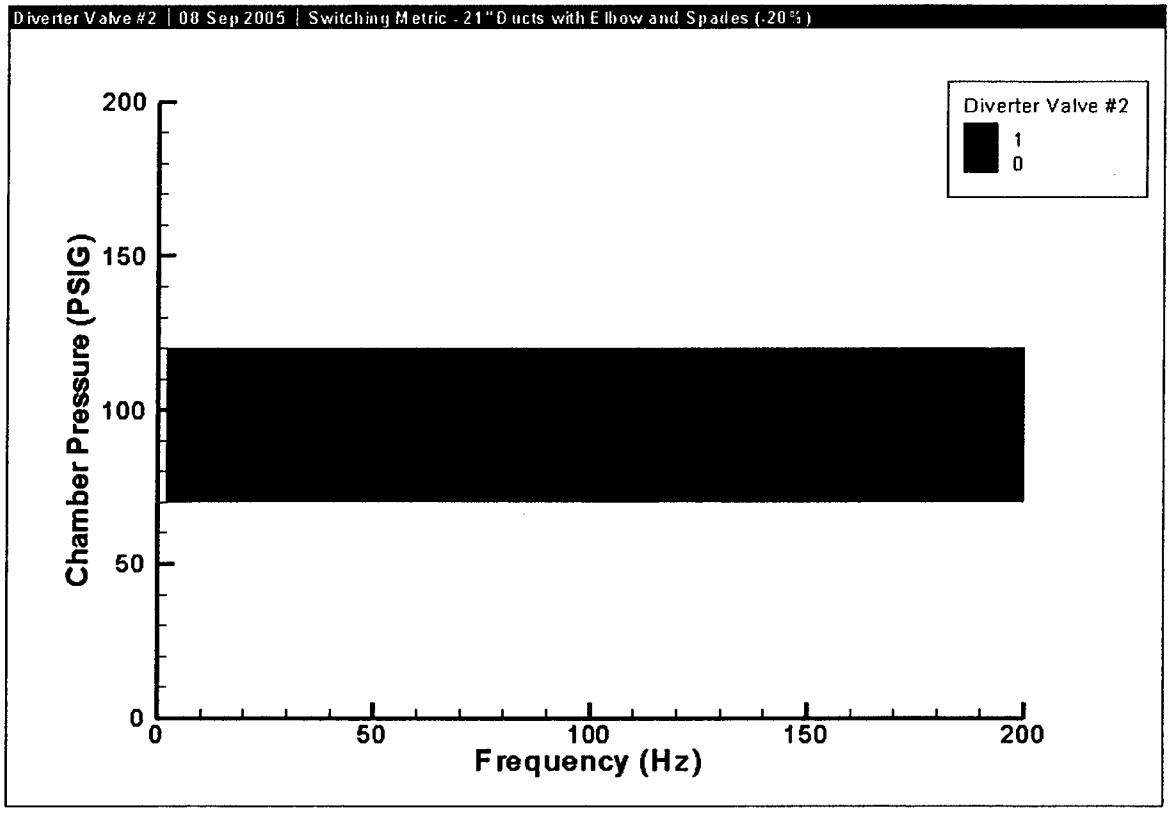

Figure 4.27 Improved pulse quality and switching with addition of 90^0 bend onto straight medium length duct (P_{ch} = 70 to 120 psig)

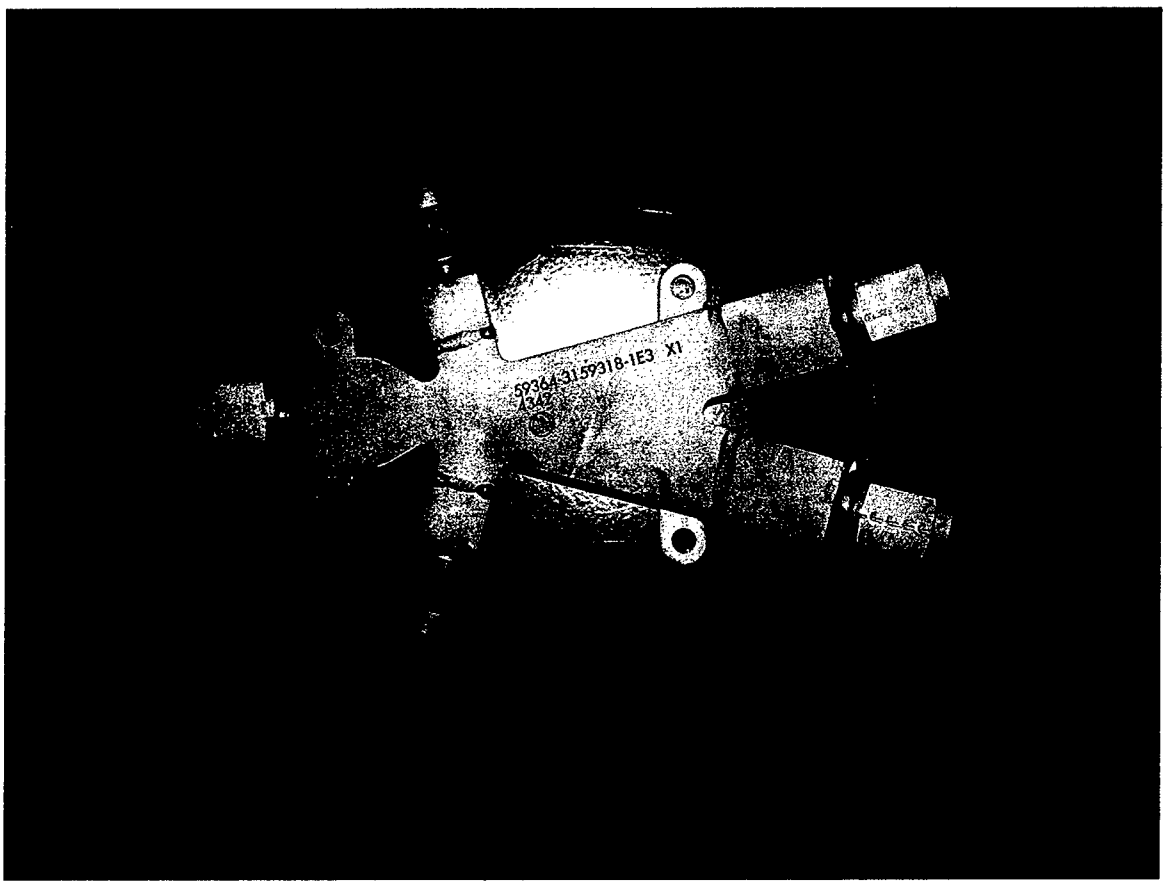

Figure 4.28 The Honeywell redesigned pilot oscillator valve.

Old Pilot Valve

New Pilot Valve

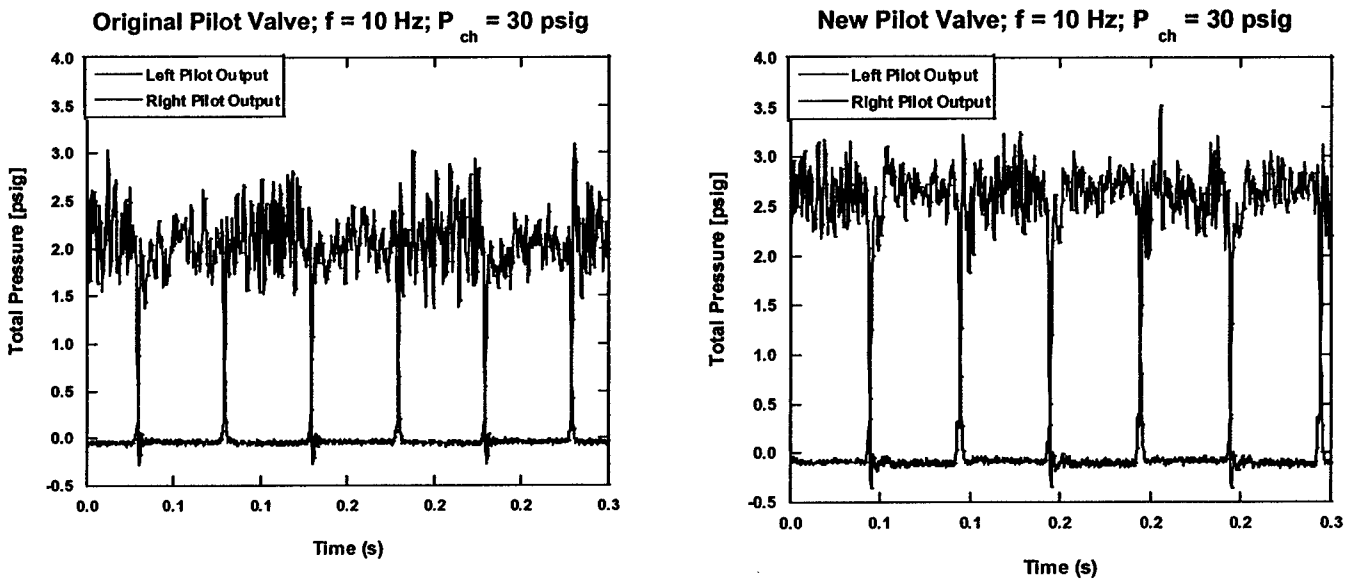

F = 10 Hz

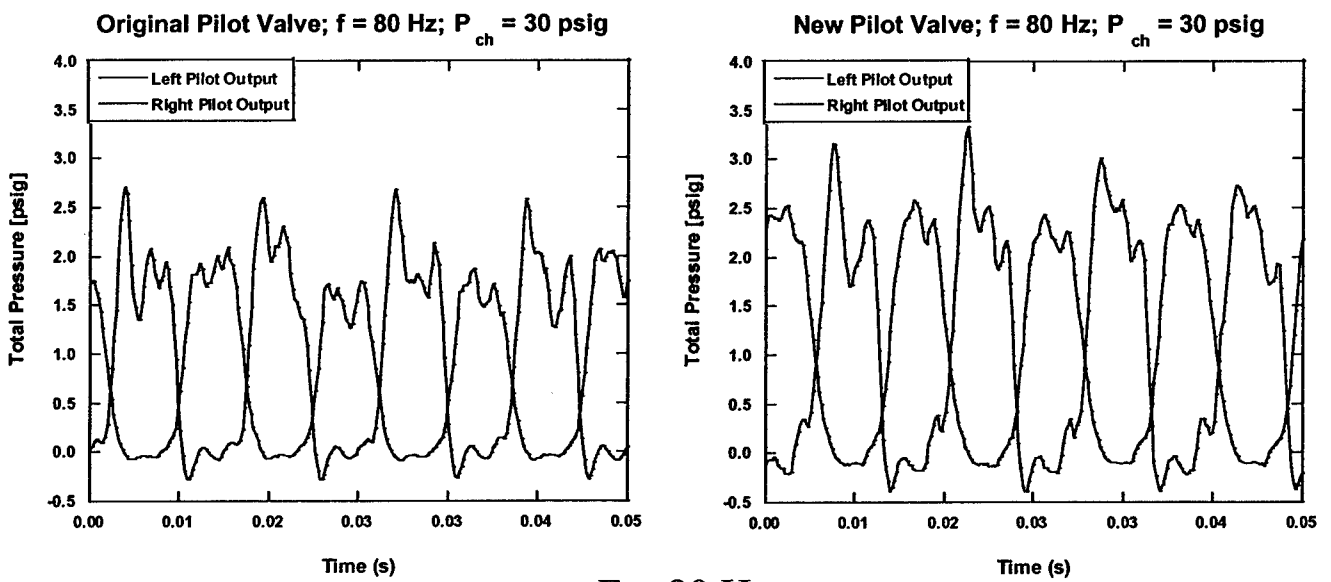

F = 80 Hz

Figure 4.29 Comparison of old and new pilot valve performance at P_{ch} = 30 psig; Output total pressure signal.

Old Pilot Valve

New Pilot Valve

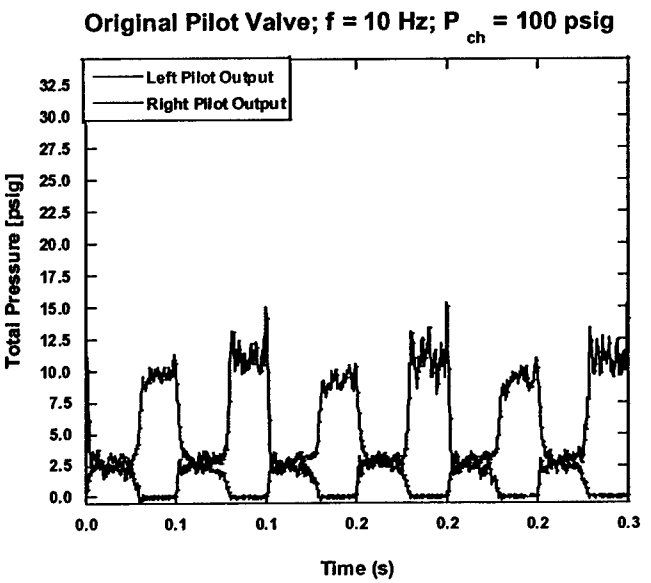

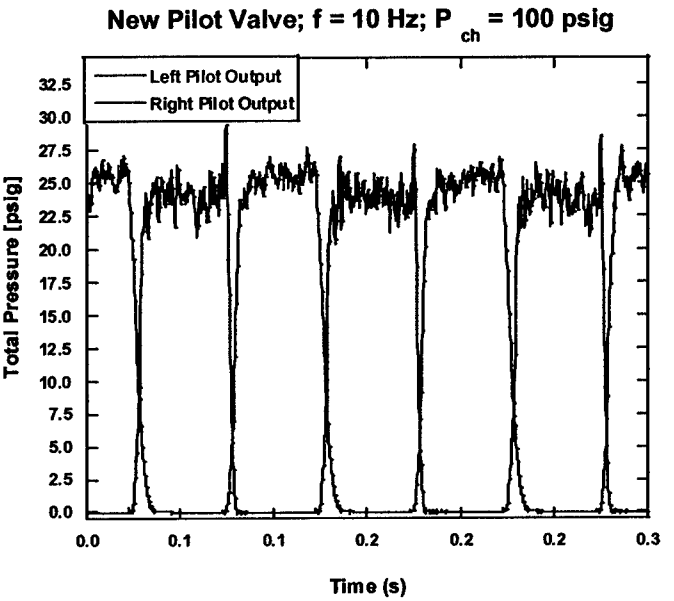

f = 10 Hz

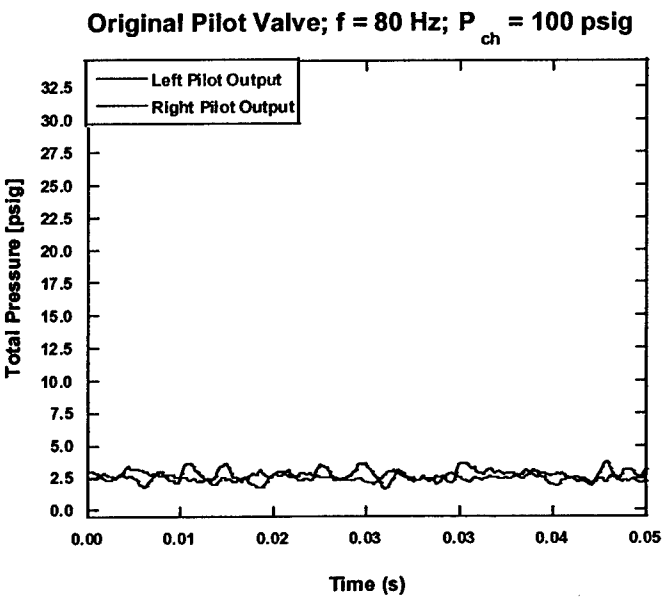

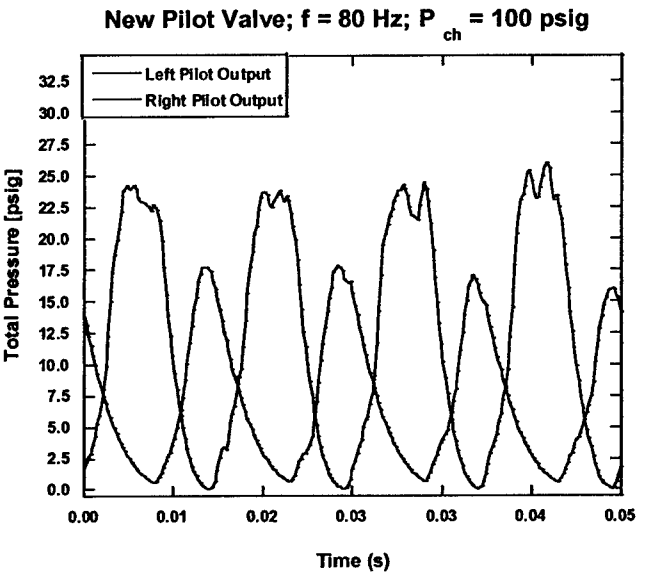

f = 80 Hz

Figure 4.30 Comparison of old and new pilot valve performance at P_{ch} = 100 psig; Output total pressure signal.

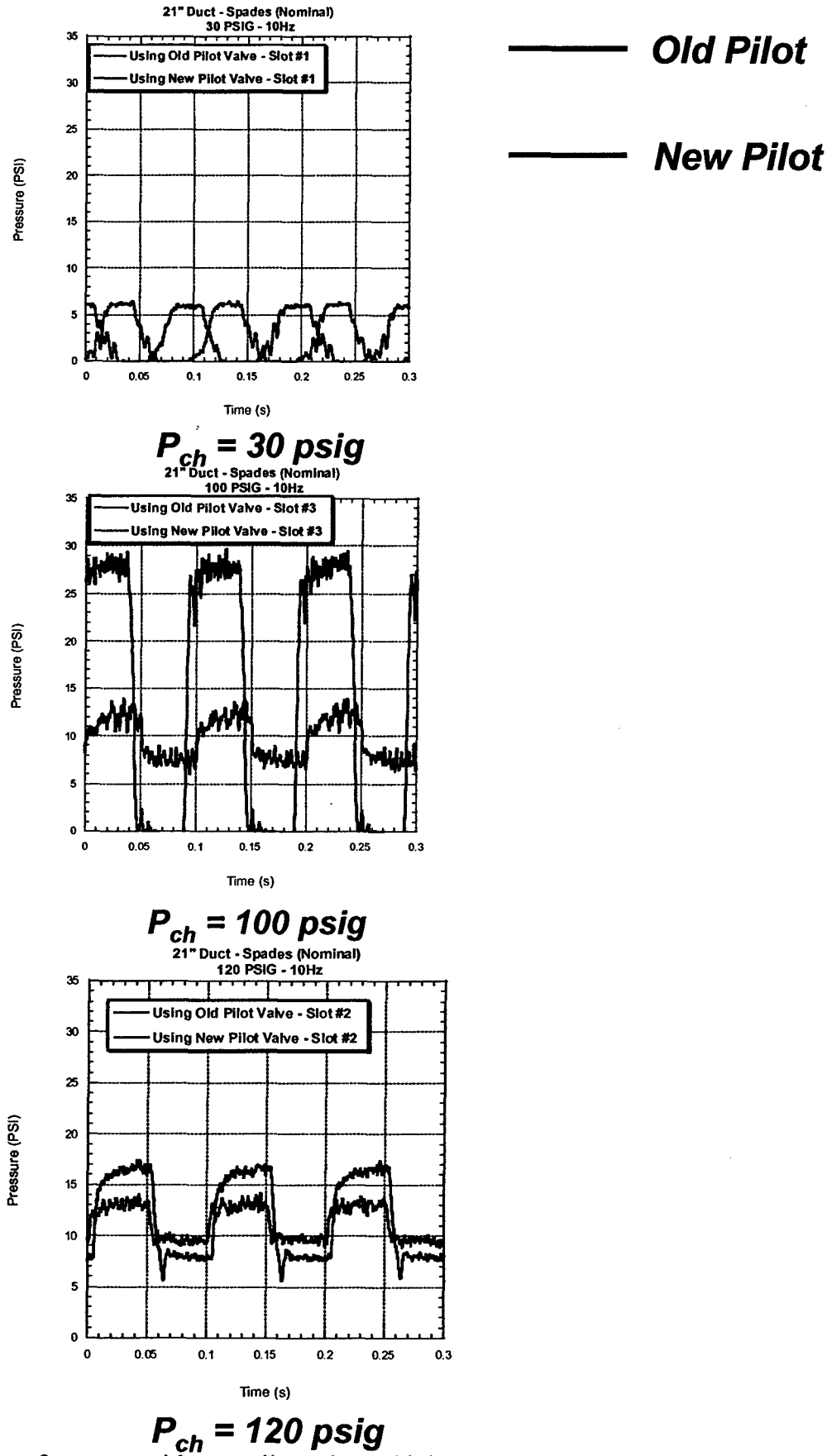

Figure 4.31 Improved system performance with new pilot valve at higher pressures; medium duct length.

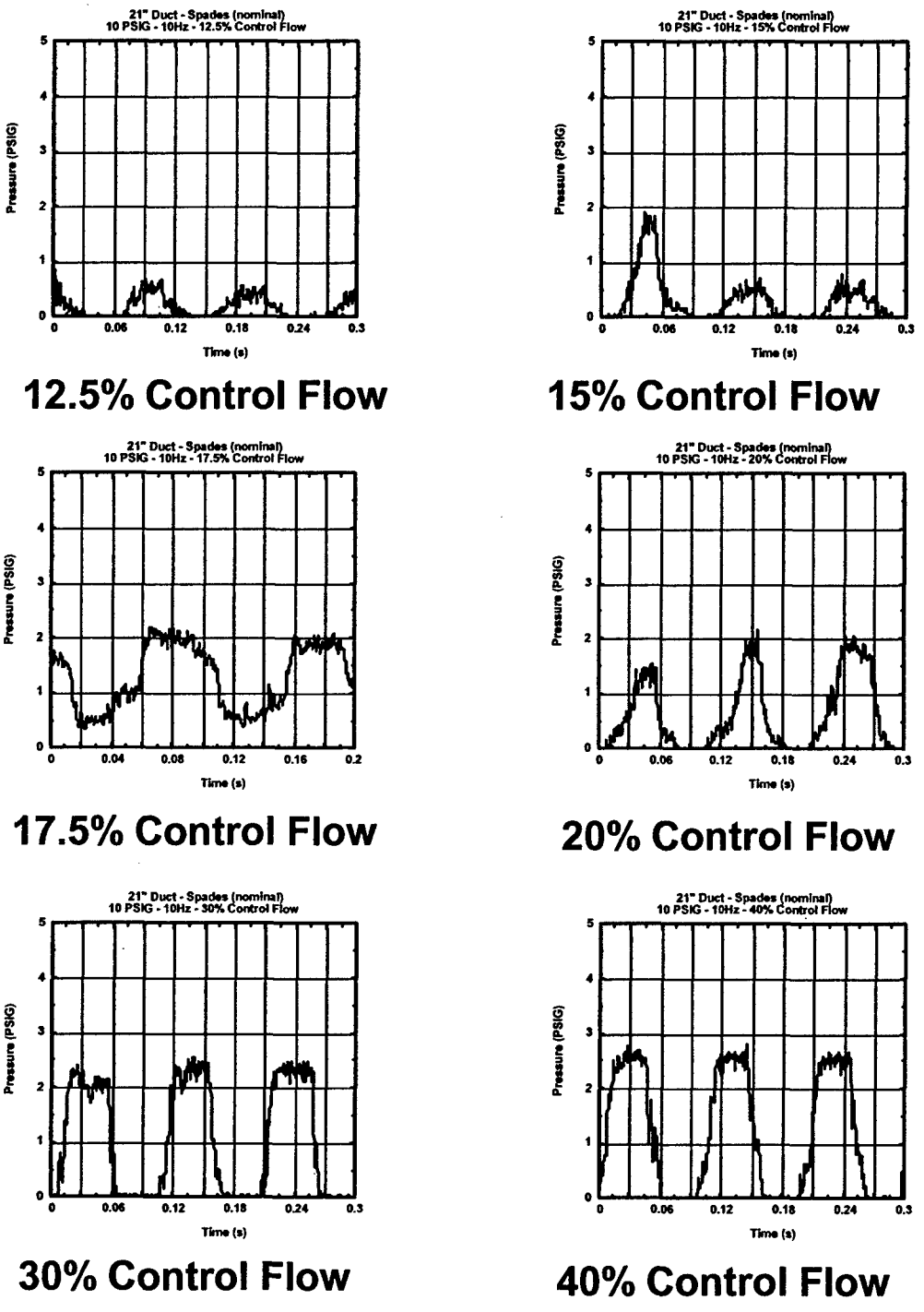

Figure 4.32 Improved system performance with increasing control flow; P_{ch} = 10 psig, f = 10 Hz, medium duct length.

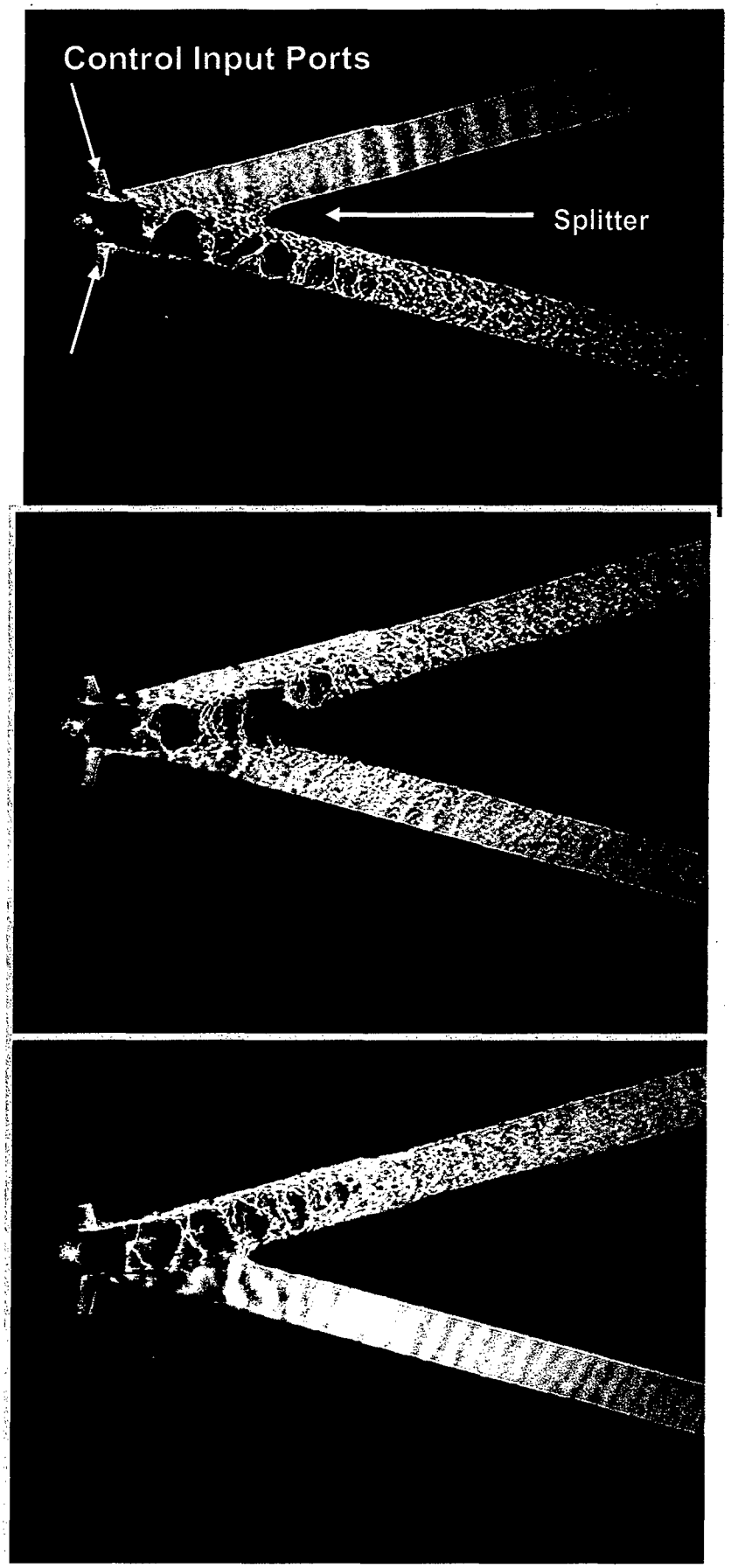

Figure 4.33 Shadowgraph of diverter valve internal flow field at P_{ch} = 40 psig; f = 5 Hz; 10% control flow; medium duct length.

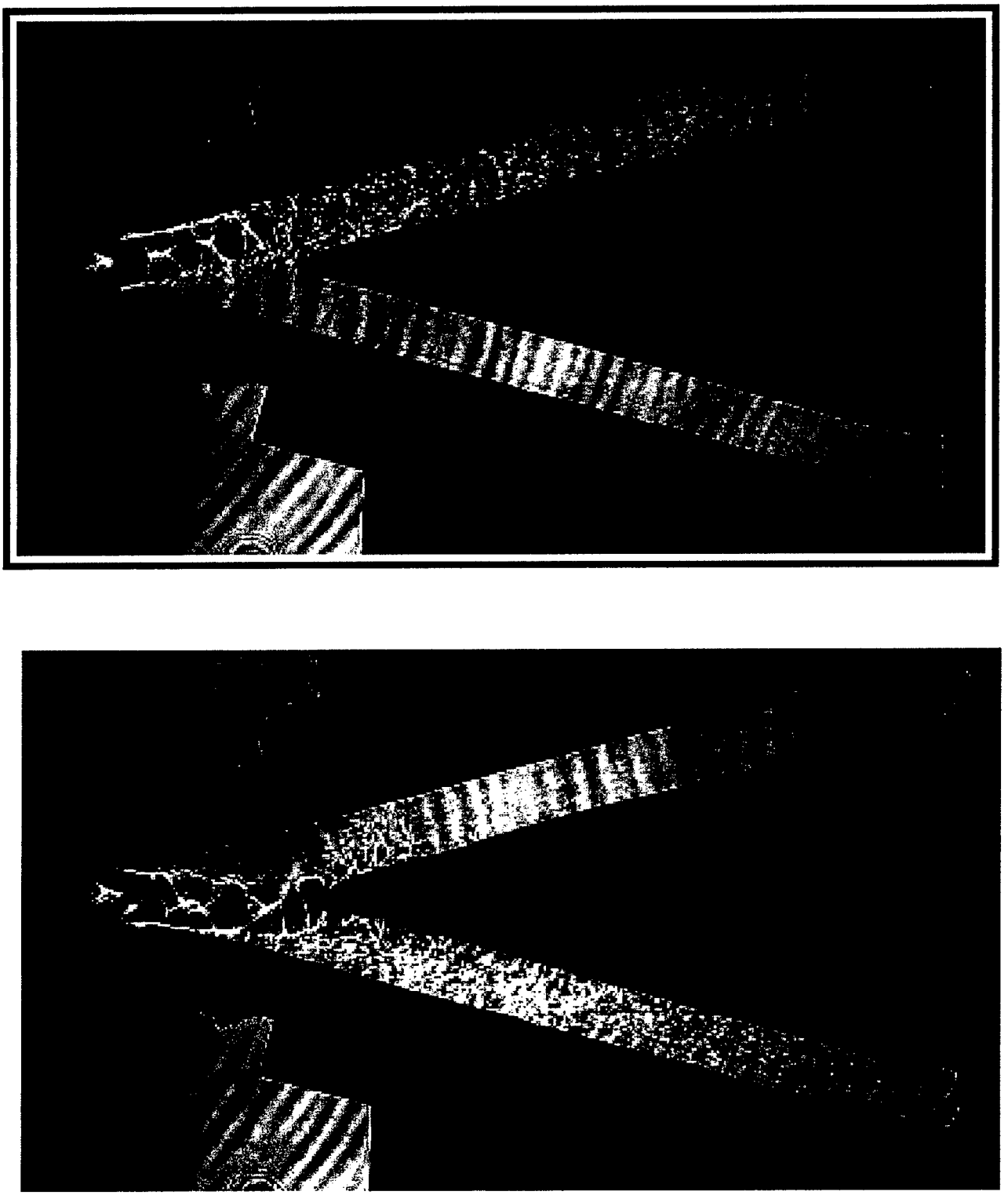

Figure 4.34 Shadowgraph of diverter valve internal flow field at P_{ch} = 30 psig; f = 15 Hz; 10% control flow; medium duct length.

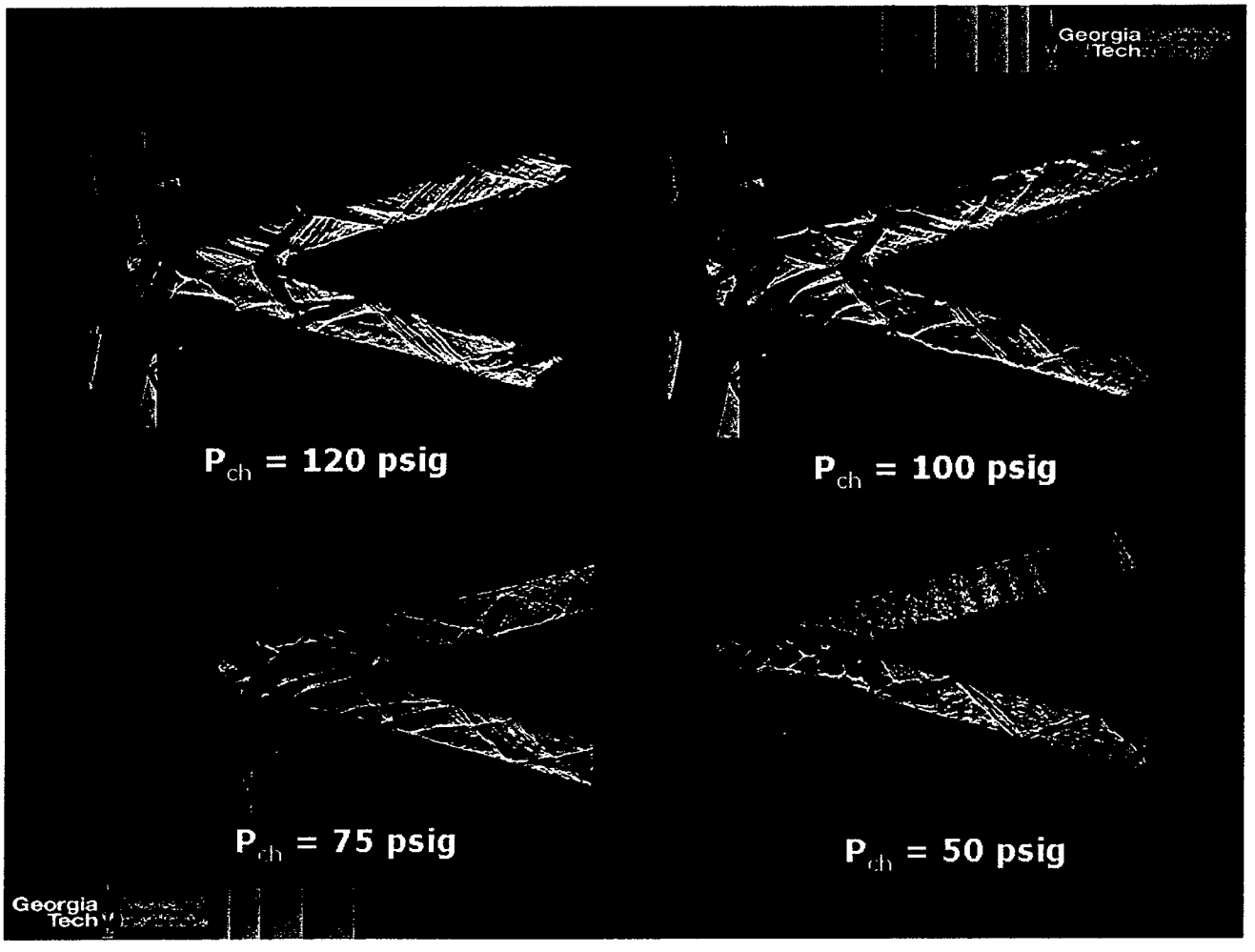

Figure 4.35 Internal flow field at ever-increasing chamber pressure. Both entire passages become filled with shock and expansion waves.

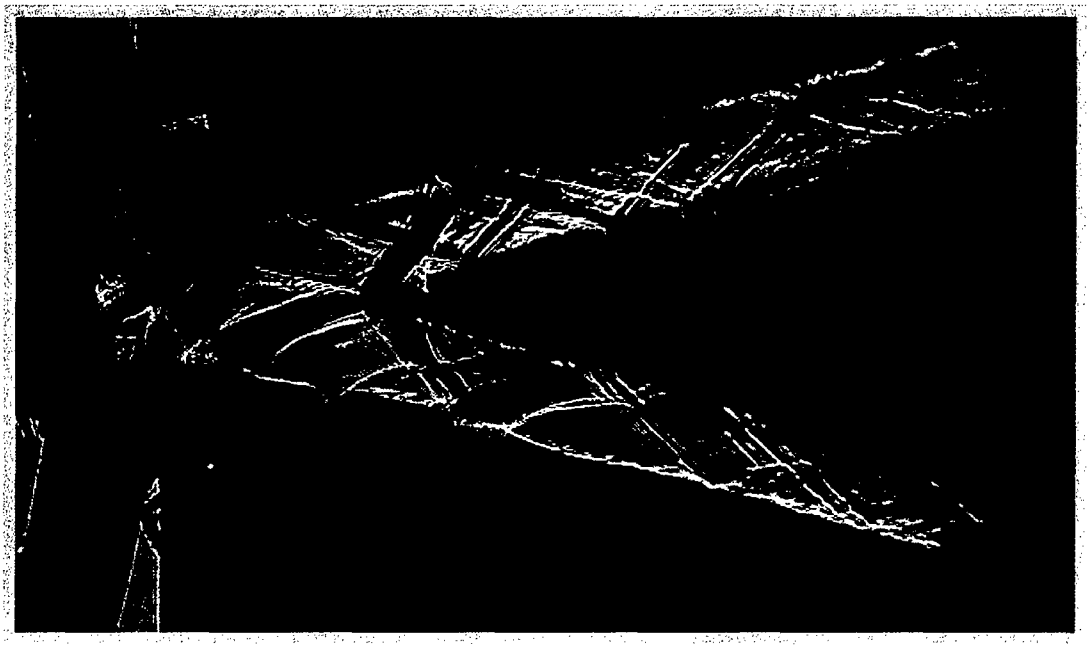

No duct attached

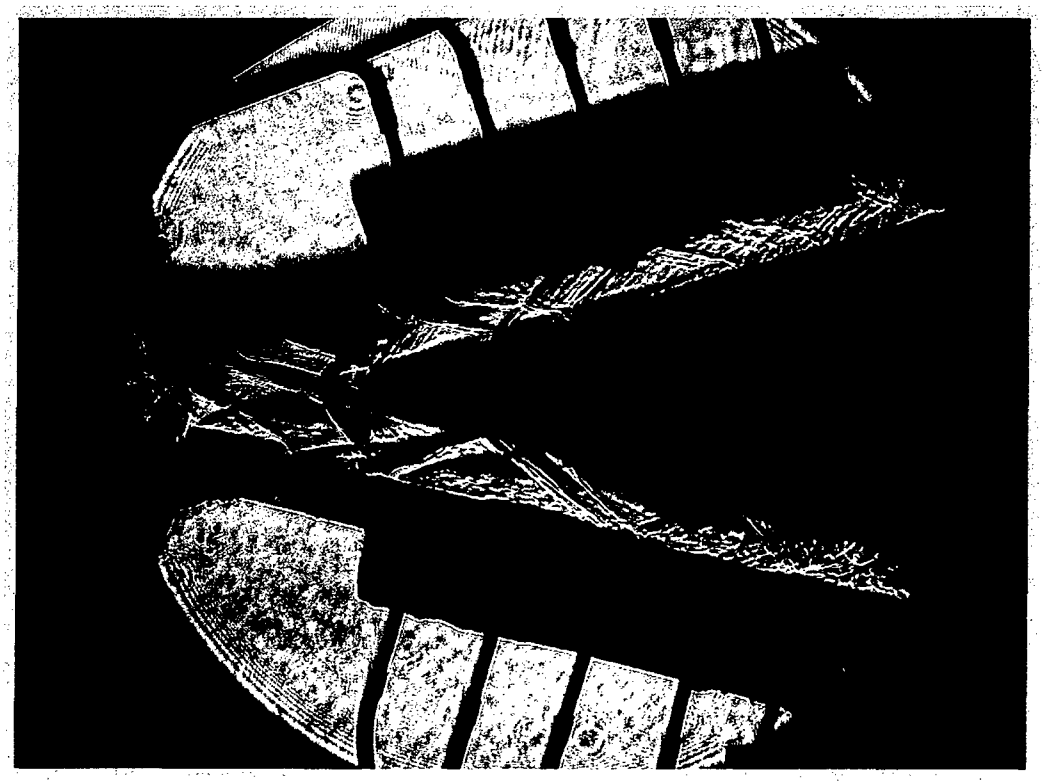

Medium duct attached

Figure 4.36 Internal flow field at P_{ch}=100 psig with and without distribution duct attached.

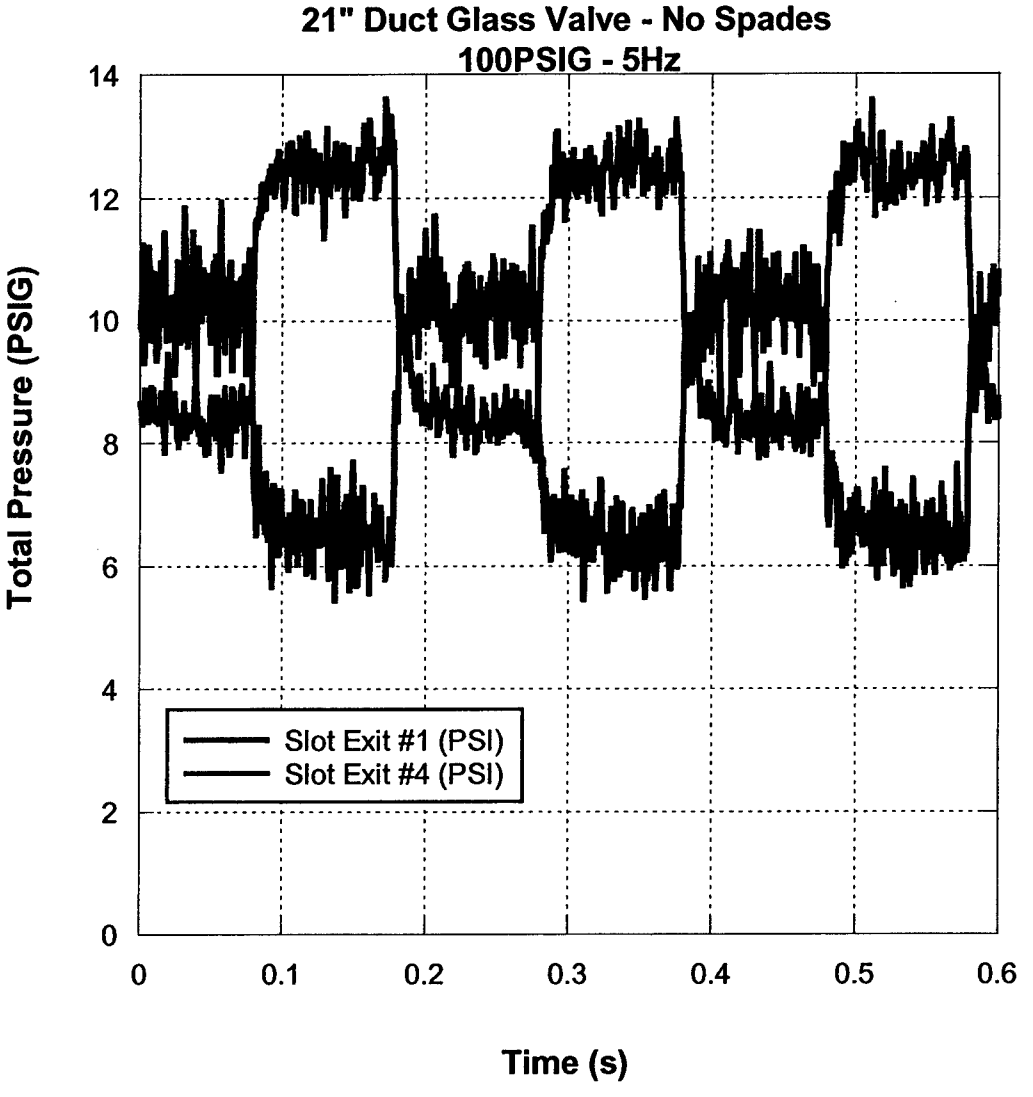

Figure 4.37 Large DC offsets resulting from flow fields like that in Figure 3.6.

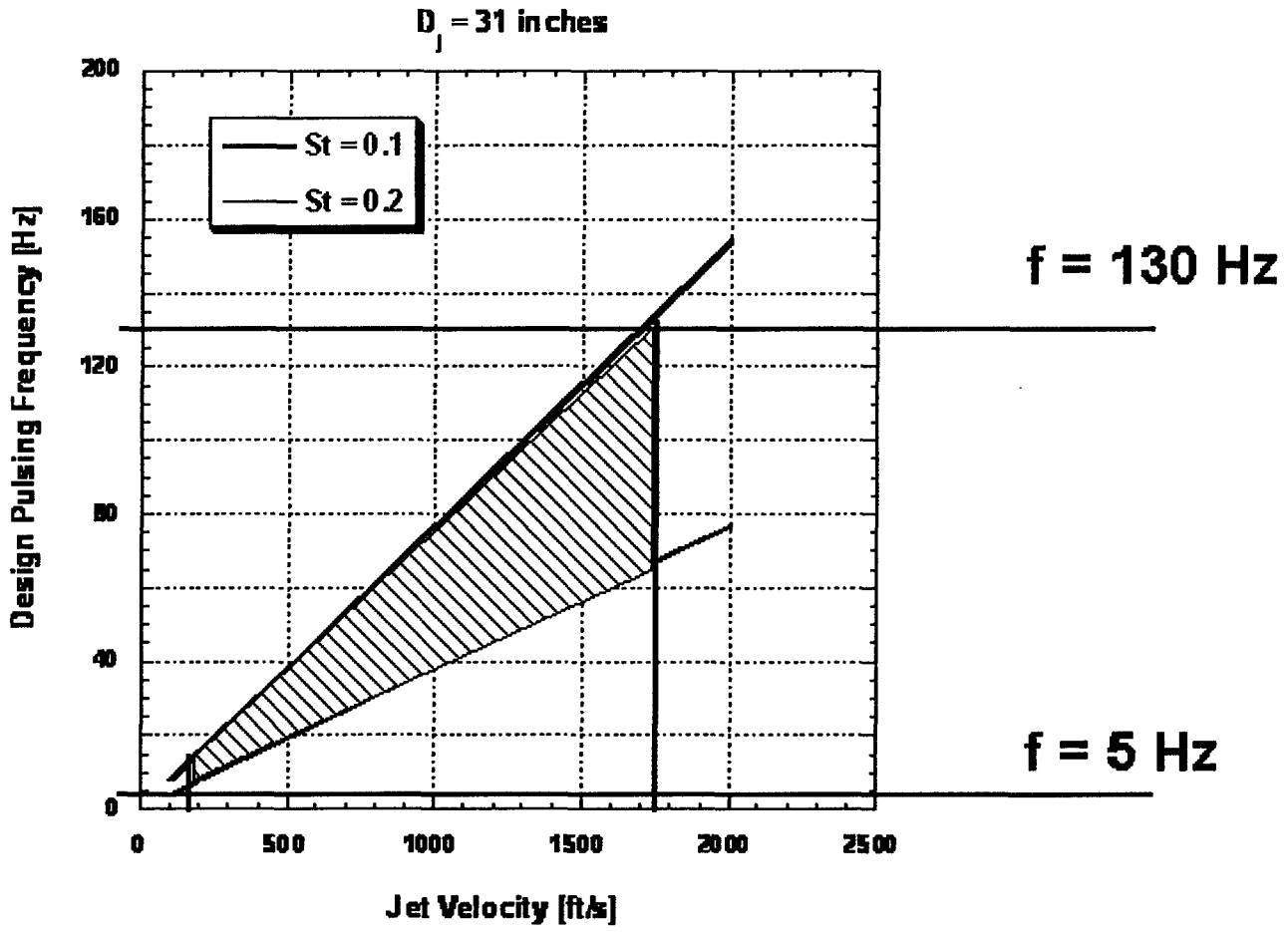

Figure 5.1 Frequency design space for ACE system to optimally mix a 30-inch diameter jet.